DISSERTATION

INFLUENCE OF POLYMERIC NANOWIRE TOPOGRAPHY ON THE DIFFERENTIATION OF ADIPOSE-DERIVED STEM CELLS

Submitted by

Nathan Anthony Trujillo

Department of Mechanical Engineering

In partial fulfillment of the requirements

For the Degree of Doctor of Philosophy

Colorado State University

Fort Collins, Colorado

Summer 2014

Doctoral Committee:

Advisor: Ketul Popat

John Williams
Lakshmi Prasad Dasi
Matt Kipper

ABSTRACT

INFLUENCE OF POLYMERIC NANOWIRE TOPOGRAPHY ON THE DIFFERENTIATION OF ADIPOSE-DERIVED STEM CELLS

Considering the many advances in tissue engineering, there are still significant challenges associated with restructuring, repairing, or replacing damaged tissue in the body. Recently biodegradable synthetic scaffolds have shown to be a promising alternative. However, based on the application, it is essential that the scaffold possess specific surface properties that promote cell-scaffold interactions and aid in extracellular matrix deposition. In this work, we present a novel solvent-free, template-synthesis technique for creating substrate-bound nanowire scaffolds from polycaprolactone, a biocompatible and biodegradable polymer. Nanowire surfaces were also fabricated from polycaprolactone that included 1 wt% hydroxyapatite nanoparticles for osteogenic studies. The fundamental concept behind successful synthetic tissue-engineered scaffolds is to promote progenitor cell migration, adhesion, proliferation, and induce differentiation, extracellular matrix synthesis, and finally integration with host tissue. Recently, lipoaspirate tissue has been identified as a viable alternative source for mesenchymal stem cells because it contains a supportive stroma that can easily be isolated. Adipose derived stem cells can differentiate into a variety of mesodermal lineages including the osteogenic, chondrogenic, and adipogenic phenotypes. The results indicated that during the growth period *i.e.*, initial 7 days of culture, the nanowire surfaces supported adhesion, proliferation, and viability of the cells in addition to morphological changes. Osteogenic, chondrogenic, and adipogenic differentiation potential of adipose derive stem cells was evaluated with and without differentiation supplements

to determine the influence of nanowire architecture on mechanotrasnduction. It was determined that nanowire topography stimulated the expression of osteogenic marker proteins, osteocalcin and osteopontin, as well as mineralization and alkaline phosphatase activity.

ACKNOWLEDGEMENTS

This research is supported by the National Institute of Arthritis and Musculoskeletal and Skin Diseases of the National Institutes of Health under Award Number 5-R21-AR057341-02.

First and foremost I would like to thank my advisor, Dr. Ketul Popat, for his insight, leadership, and guidance. Thank you to my committee members: Dr. John Williams, Dr. Lakshmi Prasad Dai, Dr. Matt Kipper, and Dr. Melissa Reynolds for their assistance and for taking the time to review this dissertation outside of their demanding schedules. Finally I would also like to thank my colleagues and friends in the BSμηEL for their support in this research.

DEDICATION

This dissertation is dedicated to my family. To my parents, Ron and Debbie, thank you so much for believing that I could achieve whatever goals I set for myself. To my sister and brother, Nicole and Noah, thank you for your constant encouragement.

TABLE OF CONTENTS

INTRODUCTION

The goal of this research was to evaluate the influence of nanowire arrays on the differentiation potential of adipose-derived stem cells into multiple lineages which include osteogenic, chondrogenic and adipogenic phenotypes. In brief, vertically oriented, high-aspect-ratio nanowires were extruded from polycaprolactone (a biodegradable and bioinert polymer) using a solvent-free thermogravimetric technique. Smooth polycaprolactone was used as a control surface and surfaces containing nanowire arrays were used as the treatment group. Previous studies have shown that nanowire surfaces promote osteogenic differentiation of murine mesenchymal stem cells when supplemented with osteogenic media. This study uses human adipose-derived stem cells and observes the behavior of these cells on nanowire surfaces with and without differentiation media to determine potential application for nanowire surfaces as an implantable biomedical device.

This research investigated both the short-term growth potential and long-term differentiation behavior of adipose derived stem cells. Adhesion, proliferation, migration, morphology and viability were studied during the initial 7-day growth period following cell attachment to the surfaces. During the following weeks, differentiation was examined by observing marker protein expression through immunofluorescence and extracellular matrix production using histological staining. The nature of this work has been arranged into five research aims starting with fabrication and characterization of the nanowire scaffolds followed by observing osteogenic, chondrogenic, and adipogenic differentiation with and without the influence of biochemical cues in the media conditions. The fundamental hypothesis is that a biomimetic nanowire architecture may provide a more favorable template stem cell functionality, interaction, and differentiation.

HYPOTHESIS AND SPECIFIC AIMS

Previous research in our lab has shown the ability for various cell types to adhere, proliferate, and maintain functionality on polycaprolactone nanowire surfaces; however we have not investigated the ability of these surfaces to induce differentiation without the use of biochemical cues or supplements from the media. The research presented here attemps to examine how the topography of polymeric nanowire surfaces influences differentiation of adipose derived stem cells (ADSCs). Investigations of the surfaces and cell behavior is guided by the following fundamental hypothesis and five specific aims:

Fundamental Hypothesis: Polycaprolactone (PCL) nanowire surfaces provide an advantageous interface for adipose derived stem cell functionality and differentiation eventually leading to enhanced biomaterial implant integration.

Hypothesis (1): Polycaprolactone (PCL) nanowire arrays engineered to have uniform, vertically oriented, immobilized, high aspect ratio nanoscale surface features with properties will exhibit suitable for cell growth and maintenance.

Specific Aim 1: Fabricate and characterize a highly oriented, vertical array of immobilized PCL nanowire arrays and characterize their bulk and surface properties. This research is discussed in Chapter 2.

(a) Fabricate highly reproducible PCL nanowire arrays using a solvent free nanotemplating process.

(b) Evaluate the bulk mechanical and thermal characteristics of PCL.

(c) Evaluate the surface characteristics of PCL nanowire arrays.

Hypothesis (2): PCL nanowire arrays provide a favorable template for osteoblast differentiation of ADSCs when cultured under osteogenic conditions.

Specific Aim 2: Determine the effect of PCL nanowrie surfaces on ADSC differentiation into osteoblasts using osteogenic differentiation media. This research is discussed in Chapter 3.

(a) Evaluate the effect of micro/nano structured surface topography on ADSC adhesion, proliferation viablility, and morphology.

(b) Measure the influence of micro/nano-topography on ADSC osteogenic differentiation by immunofluorescence of the osteogenic marker proteins osteocalcin and osteopontin

(c) Measure extracellular matrix production through histological staining and quantification of alkaline phosphatase activity

Hypothesis (3): PCL nanowire arrays provide a favorable template for osteoblast differentiation of ADSCs when cultured under chondrogenic conditions.

Specific Aim 3: Determine the effect of PCL nanowrie surfaces on ADSC differentiation into chondrocytes using chondrogenic differentiation media. This research is discussed in Chapter 4.

(a) Evaluate the effect of micro/nano structured surface topography on ADSC adhesion, proliferation viablility, and morphology.

(b) Measure the influence of micro/nano-topography on ADSC chondrogenic differentiation by immunofluorescence of chondrogenic marker proteins sox9 and collagen 2.

(c) Measure extracellular matrix production through histological staining and quantification of sulfated glycosaminoglycan (GAG) formation

Hypothesis (4): PCL nanowire arrays provide a favorable template for adipocyte differentiation of ADSCs when cultured under adipogenic conditions.

Specific Aim 4: Determine the effect of PCL nanowrie surfaces on ADSC differentiation into adipocytes using adipogenic differentiation and maintenance media. This research is discussed in Chapter 5.

(a) Evaluate the effect of micro/nano structured surface topography on ADSC adhesion, proliferation viablility, and morphology.

(b) Measure the influence of micro/nano-topography on ADSC adipogenic differentiation by immunofluorescence of adipogenic marker proteins PPARγ and adiponectin.

(c) Measure extracellular matrix production through histological staining and quantification of lipid accumulation

Hypothesis (5): PCL nanowire arrays provide a favorable template for ADSC differentiation potential into one or more of the following cell phenotypes: osteoblasts, chondrocytes, or adipocytes using only ADSC growth media without the presence of differentiation supplements.

Specific Aim 5: Determine the effect of PCL nanowire arrays on osteogenic, chondrogenic, and adipogenic ADSC differentiation without the use of differentiation media and determine if the

surface nanotopgraphy alone has a significant effect on differentiation. This research is discussed in Chapter 6.

(a) Evaluate the effect of micro/nano structured surface morphology on ADSC adhesion and proliferation.

(b) Measure the influence of micro/nano-topography on ADSC osteogenic differentiation by immunofluorescence, measure extracellular matrix production using histological staining of calcium phosphate, and quantify alkaline phosphatase activity.

(c) Measure the influence of micro/nano-topography on ADSC chondrogenic differentiation by immunofluorescence, measure extracellular matrix production, and quantify sulfated glycosaminoglycan (GAG) formation.

(d) Measure the influence of micro/nano-topography on ADSC adipogenic differentiation by immunofluorescence, measure extracellular matrix production, and quantify lipid accumulation.

CHAPTER 1

INTRODUCTION AND LITERATURE REVIEW

1.1 The role of biomaterials in tissue engineering

One of the most commonly used definitions of the word biomaterial is "a nonviable material used in a medical device, intended to interact with biological systems" [1]. However biomaterials have a wide range of applications where synthetic and natural materials interface with biology [1]. The first main objectives of tissue repair and biomaterials have roots in ancient times with early evidence dating back at least 2,500 years. The Etruscan civilization learned to replace missing teeth with bridges made from the bones of oxen and Chinese literature has records of the first dental amalgam for reparation of decayed teeth [2]. As biological science developed in the 20th century, more sophisticated biomaterials began emerging that have the ability to interact with cells to influence a particular biological response, unlike traditional bioinert materials [3]. In order for biomaterials to have successful interaction they must be capable of supporting the structure and maintaining the function of the tissue by bonding with transplanted or host cells [4]. In addition, the biomaterials must ideally be biocompatible, promote cellular and tissue development, and possess the proper mechanical properties [4].

The nature and definition of biomaterials has changed considerably in the past 50 years. The goal of first generation biomaterial design was to match the mechanical and physical properties of the bioinert material to the host tissue with minimal toxic effect or damage [5, 6]. As the field began shifting to the design of second generation biomaterials, the emphasis shifted to the addition of bioactive components that would stimulate a controlled reaction or physiological response [5, 7]. In addition, as second generation biomaterial design advanced,

scientists began developing resorbable and degradable biomaterials, which exhibit a controlled chemical breakdown over time to allow the host tissue to take over during the regeneration process [8]. To avoid risk of inflammatory or foreign body reactions, the degradation products must be removed from the body via metabolic pathways at concentrations that are tolerable for the contact tissue and the rest of the body [9]. So the combination of first and second generation biomaterials has proven capabilities to support the healing site, be bioactive, and also have biodegradable properties [8]. Third generation biomaterials are also now currently moving in the direction to stimulate specific cellular responses at the molecular level [5, 10].

One of the core challenges of third generation tissue engineering is combining a biomaterial scaffold with live, functional cells [11]. The classic model relies on a combination of biomaterial scaffolds, cells, and bioactive molecules working together to integrate successfully with the host tissue and begin the process of regeneration [12, 13]. The desire is for cells on the biomaterial to have system-specific response whether that be the secretion of extracellular matrix, the interaction of cells with each other, biosynthesis of proteins, or differentiated metabolic activities [11]. In essence, the tissue engineering process can basically be defined by three steps involving the isolation of cells, biomaterial impregnation or seeding, and maturation of the cell-biomaterial construct as the material slowly biodegrades [14-16]. Ultimately, the fundamental hypothesis is that if these three steps are met, the regeneration of lost or damaged tissue can occur successfully.

1.2 Biodegradable polymeric materials

Prior to entering the new millennium, the standard of biomaterials saw a major shift from biostable materials to biodegradable materials for tissue engineering applications [17, 18]. In

order for a biodegradable biomaterial to be successful, it must possess the following properties: the material should not induce a sustained inflammatory/toxic response, it should have an acceptable shelf life, it should have a degradation time that matches the regeneration rate of the tissue, it should have appropriate mechanical properties, the degradation products should be non-toxic and cleared through metabolic pathways, and the material should be easily processed and sterilized [19-21]. Biodegradable polymers can be broadly classified into two different groups: biologically derived (or natural) polymers and synthetic polymers [21, 22]. Both natural and synthetic polymer biomaterials undergo biodegradation by either cleavage of hydrolytically or enzymatically sensitive bonds that are present in the backbone with most natural polymers degrading by the latter mode [23].

Natural polymers are the first biodegradable biomaterials to be used clinically, and they are generally non-toxic, even at high concentrations [21, 24]. Additionally, they are bioactive by readily presenting receptor-binding ligands and an inherent ability to degrade and remodel via cell-secreted enzymes [21, 24, 25]. Examples of natural biopolymers include proteins (collagen, elastin, fibrin), polynucleotides (DNA, RNA), and polysaccharides (hyaluronic acid, chitosan, chondroitin sulfate) [21]. Tissue engineering and regenerative medicine have benefited from natural polymers. They are well established clinically as therapeutic biomaterials and are models for various engineering principles [25]. Synthetic polymer biomaterials, on the other hand, possess many qualities that are unique from natural polymers. Synthetic polymers are generally biologically inert and uniform from one batch to the next. Furthermore, their mechanical properties can be tailored for specific biomedical applications [21, 26]. The use of synthetic polymers has grown tremendously over the years and have become very attractive materials for various medical applications such as sutures, wound dressings, drug delivery devices, orthopedic

fixation devices, vascular grafts, and stents [23, 27]. Although there are several hydrolytically synthetic degradable polymers used as biomaterials, polyesters remain among the most widely used having been adopted in surgery for 40 years for sutures and bone fixation devices [28, 29]. Degradable aliphatic polyesters are derived from three different monomers: lactide, glycolide, and caprolactone and are very common in clinical use [28, 30, 31]. One example of a successful clinical product that uses aliphatic polyesters is Dermagraft™ which is a human fibroblast derived dermal substitute [32]. When synthetic polymers were introduced in the early days of tissue engineering, degradable polyesters based on lactide and glycolide monomers were among the first materials used for scaffold construction [32]. However, polycaprolactone is an aliphatic polyester that has attracted increasing interest in the tissue engineering community over the past 10-15 years [33].

1.3 Polycaprolactone as a suitable biomaterial

Polycaprolactone (PCL) is semicrystalline and a biocompatible polyester that is derived from the monomeric unit 'ε-caprolactone' [21]. Since it belongs to the polyester family, it is biodegradable, however, the rate of degradation is very slow [34] in comparison with other polyesters such as polyglycolic acid (PGA) and polylactic acid (PLA) [35] Similar to other synthetic polymers, PCL undergoes hydrolytic degradation due to the presence of hydrolytically labile aliphatic ester linkages, and its readily-metabolized degradation products add to its appeal in biological applications [21, 36]. The biodegradation rate of a thick piece of PCL material is on the order of 2-3 years in the absence of enzymes [37] and surface erosion typically occurs from the bulk PCL material during hydrolysis degradation [38].

PCL is highly processible as it is soluble in a wide range of organic solvents. It has a low melting point (approx. +60 °C) and glass transition temperature (approx. −60 °C) while having the ability to form miscible blends with a wide range of polymers [35]. Its slow degradation rate, high permeability to drugs, and non-toxicity has made PCL a viable candidate material as a long-term drug/vaccine delivery vehicle [22]. The long-term contraceptive device Capronor®, is composed of PCL and has been developed for the long-term, zero-order release of the prescription drug levonorgestrel [22]. Extensive research is ongoing to develop various micro- and nano-sized drug delivery vehicles based on PCL [33]. Due to its excellent biocompatibility, PCL has also been extensively investigated as scaffolds for tissue engineering. A recent study demonstrated the feasibility of using a composite matrix composed of PCL and hyaluronic acid as a potential meniscus substitute [39]. Composites of PCL with calcium phosphate-based ceramics such as hydroxyapatite are also currently being investigated as suitable scaffolds for bone tissue engineering [40].

To increase the degradation rate of PCL, several co-polymeric systems containing PCL have been investigated including co-polymers with other polyesters. Co-polymer systems of ε-caprolactone with DL-lactide have yielded materials with more rapid degradation rates [21]. Similarly, a co-polymer of ε-caprolactone and glycolide resulted in fibers that were less stiff compared to those made of polyglycolide, and this composite polymer is currently on the market as a monofilament suture (MONACRYL®) [21]. A few examples of potential substrate applications include controlled drug delivery systems [41], tissue-engineered skin [42] axonal regeneration [43], and scaffolds for supporting fibroblasts and osteoblasts growth [44] (**Figure 1.1**). In addition, PCL has resulted in US-FDA approval of a number of medical devices [45-49].

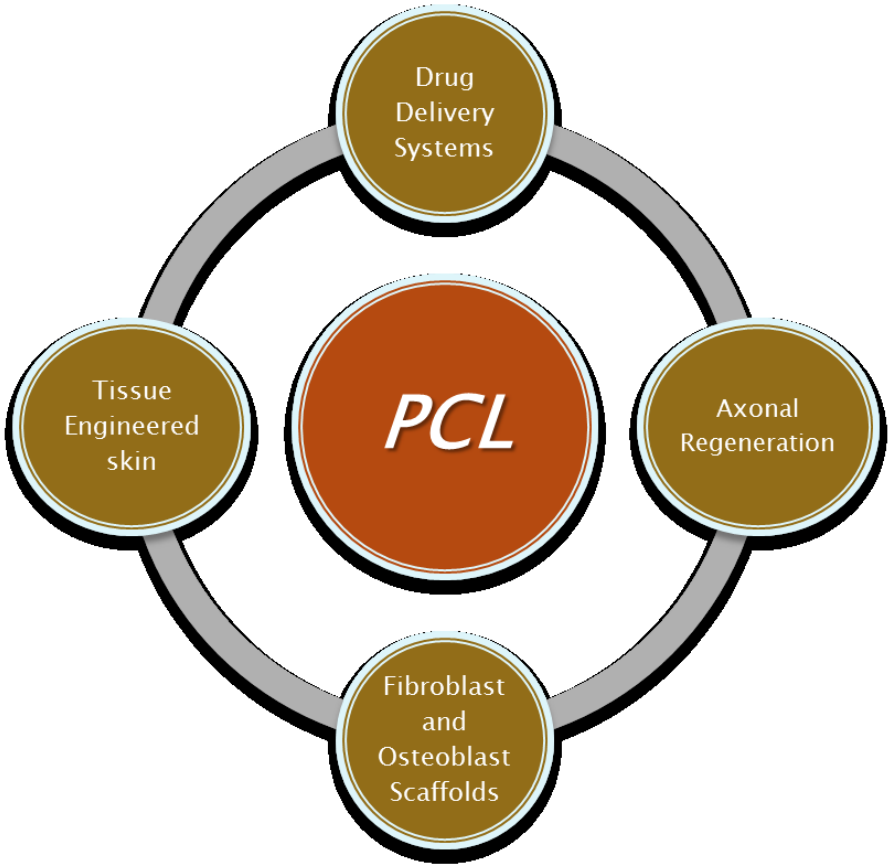

Figure 1.1: Multiple examples of potential tissue engineering applications and biomedical devices for PCL.

1.4 Adipose derived stem cells as an alternative source for stem cell therapies

Tissue engineering and regenerative medicine is an interdisciplinary field that involves biology, medicine, and engineering. Over the years it has evolved in parallel with many recent advances in biotechnology [50]. In addition to fabricating biocompatible artificial scaffolds, tissue engineering scientists are now looking toward stem cell therapies to repair damaged or failing organs in the body [51, 52]. Stem cells are a unique population of cells because they possess three characteristics: self-renewal capacity, long-term viability, and multilineage potential [53, 54]. There are two types of stem cells that exist in the body: somatic stem cells and

embryonic stem cells. The ability of somatic stem cells and embryonic stem cells to differentiate into various cell phenotypes has been studied extensively. Embryonic stem cells are pluripotent cells that have the ability to differentiate into all derivatives of the three germ layers [55-58]. During the first few cell divisions after fertilization they can be thought of as totipotent as they differentiate into all of the extraembryonic tissues [59]. Although they possess great multilineage potential, research associated with embryonic stem cells is accompanied with many ethical, legal, and political concerns in addition to safety and efficacy in the realm of science [52-54]. For this reason the focus has been on using somatic stem cells, also known as adult stem cells, which have multilineage potential, but are considered to be multipotent instead of pluripotent like embryonic stem cells.

Somatic stem cells can be divided into two groups: hematopoietic stem cells and mesenchymal stem cells [60-63]. Hematopoietic stem cells are defined as cells that have the ability to differentiate into a multitude of blood cell lineages as well as produce additional stem cells through their self-renewal capacity [64-66]. Mesenchymal stem cells (MSCs) are a heterogenous population of stem cells and progenitor cells with a capacity to differentiate into numerous mesodermal and non-mesodermal lineages [67] including osteoblasts [68], chondrocytes [69], adipocytes [70], myocytes, [71], and neurons [72] . Both hematopoietic and mesenchymal stem cells can be found within the bone marrow with the stromal cell population loosely referring to non-hematopoietic cells of mesenchymal origin [73]. However due the invasiveness of the procedure to obtain stromal cells from the bone marrow, scientists have begun looking to other tissue sources for multipotent MSCs. Although MSCs are originally derived from the bone marrow, they have also been isolated from other tissues such as the periosteum, synovial membrane, synovial fluid, skeletal muscle, dermis, deciduous teeth,

pericytes, trabecular bone, infrapatellar pad, articular cartilage, and adipose tissue [74, 75]. Approximately 400,000 liposuction surgeries are performed each year in the U.S. and within each procedure, approximately 100ml to >3L of lipoaspriate tissue is removed from the patient and is routinely discarded without repurposing [50]. Adipose tissue is a mesodermally derived organ and contains an abundant population of stromal cells including stem cells [76]. These cells can be enzymatically digested out of the lipoaspirate tissue, separated via centrifugation, and isolated by examining the surface immunophenotype [50, 76]. Adipose derived stem cells (ADSCs) share many of the same characteristic of bone marrow derived MSCs including their self-renewal capacity, proliferative potential, long term viability, and the ability to undergo multilineage differentiation [54, 77] (**Figure 1.2**).

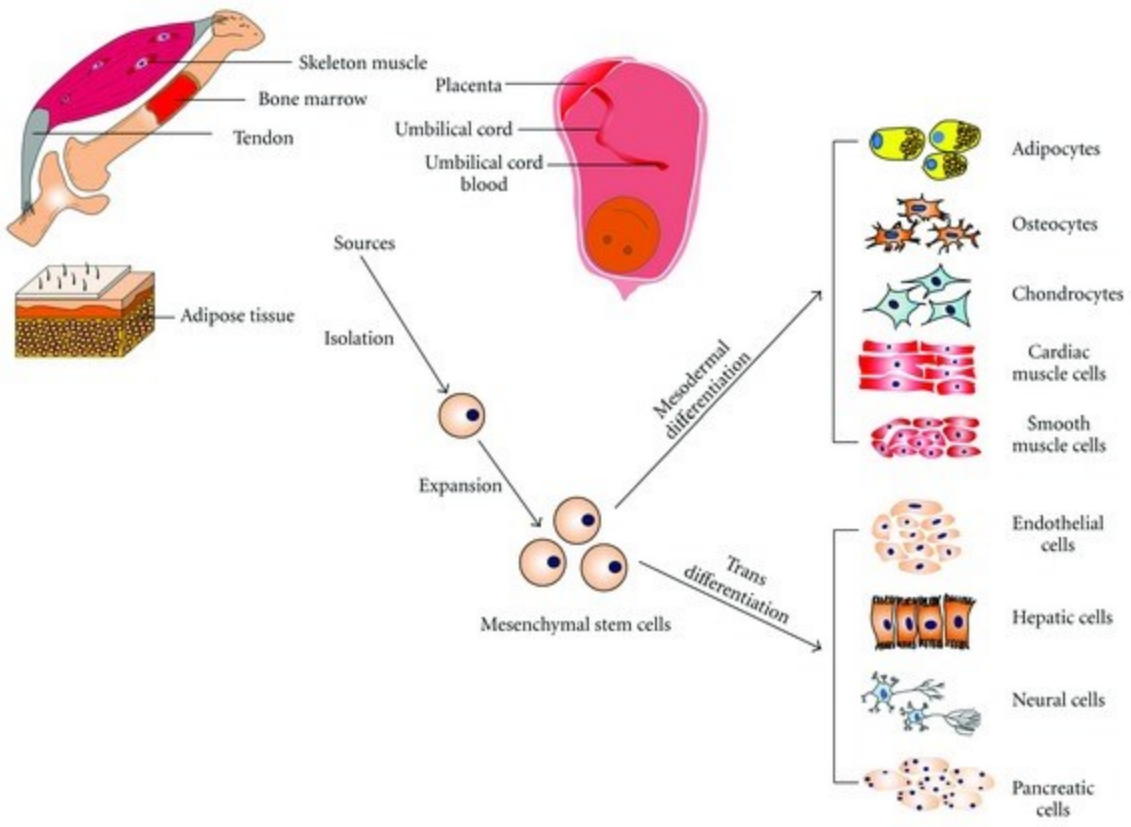

Figure 1.2: Multilineage potential of mesenchymal stem cells isolated from multiple different sources including adipose tissue, bone marrow, tendon, skeletal muscle, placenta, and the umbilical cord components.

Reprinted from [Mechanisms Underlying the Osteo- and Adipo- Differentiation of Human Mesenchymal Stem Cells] Vol. 2012 (2012), Article ID 793823, Copyright 2012, licensed under Creative Commons, CC BY 3.0.

1.5 Mechanisms that promote osteogenesis, chondrogenesis, and adipogenesis in vitro

Multipotent stem cells such as MSCs or ADSCs express various genetic markers that link to multiple cell lineages. The presence of specific markers helps to keep the cells in an undifferentiated state through negative feedback processes [78, 79]. Typically *in vitro*,

osteogenesis, chondrogenesis, or adipogenesis of stem cells is induced using added supplements in the medium in addition to other stimulations such as mechanical forces or topographical cues [80]. These supplements stimulate the expression of various transcriptions factors and the secretion of numerous matrix proteins from the cell [79]. For osteogenic induction, dexamethasone is a corticosteroid that induces the expression of runt-related transcription factor 2 (Runx2) and other born matrix proteins [81]. Ascorbic acid and β-glycerophosphate are promoters for osteoblastic transformation and therefore induce calcification of the extracellular matrix [82]. As stem cells secure their commitment and differentiation toward osteogenic cell lines, osteogenesis is regulated by Runx 2 via signaling pathways such as transforming growth factor-beta 1 (TGF-β1) and bone morphogenic protein 2 (BMP2) [80, 82, 83] . Regulation of chondrogenic induction is very similar to osteogenensis in that BMPs and TGFβs signaling pathways play important roles in the formation of chondrogenic progenitors [84]. Many recent studies have shown that specific TGF-β family members are responsible for intracellular signaling cascades that promote the expression of cartilage-specific genes [85]. The inclusion of TGF-β1 treatment *in vitro* induces MSC condensation and initiates the formation of chondrogenic progenitor cells [86]. Finally, dexamethasone, insulin, and PPARγ agonist are three key factors for induction of adipogenic differentiation *in vitro* using biochemical cues. As stated previously, dexamethasone is a synthetic glucocorticoid that acts as a powerful differentiation stimulant, and the presence of dexamethasone in the basal medium is critical for *in vitro* differentiation of MSCs into many different phenotypes [87]. Both insulin and PPARγ are very important activators of adipogensis and are responsible for regulating the differentiation process while repressing osteogenic factors [79, 80, 88]. Not only are insulin and PPARγ agonist

important for triggering the MSCs to differentiate from preadipocytes to early adipocytes, they are also responsible for maintaining the cells in a differentiated state [80].

1.6 The cell-extracellular matrix interface

The extracellular matrix (ECM) is composed of many distinct groups of molecules with very different evolutionary origins. These ECM molecules include glycosaminoglycans and proteoglycans as well as collagens and non-collagenous glycoproteins that are secreted by cells [89-91]. Originally the ECM was thought to serve only as a structural support system for tissues and cells, however, there has been a great deal of progress in understanding how the cell-ECM interactions influence cell behavior and development of tissues [90]. ECM molecules have strong interactions with receptors on the cell surface which transmit signals through the cell membrane and into the cytoplasm where a signal cascade of events is sent through the cytoskeleton to the nucleus [92]. In turn, those signals result in expression of specific genes that have a direct effect back onto the ECM [92]. The complexity of the cell-ECM interaction can produce many cellular responses leading to migration, growth, proliferation, differentiation, matrix remodeling, morphogenic signaling, homeostasis, and even pathological signals such as tumorogensis, if the conditions facilitate such behavior [93, 94]. Integrins are a group of transmembrance heterodimeric cell surface receptors and are known as the mediators of cell-cell and cell-ECM interactions [95, 96]. In addition to their role as cell adhesion receptors, each individual integrin has the ability to recognize many distinct ECM proteins and to function as signaling receptors [97, 98] (**Figure 1.3**). When an integrin binds to a particular ECM protein ligand, the integrin will transmit signals by organizing the cytoskeleton, which consequently regulate the cell shape and overall internal architecture of the cell [95]. Since integrin cytoplasmic domains interact with

the cytoskeletal components of the cell, it would be likely that the appropriate cytoskeletal organization and shape of the cell would regulate many biological responses [95, 99-103]. Integrins are true receptors of the cells with the capability of inducing biochemical signals within the cell [95]. *In vitro*, the types of cell-matrix adhesions organized by integrins is strongly affected by the material surface which is why it is important to provide cells with surfaces that more closely approximate *in vivo* environments [104].

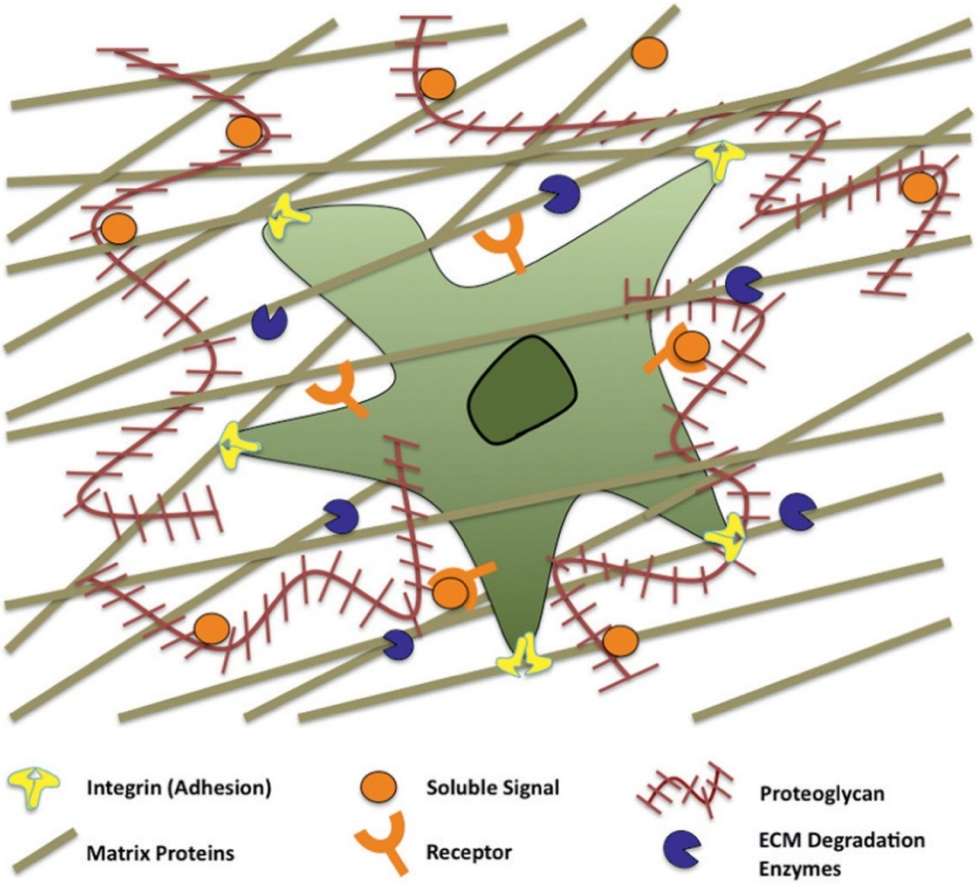

Figure 1.3: Integrins and cell receptors in contact with extracellular matrix molecules

Reprinted from [Engineering ECM signals into biomaterials] Vol. 15 (10), Pages 454-459, Copyright 2012, licensed under Creative Commons, CC BY-NC-ND 3.0

1.7 Mechanotransduction of stem cells through the cytoskeletal network

The conversion of physical force or mechanical stimuli into a biochemical response is known as mechanotransduction and is fundamental to cell physiology and development [105]. Integrins of MSCs are considered to be the direct mechanosensors and physical link between the cytoskeletal proteins of the cell and the binding site of the ECM [106-112]. The natural ECM of cells and tissues is a very complex 3D structural network of fibers, proteins, and small molecules that provides various biochemical and physical cues [113]. Geometric sensing is defined as the development of various signaling processes induced by the geometrical shape of the substrate and the spacing of different molecular adhesion sites [113]. The cytoskeleton protein network is fundamental to the cell and controls many behaviors, movements, and metabolisms of cells [114]. In general, the cytoskeleton of the cell is responsible for the following functions: it enables the cell to move and change shape via synchronized forces, it is responsible for the spatial organization of the cell contents, and it physical and biochemically connects the cells to the extracellular environment [115]. The three main components that make up the cytoskeletal network include microfilaments, microtubules, and intermediate filaments. Actin filaments are globular proteins that form a parallel double helix to form microfilaments [114, 115]. These microfilaments support the projections of the cell membrane (filopodia and lamellipodia) which are involved in cell sensing and cell migration [114, 116, 117]. Microtubules are composed of tubulin and orient out from the center of the centrosome near the nucleus through the cell cytoplasm. Similar to microfilaments, microtubules help control cell shape and movement. In addition they provide a system of travel and transport for membrane bound organelles [114, 115, 118]. Finally, intermediate filaments consist of a family of cytoplasmic protein fibers that are constructed as woven rope arrays around the cell nucleus out to the cell boundary. Cytoplasmic

fibers are divided into many types, but in brief, together they are responsible for maintaining the tensional integrity of the cell [114, 115]. The cytoskeleton can be viewed as an interconnected network of actin, intermediate filaments, and microtubules combined [119-121]. The internal pressure within a cell is controlled by osmotic processes. The transduction of mechanical signals to the nucleus through the cytoskeleton network and balanced by osmotic pressures is known as percolation (**Figure 1.4**). It is proposed that the ordered network can be thought of as a "spider web" where the signals from focal adhesions on the cell membrane can travel through multiple pathways if there are enough cytoskeletal fibers in connection. If there are more connections within the cytoskeleton, then the signal can propogate faster which can result is quicker biochemical response [114, 122]. There are many ways mechanotransduction can have an effect on stem cell behavior, however, within the scope of this research, geometry and mechanosensing of integrins coupled with percolation of the cytoskeletal network are assumed to play the one of the primary roles.

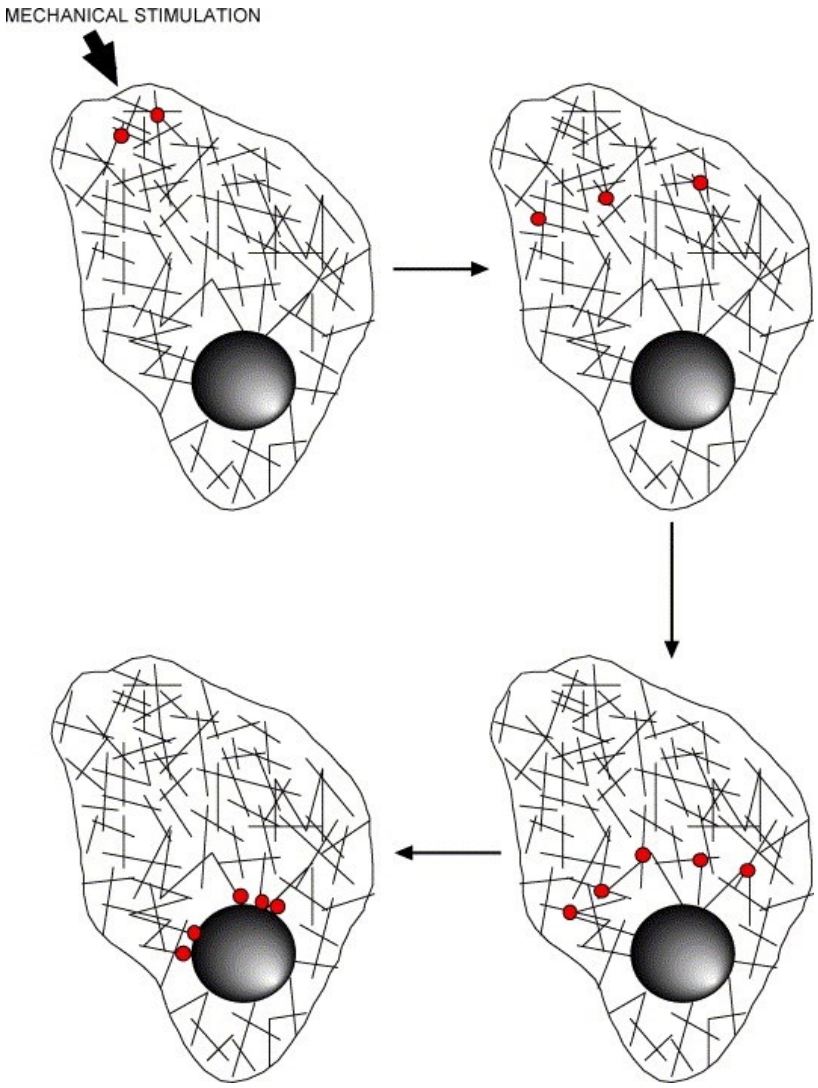

Figure 1.4: Percolation of signal transduction through the cytoskeletal network following mechanical stimulation

Reprinted from Topgraphically induced direct cell mechanotransduction, Vol. 27, Issue 9, Matthew J. Dalby, Pages 730-742, Copyright (2005), with permission from Elsevier.

1.8 The influence of micro- and nanotopography on stem cell behavior and differentiation

Even though mechanical properties at the macroscale level play a large role in the direction of stem cell fate, many tissues have similar elasticities and stiffnesses. It is believed

that the topographical patterns of the ECM on the micro and nano-scales could also be a powerful regulator of stem cell differentiation [123, 124]. A combination of the mechanical, chemical, and physical properties including size, shape, and surface texturization can regulate biological responses and provide mechanical stimuli to stem cells [125].

When designing biomaterials for modulation and control of stem cell environments, it is important to design the substrate to have properties that mimic the hierarchical structure of the native tissue [126]. Although there are extensive 3D topographical structures of cell microenvironments in vivo, most in vitro studies for cell culture have been done on 2D flat rigid substrates that do not mimic the complexity of the ECM in natural tissues [113, 127]. It has been shown that cells will encounter many topographical features that range from protein folding to collagen banding *in vivo*, and there is a strong relationship between the cell and the various nanoscale features *in vivo* [124]. Many studies have shown that both micrometer and nanometer scale features of a biomaterial surface can significantly influence the behavior of stem cells in terms of adhesion, proliferation, morphology, migration, and ultimately differentiation [128-135]. A study in asymmetrical micropatterning has shown that feature size can regulate whether MSCs commit to differentiating into osteogenic or adipogenic lineages [113, 136]. Changes in nanotopography can affect cells by introducing changes in the number, size and arrangement of focal adhesions; redistribution of the cytoskeletal network with the nucleus; and altered cell morphologies [137, 138]. Vogel and Sheetz also consider that geometric form sensing of the cell can be affected by nanoscale surface features such as nanopost, nanofibers, nanogrooves, and nanopits. Concave and convex curvature on the nanoscale level may have an effect on protein release or the opening of transmembrane ion channels [113]. Not only do microscale and nanoscale features initiate immediate responses from MSCs, mechanosensing can also produce

intracellular and extracellular events and cause the cell to monitor its environment over time ,which can lead to matrix and tissue remodeling as the cells differentiate over time into various phenotypes [113, 139] (**Figure 1.5**).

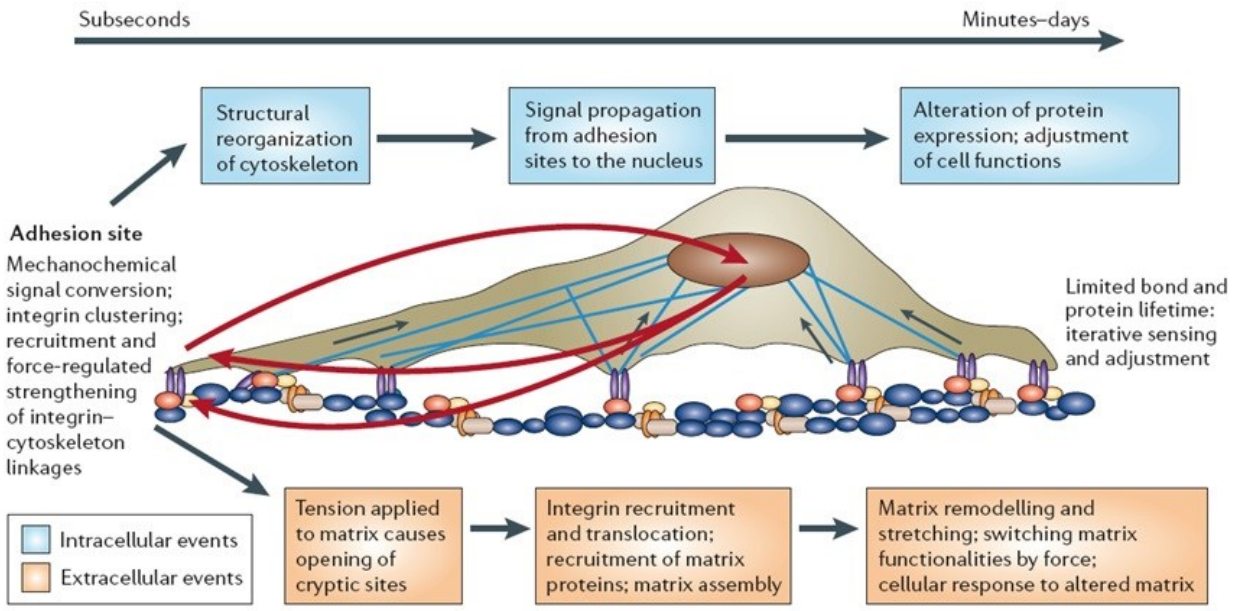

Figure 1.5: Intracellular and extracellular events of mechanotransduction, alteration of protein expression, and matrix remodeling following initial adhesion of a cell to the ECM.

Reprinted by permission from Macmillan Publishers Ltd: [Nature Reviews Molecular Cell Biology] (Vogel, V. and M. Sheetz, Local force and geometry sensing regulate cell functions. Nat Rev Mol Cell Biol, 2006. 7(4): p. 265-75) Copyright (2006).

When designing biomaterials for bone tissue applications, nanoscale topographies have also been shown to modulate cell behaviors on both metallic [124, 140, 141] and polymeric implant materials [142-144]. ADSCs and osteoblast functionality is heavily regulated by surface nano- and micro-topography *in vitro,* which is not surprising considering the hierarchy,

mechanical properties, and function of bone. It is suggested that nanotopography may result in improved cellular adhesion that in turn may help to increase the matrix deposition. Bone architecture has a unique structure and the hierarchy of the tissue is organized into various levels that affect adhesion [145]. Starting at the macrostructure (cancellous and cortical bone), the tissue can be broken down into osteons with Haverisan systems (~10-500um), Lamella (~3-7um), collagen fiber assemblies with individual fibrils (~0.5um), and sub-nanostructures such as bone mineral crystals and proteins (~1nm) [145]. Hydroxyapatite is the primary inorganic component of the bone matrix that resides in the gaps between type I collagen fibrils of Haversian bone [146]. Calcium phosphate crystallites such as hydroxyapatite in the bone substructure are typically nanoscale components [147-149].

Nanoscale synthetic materials are also important to consider when designing for cartilage tissue applications because the unique nanostructure of cartilage is rarely duplicated. Similar to osteoblast interaction with surrounding surfaces *in vitro*, chondrocyte functionality is also heavily regulated by nanotopography *in vitro* since the cells are naturally accustomed to interacting with a well-organized nanostructured collagen matrix [150]. The unique microarchitecture of extracellular cartilage matrix facilitates the load transfer and provides resistance to tensile, compressive, and shear stresses. Unlike other tissues, 85% of hyaline cartilage tissue consists of extracellular matrix materials and only 15% is chondrocytes [151]. The extracellular matrix overtakes the biomechanical function of the cartilage and the small number of cells are only responsible for its preservation and regeneration [151]. The most common nanostructured materials developed for chondrogenic tissue engineering applications are nanofiber scaffolds formed from polycaprolactone (PCL). These PCL scaffolds demonstrated higher in vitro expression of chondrogenic markers and had higher histological scores in

comparison with commercially available collagen scaffolds typically used for cartilage repair [152]. Examples of electrospun nanofibers scaffolds in chondrogenic applications include the use of synthetic polyesters such as polycaprolactone and poly (lactic-co-glycolic acid) for differentiations of MSCs to chondrocytes [153] as well as nanoporous structures created within the polycaprolactone nanofiber scaffolds by phase separation [152].

Finally, nanostructural features that govern adipogenic differentiation and maintenance include extracellular matrix proteins and cytoskeleton proteins [154]. Many of these proteins have a unique nanotopography in the extracellular matrix, and the design of a biomimetic scaffold for induction of adipogenesis should also contain these types of structures *in vitro*. Previous studies have demonstrated that adipogenic differentiation can be upregulated to a certain extent by changing the geometry of the scaffold to features such as nanogrooves [155]. Cells seeded on nanogroove surfaces penetrated into the grooves with the actin cytoskeleton being more aligned along the grooves, suggesting that cell-to-surface interactions as characterized by contact guidance are closely related to the adipogenesis [155]. In addition, studies have shown that tailored electroactive nanorods and hydrophobic nanopillars have been successful in not only differentiating MSCs into adipocytes, but actually increasing the rate of differentiation in comparison with flat surfaces [156, 157].

REFERENCES

1. Ratner, B.D. and S.J. Bryant, *Biomaterials: Where we have been and where we are going.* Annual Review of Biomedical Engineering, 2004. **6**: p. 41-75.
2. Eisenbarth, E., *Biomaterials for tissue engineering.* Advanced Engineering Materials, 2007. **9**(12): p. 1051-1060.
3. Rokusek, D., et al., *Interaction of human osteoblasts with bioinert and bioactive ceramic substrates.* J Biomed Mater Res A, 2005. **75**(3): p. 588-94.
4. Kim, B.S., C.E. Baez, and A. Atala, *Biomaterials for tissue engineering.* World J Urol, 2000. **18**(1): p. 2-9.
5. Hench, L.L. and J.M. Polak, *Third-generation biomedical materials.* Science, 2002. **295**(5557): p. 1014-+.
6. Keane, T.J. and S.F. Badylak, *Biomaterials for tissue engineering applications.* Seminars in Pediatric Surgery, (0).
7. Hench, L.L. and J. Wilson, *Surface-active biomaterials.* Science, 1984. **226**(4675): p. 630-6.
8. Hench, L.L. and J.M. Polak, *Third-generation biomedical materials.* Science, 2002. **295**(5557): p. 1014-7.
9. Bergsma, J.E., et al., *Biocompatibility and degradation mechanisms of predegraded and non-predegraded poly(lactide) implants: An animal study.* Journal of Materials Science-Materials in Medicine, 1995. **6**(12): p. 715-724.
10. Narayan, R.J., *The next generation of biomaterial development.* Philos Trans A Math Phys Eng Sci, 2010. **368**(1917): p. 1831-7.

11. Nerem, R.M. and A. Sambanis, *Tissue engineering: from biology to biological substitutes.* Tissue Eng, 1995. **1**(1): p. 3-13.

12. Lee, E.J., F.K. Kasper, and A.G. Mikos, *Biomaterials for tissue engineering.* Ann Biomed Eng, 2014. **42**(2): p. 323-37.

13. Langer, R., *Tissue engineering.* Mol Ther, 2000. **1**(1): p. 12-5.

14. Minuth, W.W., R. Strehl, and K. Schumacher, *Tissue engineering : essentials for daily laboratory work*. 2005, Weinheim: Wiley-VCH. xii, 314 p.

15. Vunjak-Novakovic, G., *The fundamentals of tissue engineering: scaffolds and bioreactors.* Novartis Found Symp, 2003. **249**: p. 34-46; discussion 46-51, 170-4, 239-41.

16. Bell, E., *Tissue engineering: a perspective.* J Cell Biochem, 1991. **45**(3): p. 239-41.

17. Shalaby, S.W. and K.J.L. Burg, *Absorbable and biodegradable polymers*. Advances in polymeric biomaterials series. 2004, Boca Raton, FL ; London: CRC Press. 289 p., 8 p. of plates.

18. Piskin, E., *Biodegradable Polymers as Biomaterials.* Journal of Biomaterials Science-Polymer Edition, 1995. **6**(9): p. 775-795.

19. Lloyd, A.W., *Interfacial bioengineering to enhance surface biocompatibility.* Med Device Technol, 2002. **13**(1): p. 18-21.

20. Middleton, J.C. and A.J. Tipton, *Synthetic biodegradable polymers as orthopedic devices.* Biomaterials, 2000. **21**(23): p. 2335-2346.

21. Nair, L.S. and C.T. Laurencin, *Biodegradable polymers as biomaterials.* Progress in Polymer Science, 2007. **32**(8-9): p. 762-798.

22. Nair, L.S. and C.T. Laurencin, *Polymers as biomaterials for tissue engineering and controlled drug delivery.* Tissue Engineering I: Scaffold Systems for Tissue Engineering, 2006. **102**: p. 47-90.

23. Katti, D.S., et al., *Toxicity, biodegradation and elimination of polyanhydrides.* Adv Drug Deliv Rev, 2002. **54**(7): p. 933-61.

24. Dang, J.M. and K.W. Leong, *Natural polymers for gene delivery and tissue engineering.* Adv Drug Deliv Rev, 2006. **58**(4): p. 487-99.

25. Lutolf, M.P. and J.A. Hubbell, *Synthetic biomaterials as instructive extracellular microenvironments for morphogenesis in tissue engineering.* Nature Biotechnology, 2005. **23**(1): p. 47-55.

26. Barrows, T., *Degradable implant materials: A review of synthetic absorbable polymers and their applications.* Clinical Materials, 1986. **1**(4): p. 233-257.

27. Ratner, B.D., et al., *Introduction - Biomaterials Science: An Evolving, Multidisciplinary Endeavor*, in *Biomaterials Science (Third Edition)*, B.D. Ratner, et al., Editors. 2013, Academic Press. p. xxv-xxxix.

28. Griffith, L.G., *Polymeric biomaterials.* Acta Materialia, 2000. **48**(1): p. 263-277.

29. Kulkarni, R.K., et al., *Biodegradable poly(lactic acid) polymers.* J Biomed Mater Res, 1971. **5**(3): p. 169-81.

30. Albertsson, A.C. and O. Ljungquist, *Degradable Polyesters as Biomaterials.* Acta Polymerica, 1988. **39**(1-2): p. 95-104.

31. Seppala, J.V., A.O. Helminen, and H. Korhonen, *Degradable polyesters through chain linking for packaging and biomedical applications.* Macromolecular Bioscience, 2004. **4**(3): p. 208-217.

32. Griffith, L.G., *Emerging design principles in Biomaterials and scaffolds for tissue engineering.* Reparative Medicine: Growing Tissues and Organs, 2002. **961**: p. 83-95.

33. Sinha, V.R., et al., *Poly-epsilon-caprolactone microspheres and nanospheres: an overview.* Int J Pharm, 2004. **278**(1): p. 1-23.

34. Zeng, J., et al., *Biodegradable electrospun fibers for drug delivery.* J Control Release, 2003. **92**(3): p. 227-31.

35. Woodruff, M.A. and D.W. Hutmacher, *The return of a forgotten polymer-Polycaprolactone in the 21st century.* Progress in Polymer Science, 2010. **35**(10): p. 1217-1256.

36. Pulkkinen, M., et al., *Effects of block length on the enzymatic degradation and erosion of oxazoline linked poly-epsilon-caprolactone.* European Journal of Pharmaceutical Sciences, 2007. **31**(2): p. 119-128.

37. Kulkarni, A., et al., *Enzymatic chain scission kinetics of poly(epsilon-caprolactone) monolayers.* Langmuir, 2007. **23**(24): p. 12202-7.

38. von Burkersroda, F., L. Schedl, and A. Gopferich, *Why degradable polymers undergo surface erosion or bulk erosion.* Biomaterials, 2002. **23**(21): p. 4221-31.

39. Chiari, C., et al., *A tissue engineering approach to meniscus regeneration in a sheep model.* Osteoarthritis and Cartilage, 2006. **14**(10): p. 1056-1065.

40. Lu, L., et al., *Porogen based solid freeform fabrication of polycaprolactone-calcium phosphate scaffolds for tissue engineering.* Virtual and Rapid Manufacturing, 2008: p. 87-96.

41. Allen, C., et al., *Polycaprolactone-b-poly(ethylene oxide) copolymer micelles as a delivery vehicle for dihydrotestosterone.* Journal of Controlled Release, 2000. **63**(3): p. 275-286.

42. Woei, K., et al., *Evaluation of ultra-thin poly(epsilon-caprolactone) films for tissue-engineered skin.* Tissue Engineering, 2001. **7**(4): p. 441-455.

43. Koshimune, M., et al., *Creating bioabsorbable Schwann cell coated conduits through tissue engineering.* Bio-Medical Materials and Engineering, 2003. **13**(3): p. 223-229.

44. Hutmacher, D.W., et al., *Mechanical properties and cell cultural response of polycaprolactone scaffolds designed and fabricated via fused deposition modeling.* Journal of Biomedical Materials Research, 2001. **55**(2): p. 203-216.

45. Bezwada, R.S., et al., *Monocryl suture, a new ultra-pliable absorbable monofilament suture.* Biomaterials, 1995. **16**(15): p. 1141-8.

46. Cui, W.U., et al., *In situ growth of hydroxyapatite within electrospun poly(DL-lactide) fibers.* Journal of Biomedical Materials Research Part A, 2007. **82A**(4): p. 831-841.

47. Darney, P.D., et al., *Clinical evaluation of the Capronor contraceptive implant: preliminary report.* Am J Obstet Gynecol, 1989. **160**(5 Pt 2): p. 1292-5.

48. Pitt, C.G., et al., *Aliphatic polyesters II. The degradation of poly (DL-lactide), poly (epsilon-caprolactone), and their copolymers in vivo.* Biomaterials, 1981. **2**(4): p. 215-20.

49. Woodward, S.C., et al., *The intracellular degradation of poly(epsilon-caprolactone).* J Biomed Mater Res, 1985. **19**(4): p. 437-44.

50. Gimble, J.M., A.J. Katz, and B.A. Bunnell, *Adipose-derived stem cells for regenerative medicine.* Circ Res, 2007. **100**(9): p. 1249-60.

51. Butler, D.L., S.A. Goldstein, and F. Guilak, *Functional tissue engineering: the role of biomechanics.* J Biomech Eng, 2000. **122**(6): p. 570-5.

52. Gimble, J. and F. Guilak, *Adipose-derived adult stem cells: isolation, characterization, and differentiation potential.* Cytotherapy, 2003. **5**(5): p. 362-9.

53. Rodriguez, A.M., et al., *The human adipose tissue is a source of multipotent stem cells.* Biochimie, 2005. **87**(1): p. 125-128.

54. Zuk, P.A., et al., *Human adipose tissue is a source of multipotent stem cells.* Molecular Biology of the Cell, 2002. **13**(12): p. 4279-4295.

55. Rippon, H.J., et al., *Embryonic stem cells as a source of pulmonary epithelium in vitro and in vivo.* Proc Am Thorac Soc, 2008. **5**(6): p. 717-22.

56. Rippon, H.J., et al., *Derivation of distal lung epithelial progenitors from murine embryonic stem cells using a novel three-step differentiation protocol.* Stem Cells, 2006. **24**(5): p. 1389-98.

57. Rippon, H.J., et al., *Initial observations on the effect of medium composition on the differentiation of murine embryonic stem cells to alveolar type II cells.* Cloning Stem Cells, 2004. **6**(2): p. 49-56.

58. Rippon, H.J. and A.E. Bishop, *Embryonic stem cells.* Cell Prolif, 2004. **37**(1): p. 23-34.

59. Nichols, J., et al., *Formation of pluripotent stem cells in the mammalian embryo depends on the POU transcription factor Oct4.* Cell, 1998. **95**(3): p. 379-91.

60. Bianco, P. and P.G. Robey, *Stem cells in tissue engineering.* Nature, 2001. **414**(6859): p. 118-21.

61. Bianco, P., et al., *Bone marrow stromal stem cells: nature, biology, and potential applications.* Stem Cells, 2001. **19**(3): p. 180-92.

62. Caplan, A.I., *The mesengenic process.* Clin Plast Surg, 1994. **21**(3): p. 429-35.

63. Weissman, I.L., D.J. Anderson, and F. Gage, *Stem and progenitor cells: origins, phenotypes, lineage commitments, and transdifferentiations.* Annu Rev Cell Dev Biol, 2001. **17**: p. 387-403.

64. Keller, G., *Hematopoietic stem cells.* Curr Opin Immunol, 1992. **4**(2): p. 133-9.

65. Smith, C. and B. Storms, *Hematopoietic stem cells.* Clin Orthop Relat Res, 2000(379 Suppl): p. S91-7.

66. Goodell, M.A., et al., *Isolation and functional properties of murine hematopoietic stem cells that are replicating in vivo.* Journal of Experimental Medicine, 1996. **183**(4): p. 1797-1806.

67. Liu, Z.J., Y. Zhuge, and O.C. Velazquez, *Trafficking and differentiation of mesenchymal stem cells.* J Cell Biochem, 2009. **106**(6): p. 984-91.

68. Jaiswal, N., et al., *Osteogenic differentiation of purified, culture-expanded human mesenchymal stem cells in vitro.* J Cell Biochem, 1997. **64**(2): p. 295-312.

69. Mackay, A.M., et al., *Chondrogenic differentiation of cultured human mesenchymal stem cells from marrow.* Tissue Engineering, 1998. **4**(4): p. 415-428.

70. Krontiras, P., P. Gatenholm, and D.A. Hagg, *Adipogenic differentiation of stem cells in three-dimensional porous bacterial nanocellulose scaffolds.* J Biomed Mater Res B Appl Biomater, 2014.

71. Westerweel, P.E. and M.C. Verhaar, *Directing myogenic mesenchymal stem cell differentiation.* Circ Res, 2008. **103**(6): p. 560-1.

72. Zhao, L.R., et al., *Human bone marrow stem cells exhibit neural phenotypes and ameliorate neurological deficits after grafting into the ischemic brain of rats.* Experimental Neurology, 2002. **174**(1): p. 11-20.

73. Deans, R.J. and A.B. Moseley, *Mesenchymal stem cells: biology and potential clinical uses.* Exp Hematol, 2000. **28**(8): p. 875-84.

74. Pittenger, M.F., et al., *Multilineage potential of adult human mesenchymal stem cells.* Science, 1999. **284**(5411): p. 143-7.

75. Lodi, D., T. Iannitti, and B. Palmieri, *Stem cells in clinical practice: applications and warnings.* J Exp Clin Cancer Res, 2011. **30**: p. 9.

76. Strem, B.M., et al., *Multipotential differentiation of adipose tissue-derived stem cells.* Keio J Med, 2005. **54**(3): p. 132-41.

77. De Ugarte, D.A., et al., *Comparison of multi-lineage cells from human adipose tissue and bone marrow.* Cells Tissues Organs, 2003. **174**(3): p. 101-9.

78. Tremain, N., et al., *MicroSAGE analysis of 2,353 expressed genes in a single cell-derived colony of undifferentiated human mesenchymal stem cells reveals mRNAs of multiple cell lineages.* Stem Cells, 2001. **19**(5): p. 408-18.

79. Kolf, C.M., E. Cho, and R.S. Tuan, *Mesenchymal stromal cells. Biology of adult mesenchymal stem cells: regulation of niche, self-renewal and differentiation.* Arthritis Research & Therapy, 2007. **9**(1): p. 204.

80. Zhang, Y., et al., *Mechanisms underlying the osteo- and adipo-differentiation of human mesenchymal stem cells.* ScientificWorldJournal, 2012. **2012**: p. 793823.

81. Igarashi, M., et al., *Inductive effects of dexamethasone on the gene expression of Cbfa1, Osterix and bone matrix proteins during differentiation of cultured primary rat osteoblasts.* Journal of Molecular Histology, 2004. **35**(1): p. 3-10.

82. Gupta, A., et al., *Osteo-maturation of adipose-derived stem cells required the combined action of vitamin D3, beta-glycerophosphate, and ascorbic acid.* Biochem Biophys Res Commun, 2007. **362**(1): p. 17-24.

83. Lee, M.H., et al., *BMP-2-induced Runx2 expression is mediated by Dlx5, and TGF-beta 1 opposes the BMP-2-induced osteoblast differentiation by suppression of Dlx5 expression.* Journal of Biological Chemistry, 2003. **278**(36): p. 34387-34394.

84. Roelen, B.A. and P. Dijke, *Controlling mesenchymal stem cell differentiation by TGFBeta family members.* J Orthop Sci, 2003. **8**(5): p. 740-8.

85. Tuli, R., et al., *Transforming growth factor-beta-mediated chondrogenesis of human mesenchymal progenitor cells involves N-cadherin and mitogen-activated protein kinase and Wnt signaling cross-talk.* J Biol Chem, 2003. **278**(42): p. 41227-36.

86. Wang, W., D. Rigueur, and K.M. Lyons, *TGFbeta signaling in cartilage development and maintenance.* Birth Defects Res C Embryo Today, 2014. **102**(1): p. 37-51.

87. Grigoriadis, A.E., J.N. Heersche, and J.E. Aubin, *Differentiation of muscle, fat, cartilage, and bone from progenitor cells present in a bone-derived clonal cell population: effect of dexamethasone.* J Cell Biol, 1988. **106**(6): p. 2139-51.

88. Klemm, D.J., et al., *Insulin-induced adipocyte differentiation. Activation of CREB rescues adipogenesis from the arrest caused by inhibition of prenylation.* J Biol Chem, 2001. **276**(30): p. 28430-5.

89. Rozario, T. and D.W. DeSimone, *The extracellular matrix in development and morphogenesis: a dynamic view.* Developmental Biology, 2010. **341**(1): p. 126-40.

90. Martins-Green, M. and M.J. Bissell, *Cell-ECM interactions in development.* Seminars in Developmental Biology, 1995. **6**(2): p. 149-159.

91. Hay, E., *Collagen and Embryonic Development*, in *Cell Biology of Extracellular Matrix*, E. Hay, Editor. 1981, Springer US. p. 379-409.

92. Bissell, M.J., H.G. Hall, and G. Parry, *How Does the Extracellular-Matrix Direct Gene-Expression.* Journal of Theoretical Biology, 1982. **99**(1): p. 31-68.

93. Dutta, R.C. and A.K. Dutta, *Comprehension of ECM-cell dynamics: a prerequisite for tissue regeneration.* Biotechnol Adv, 2010. **28**(6): p. 764-9.

94. Hynes, R.O., *Cell adhesion: old and new questions.* Trends Cell Biol, 1999. **9**(12): p. M33-7.

95. Juliano, R.L. and S. Haskill, *Signal transduction from the extracellular matrix.* J Cell Biol, 1993. **120**(3): p. 577-85.

96. Hynes, R.O., *Integrins: versatility, modulation, and signaling in cell adhesion.* Cell, 1992. **69**(1): p. 11-25.

97. Meredith, J.E., B. Fazeli, and M.A. Schwartz, *The Extracellular-Matrix as a Cell-Survival Factor.* Molecular Biology of the Cell, 1993. **4**(9): p. 953-961.

98. Hall, D.E., et al., *The alpha 1/beta 1 and alpha 6/beta 1 integrin heterodimers mediate cell attachment to distinct sites on laminin.* J Cell Biol, 1990. **110**(6): p. 2175-84.

99. Horwitz, A., et al., *Interaction of plasma membrane fibronectin receptor with talin--a transmembrane linkage.* Nature, 1986. **320**(6062): p. 531-3.

100. Otey, C.A., F.M. Pavalko, and K. Burridge, *An Interaction between Alpha-Actinin and the Beta-1 Integrin Subunit Invitro.* Journal of Cell Biology, 1990. **111**(2): p. 721-729.

101. Ben-Ze'ev, A., et al., *Cell-cell and cell-matrix interactions differentially regulate the expression of hepatic and cytoskeletal genes in primary cultures of rat hepatocytes.* Proc Natl Acad Sci U S A, 1988. **85**(7): p. 2161-5.

102. Ingber, D.E., *Control of capillary growth and differentiation by extracellular matrix. Use of a tensegrity (tensional integrity) mechanism for signal processing.* Chest, 1991. **99**(3 Suppl): p. 34S-40S.

103. Ingber, D.E. and J. Folkman, *How Does Extracellular-Matrix Control Capillary Morphogenesis.* Cell, 1989. **58**(5): p. 803-805.

104. Cukierman, E., R. Pankov, and K.M. Yamada, *Cell interactions with three-dimensional matrices.* Curr Opin Cell Biol, 2002. **14**(5): p. 633-9.

105. Orr, A.W., et al., *Mechanisms of mechanotransduction.* Dev Cell, 2006. **10**(1): p. 11-20.

106. Ingber, D., *Mechanical signaling.* Ann N Y Acad Sci, 2002. **961**: p. 162-3.

107. Ingber, D.E., *Integrins, tensegrity, and mechanotransduction.* Gravit Space Biol Bull, 1997. **10**(2): p. 49-55.

108. Ross, T.D., et al., *Integrins in mechanotransduction.* Curr Opin Cell Biol, 2013. **25**(5): p. 613-8.

109. Schwartz, M.A., M.D. Schaller, and M.H. Ginsberg, *Integrins: emerging paradigms of signal transduction.* Annu Rev Cell Dev Biol, 1995. **11**: p. 549-99.

110. Wang, N., J.P. Butler, and D.E. Ingber, *Mechanotransduction across the Cell-Surface and through the Cytoskeleton.* Science, 1993. **260**(5111): p. 1124-1127.

111. Ingber, D.E., *Cellular Tensegrity - Defining New Rules of Biological Design That Govern the Cytoskeleton.* Journal of Cell Science, 1993. **104**: p. 613-627.

112. Stupack, D.G., *The biology of integrins.* Oncology (Williston Park), 2007. **21**(9 Suppl 3): p. 6-12.

113. Vogel, V. and M. Sheetz, *Local force and geometry sensing regulate cell functions.* Nat Rev Mol Cell Biol, 2006. **7**(4): p. 265-75.

114. Dalby, M.J., *Topographically induced direct cell mechanotransduction.* Med Eng Phys, 2005. **27**(9): p. 730-42.

115. Fletcher, D.A. and R.D. Mullins, *Cell mechanics and the cytoskeleton.* Nature, 2010. **463**(7280): p. 485-92.

116. Spooner, B.S., K.M. Yamada, and N.K. Wessells, *Microfilaments and cell locomotion.* J Cell Biol, 1971. **49**(3): p. 595-613.

117. Wessells, N.K., B.S. Spooner, and M.A. Luduena, *Surface movements, microfilaments and cell locomotion.* Ciba Found Symp, 1973. **14**: p. 53-82.

118. Stearns, T., *Molecules of the Cytoskeleton - Amos,La, Amos,Wb.* Science, 1992. **257**(5075): p. 1422-1422.

119. Heuser, J.E. and M.W. Kirschner, *Filament organization revealed in platinum replicas of freeze-dried cytoskeletons.* J Cell Biol, 1980. **86**(1): p. 212-34.

120. Bridgman, P.C. and T.S. Reese, *The structure of cytoplasm in directly frozen cultured cells. I. Filamentous meshworks and the cytoplasmic ground substance.* J Cell Biol, 1984. **99**(5): p. 1655-68.

121. Mitchison, T.J., *Compare and contrast actin filaments and microtubules.* Mol Biol Cell, 1992. **3**(12): p. 1309-15.

122. Forgacs, G., *On the possible role of cytoskeletal filamentous networks in intracellular signaling: an approach based on percolation.* J Cell Sci, 1995. **108 (Pt 6)**: p. 2131-43.

123. Clause, K.C., L.J. Liu, and K. Tobita, *Directed stem cell differentiation: the role of physical forces.* Cell Commun Adhes, 2010. **17**(2): p. 48-54.

124. Dalby, M.J., et al., *The control of human mesenchymal cell differentiation using nanoscale symmetry and disorder.* Nature Materials, 2007. **6**(12): p. 997-1003.

125. Armentano, I., et al., *Biodegradable polymer matrix nanocomposites for tissue engineering: A review.* Polymer Degradation and Stability, 2010. **95**(11): p. 2126-2146.

126. D'Angelo, F., et al., *Mechanotransduction: Tuning Stem Cells Fate.* Journal of Functional Biomaterials, 2011. **2**(2): p. 67-87.

127. Kim, D.H., et al., *Matrix nanotopography as a regulator of cell function.* Journal of Cell Biology, 2012. **197**(3): p. 351-360.

128. Tan, J. and W.M. Saltzman, *Biomaterials with hierarchically defined micro- and nanoscale structure.* Biomaterials, 2004. **25**(17): p. 3593-3601.

129. Ito, Y., *Surface micropatterning to regulate cell functions.* Biomaterials, 1999. **20**(23-24): p. 2333-42.

130. Brunette, D.M. and B. Chehroudi, *The effects of the surface topography of micromachined titanium substrata on cell behavior in vitro and in vivo.* J Biomech Eng, 1999. **121**(1): p. 49-57.

131. Tan, J., H. Shen, and W.M. Saltzman, *Micron-scale positioning of features influences the rate of polymorphonuclear leukocyte migration.* Biophys J, 2001. **81**(5): p. 2569-79.

132. Wilkinson, C.D.W., et al., *The use of materials patterned on a nano- and micro-metric scale in cellular engineering.* Materials Science & Engineering C-Biomimetic and Supramolecular Systems, 2002. **19**(1-2): p. 263-269.

133. Curtis, A. and C. Wilkinson, *Topographical control of cells.* Biomaterials, 1997. **18**(24): p. 1573-83.

134. Rajnicek, A., S. Britland, and C. McCaig, *Contact guidance of CNS neurites on grooved quartz: influence of groove dimensions, neuronal age and cell type.* J Cell Sci, 1997. **110 (Pt 23)**: p. 2905-13.

135. Webster, T.J., et al., *Enhanced functions of osteoblasts on nanophase ceramics.* Biomaterials, 2000. **21**(17): p. 1803-10.

136. McBeath, R., et al., *Cell shape, cytoskeletal tension, and RhoA regulate stem cell lineage commitment.* Developmental Cell, 2004. **6**(4): p. 483-495.

137. Biggs, M.J., et al., *Regulation of implant surface cell adhesion: characterization and quantification of S-phase primary osteoblast adhesions on biomimetic nanoscale substrates.* J Orthop Res, 2007. **25**(2): p. 273-82.

138. Dalby, M.J., et al., *Nanotopographical stimulation of mechanotransduction and changes in interphase centromere positioning.* Journal of Cellular Biochemistry, 2007. **100**(2): p. 326-338.

139. Badylak, S.E., *The extracellular matrix as a scaffold for tissue reconstruction.* Seminars in Cell & Developmental Biology, 2002. **13**(5): p. 377-383.

140. Biggs, M.J.P., et al., *The use of nanoscale topography to modulate the dynamics of adhesion formation in primary osteoblasts and ERK/MAPK signalling in STRO-1+enriched skeletal stem cells.* Biomaterials, 2009. **30**(28): p. 5094-5103.

141. Olivares-Navarrete, R., et al., *Direct and indirect effects of microstructured titanium substrates on the induction of mesenchymal stem cell differentiation towards the osteoblast lineage.* Biomaterials, 2010. **31**(10): p. 2728-2735.

142. Ruckh, T.T., et al., *Osteogenic differentiation of bone marrow stromal cells on poly(epsilon-caprolactone) nanofiber scaffolds.* Acta Biomaterialia, 2010. **6**(8): p. 2949-2959.

143. Bechara, S., L. Wadman, and K.C. Popat, *Electroconductive polymeric nanowire templates facilitates in vitro C17.2 neural stem cell line adhesion, proliferation and differentiation.* Acta Biomaterialia, 2011. **7**(7): p. 2892-2901.

144. Porter, J.R., A. Henson, and K.C. Popat, *Biodegradable poly(epsilon-caprolactone) nanowires for bone tissue engineering applications.* Biomaterials, 2009. **30**(5): p. 780-788.

145. Rho, J.Y., L. Kuhn-Spearing, and P. Zioupos, *Mechanical properties and the hierarchical structure of bone.* Med Eng Phys, 1998. **20**(2): p. 92-102.

146. Palmer, L.C., et al., *Biomimetic Systems for Hydroxyapatite Mineralization Inspired By Bone and Enamel.* Chemical Reviews, 2008. **108**(11): p. 4754-4783.

147. Sato, M. and T.J. Webster, *Nanobiotechnology: implications for the future of nanotechnology in orthopedic applications.* Expert Rev Med Devices, 2004. **1**(1): p. 105-14.

148. Stevens, M.M. and J.H. George, *Exploring and engineering the cell surface interface.* Science, 2005. **310**(5751): p. 1135-8.

149. Taton, T.A., *Nanotechnology. Boning up on biology.* Nature, 2001. **412**(6846): p. 491-2.

150. Burns, K., C. Yao, and T.J. Webster, *Increased chondrocyte adhesion on nanotubular anodized titanium.* Journal of Biomedical Materials Research Part A, 2009. **88A**(3): p. 561-568.

151. Brandt, J., et al., *Nanostructured Materials for Skeletal Repair.* Layered Nanostructures - Polymers with Improved Properties, 2010. **294-I**: p. 109-119.

152. Christensen, B.B., et al., *A novel nano-structured porous polycaprolactone scaffold improves hyaline cartilage repair in a rabbit model compared to a collagen type I/III scaffold: in vitro and in vivo studies.* Knee Surgery Sports Traumatology Arthroscopy, 2012. **20**(6): p. 1192-1204.

153. von der Mark, K., et al., *Nanoscale engineering of biomimetic surfaces: cues from the extracellular matrix.* Cell and Tissue Research, 2010. **339**(1): p. 131-153.

154. Kilian, K.A., et al., *Geometric cues for directing the differentiation of mesenchymal stem cells.* Proc Natl Acad Sci U S A, 2010. **107**(11): p. 4872-7.

155. Kim, M.S., et al., *Effect of nanogroove geometry on adipogenic differentiation.* Nanotechnology, 2011. **22**(49).

156. Luo, W. and M.N. Yousaf, *Tailored electroactive nanorods for biospecific cell adhesion and differentiation.* Chemical Communications, 2009(10): p. 1237-1239.

157. Brammer, K.S., et al., *Hydrophobic nanopillars initiate mesenchymal stem cell aggregation and osteo-differentiation.* Acta Biomater, 2011. **7**(2): p. 683-90.

CHAPTER 2

FABRICATION AND CHARACTERIZATION OF PCL AND HIGH-ASPECT-RATIO NANOWIRE SURFACES

2.1 Introduction

In tissue engineering, cells are often implanted or seeded onto artificial biomaterials known as scaffolds which provide the necessary structure for growth, maintenance, and differentiation of the cells in the early stages of tissue repair. In regard to polymer scaffold materials, polycaprolactone (PCL) has emerged as a promising implant material because it is biodegradable polyester with good mechanical strength and a low degradation rate [1]. PCL is a semi-crystalline, biocompatible, aliphatic polyester that has been frequently utilized for tissue engineering applications over the past 10–15 years [2]. It is a biodegradable polyester by hydrolysis of its ester linkages in physiological conditions and its degradation products are easily bioresorbed or removed naturally in metabolic pathways such as the citric acid cycle [1]. The slow degradation rate of PCL and its non-acidic degradation pathways add to its appeal in biological applications [3, 4]. As a result, it recently has been regarded as a compatible scaffold material for both hard and soft tissues as well as various applications for providing tissues and cells with appropriate medicine [5-11]. A few examples of potential substrate applications include controlled drug delivery systems [12], tissue-engineered skin [13] axonal regeneration [14] and scaffolds for supporting fibroblasts and osteoblasts growth [15]. In addition, it has resulted in US-FDA approval of a number of medical devices [16-20].

One of the reasons it is an advantageous polymer material for this research is because it also has a low melting point between 60-65°C, which can be utilized in various fabrication

methods including the method described here. In this study, we have used a solvent-free gravimetric template synthesis technique for fabricating controlled arrays of high-aspect-ratio, substrate-bound nanowire surfaces from PCL.

2.2 Methods

2.2.1 Fabrication of smooth PCL and nanowire surfaces

A novel template synthesis technique (**Figure 2.1**) was utilized for fabrication of PCL nanowire surfaces. PCL powder with a molecular weight of 50,000 Da sintered for 10 minutes at 115ºC. The sintered powder was allowed to cool to room temperature and smooth PCL (notation: **PCL**) discs (10mm) were punched using a standard aluminum hole punch. A similar method was used to fabricate smooth PCL discs with 1wt% HAp nanoparticles (< 200nm) (notation: **hPCL**) where PCL powder was homogenously mixed with HAp nanoparticles. PCL and hPCL discs were gravimetrically extruded though the pores of inorganic aluminum oxide membranes (ANOPORE^{TM}) with 100nm diameter pore size for 20 min at 70ºC. The alumina membranes were dissolved in 1M NaOH for 75 min followed by profuse rinsing in DI water to release substrate bound nanowire surfaces with (notation: **hNW**) and without HAp (**NW**).

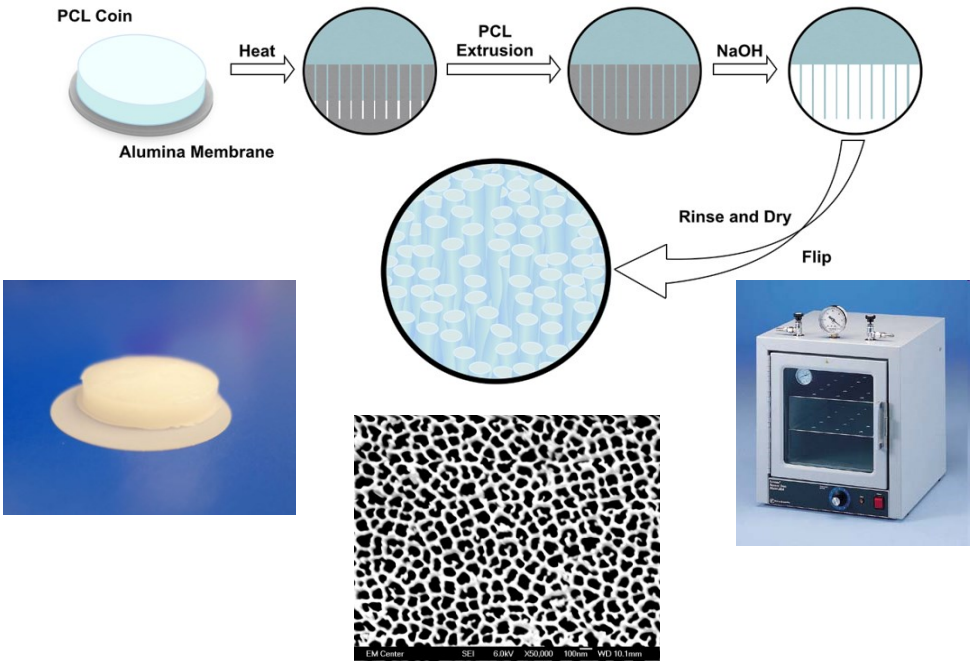

Figure 2.1: Thermogravimetric nanowire extrusion process using bulk PCL using 0.1µm alumina membrane and 1M NaOH

2.2.2 Scanning Electron Microscopy and EDS Analysis

Scanning electron microscopy (SEM) (JEOL JSM-6500F SEM) was used to obtain images of the surface nanotopographies to ensure the absence of alumina and NaOH on NW and hNW surfaces. To confirm the presence of hydroxyapatite nanopowder on hPCL and hNW surfaces, energy dispersive spectroscopy (EDS) was used in conjunction with SEM imaging to determine the concentrations of calcium and phosphorus. First, samples were sputter coated with an ultra-thin film of carbon to create a conductive surface before insertion into the SEM chamber. Carbon was used instead of traditional gold sputter coating because gold is known to

inhibit the detection of phosphorus when using EDS analysis. Images were obtained at 100x magnification and 5 areas on each sample were subjected to EDS acquisition using spectrum processing and spectral imaging on the EDS NSS analyzing software. Quantitative results were given for the calcium and phosphorus peaks.

2.2.3 Thermal characterization and analysis of PCL

Differential scanning calorimetry (DSC) was conducted using TA modulated 2920 DSC, equipped with a subambient accessory to determine the thermal transition of the 50,000 Da powder PCL. In this case, it was utilized to determine the melting temperature of the 50,000 Da powder PCL prior to sample fabrication and nanowire extrusion. PCL samples were placed in the DSC and cooled using liquid nitrogen. Once the samples stabilized at -80°C, the temperature was slowly ramped up to 100°C over the course of 20 min to visualize the heat flow characteristics. In addition thermogravimetic analysis was conducted using a TA TGA 2950 thermogravimetric analyzer to determine the thermal stability and decomposition kinetics. In brief, PCL samples were weighed and placed in the TGA analyzer at room temperature. Starting at room temperature, the TGA slowly increased the temperature to 100°C and recorded the weight percentage until the samples reached 100% degradation.

2.2.4 Contact angle surface tension and wettability

The material wet-ability on all surfaces was evaluated using a static sessile water-drop method. Images were taken immediately following DI water/substrate contact. A contact angle goniometer was used to identify the degree of phase separation, formed between the liquid/solid interface and the liquid/vapor interface. The images were analyzed to evaluate the degree surface

hydrophobicity/ hydrophilicity, where higher angles correlate with a low surface energy and an increased hydrophobicity of the substrate. Material surface wet-ability was therefore evaluated by contact angle measurement to determine the degree of phase separation, immediately following DI water/substrate contact. Higher contact angles (at or above 90 degrees) correlate to a low surface energy and a reduced water-material interaction, indicating hydrophobic surfaces. Lower contact angles (below 90 degrees) correlate to a high surface energy and a high water-material interaction, indicating hydrophilic surfaces.

2.2.5 Uniaxial tensile testing for bulk mechanical properties

Uniaxial tensile testing was performed on flat PCL sheets of approximately 1.6mm thickness. Six samples were culled from separate PCL sheets to account for batch-to-batch variability. Prior to mechanical testing, samples were punched into dogbone shapes with a central width of 3.175mm (ASTM specification #D638-05, Qualitest USA, Plantation, FL). Hydraulic wedge grips (Model 647 MTS Systems Corporation, Eden Prairie, MN) set to 500psi were utilized to clamp each specimen with an exposed gauge length of approximately 4cm. A servo-hydraulic mechanical test system (Bionic Model 370.02 MTS Systems Corporation, Eden Prairie, MN) equipped with a 15kN axial-torsional load transducer (Model 662 20D-04 MTS Systems Corporation, Eden Prairie, MN) was used to test each sample in tension at a strain rate of 1%/s and 5%/s. Samples were speckle coated with India ink and surface images were captured during testing with a CCD camera (Flea3, Point Grey Research, Richmond, BC, Canada) at a rate of 15 frames per second to characterize material yield strength.

To calculate strain, images were analyzed using a Matlab (Mathworks, Natick, MA)-based Digital Image Correlation code (E.M.C. Jones, University of Illinois) to track the

displacement of the speckle pattern in the central region of each dogbone shaped sample. Stress was calculated by dividing the force values by the cross-sectional area of the central region of each sample. Modulus was determined by taking the slope of the linear region (0.01-0.04 strain) of each stress-strain curve, with excellent agreement to the data (r-squared = .98 ± .01). Yield stress and strain values were calculated based on the intersection of a 2% offset line.

2.2.6 Nanoindentation for surface mechanical properties

Indentation at a nanoscale, also known as nanoindentation, was performed using a Nanoindenter XP (MTS) with a Berkovich indenter tip with the area function calibrated using fused silica. A set of nine indentations with six loading/unloading cycles was done on each sample surface. All the indentations were made using 6 loading cycles (0.125, 0.3125, 0.625, 1.25, 2.5 and 5gf) with the maximum load of 50mN (5gf) and the holding time at each load step was 30s. The hardness and elastic modulus profiles were determined by the Oliver & Pharr method [21]. In brief, based on the continuous load-displacement data obtained from a complete cycle of loading and unloading during the nanoindentation test and by using the Oliver & Pharr method, the effective modulus of elasticity was calculated. Hardness is the material resistance against the surface deformation caused by the external load applied. It was calculated by dividing the normal load by the projected area of the surface.

2.3 Results and Discussion

A solvent-free nano-templating technique was utilized to fabricate substrate bound nanowire surfaces from PCL. We have also developed a method to encapsulate HAp nanoparticles within the nanoarchitecture of the nanowire surfaces without the use of any organic solvents that may have cytotoxic effects. NW and hNW surfaces were imaged using SEM to evaluate the surface nanoarchitecture as well as the uniformity (**Figure 2.2**). The images indicate presence of regular "microchannels" on the surface, which may be due to the surface tension interaction during membrane dissolution. A closer examination shows cylindrical shape of the nanowires indicating that NW and hNW surfaces have higher surface area compared to smooth surfaces.

Further, EDS was used to confirm the absence of alumina and NaOH on NW and hNW surfaces, and to confirm the presence of calcium and phosphorus on hNW surfaces. The results indicate that the NaOH dissolved the alumina membranes and the surface only shows the presence of carbon and oxygen peaks indicative of pure PCL (**Figure 2.3a**). Apart from carbon and oxygen peak, the hNW surfaces show the presence of calcium and phosphorus peaks (**Figure 2.3b**). This indicates successful incorporation of HAp nanoparticles in the nanowire architecture.

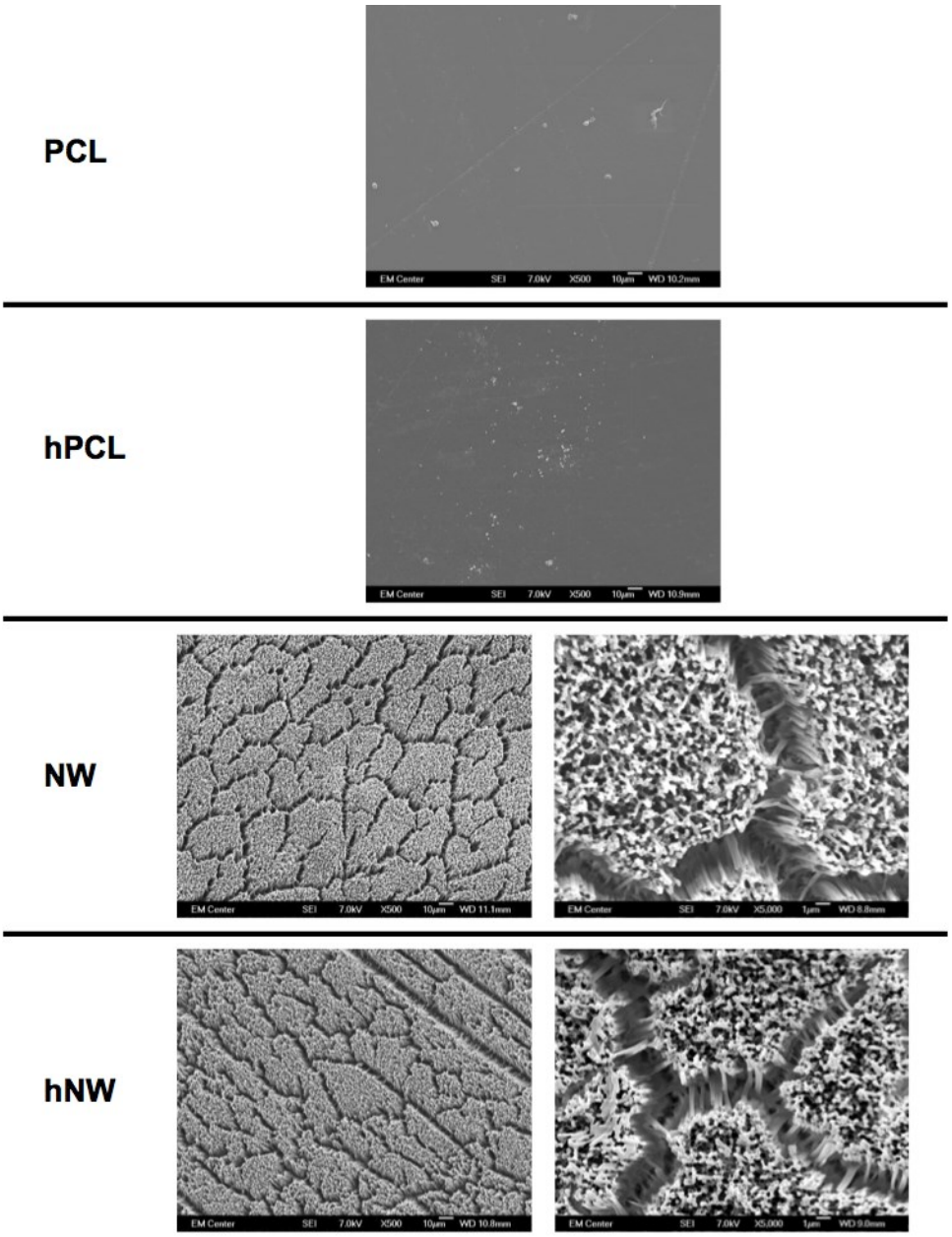

Figure 2.2: Representative SEM images of PCL, hPCL, NW, and hNW surfaces. The high magnification SEM images of NW and hNW show the nanoarchitecture.

Element Line	Weight %	Weight % Error
C K	67.73	+/- 0.40
O K	31.26	+/- 0.38
P K	0.41	+/- 0.02
P L	---	---
Ca K	0.61	+/- 0.03
Ca L	---	---
Total	100.00	

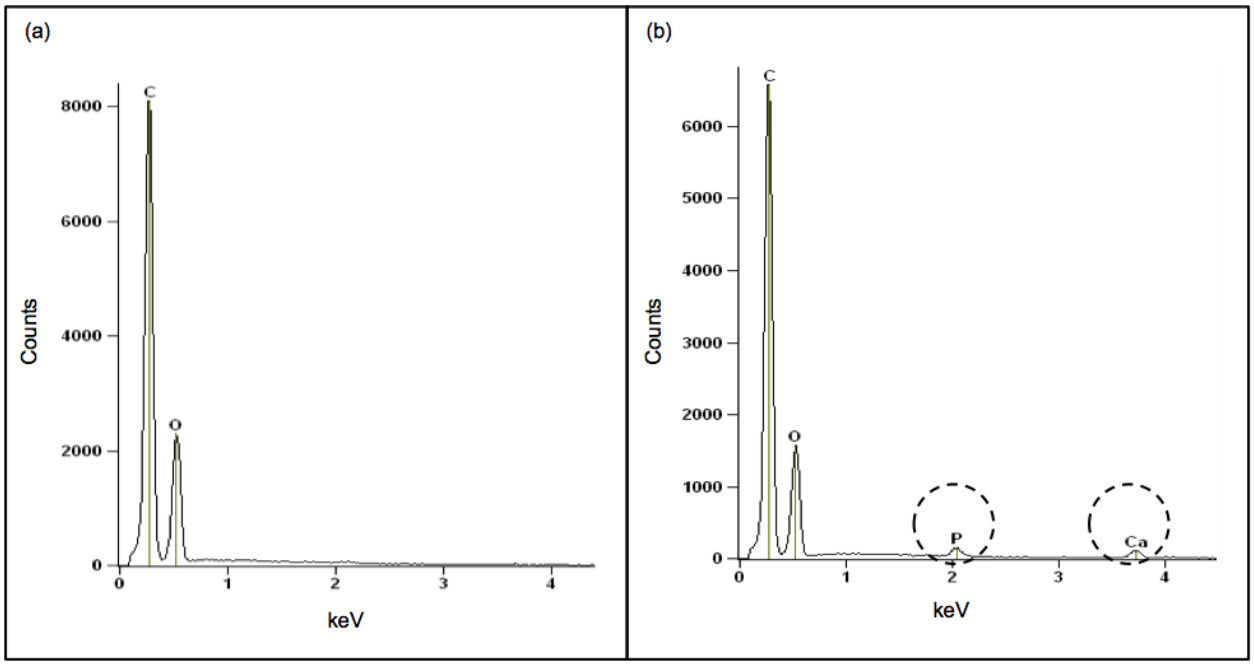

Figure 2.3: Energy dispersive spectroscopy (EDS) scans for (a) NW surfaces and (b) hNW surfaces. The presence of calcium (Ca) and phosphorus (P) in (b) indicates the presence of HAp nanoparticles on the surface.

Results of DSC determined that the melting temperature 50,000 Da polycaprolactone powder was 61.12°C. To ensure that there would be adequate extrusion of the polymer through the aluminum oxide membrane during nanowire fabrication, the polymer was thermally extruded slightly above the melting temperature at 70°C when the formation of a clear melt interface was present between the bulk material and the membrane. Results of the TGA determine that as the temperature was ramped to 500°C, the weight percent of PCL began to drop quickly between 375°C and 425°C. At 491°C, the weight percent of PCL left in the instrument was 0.09885%.

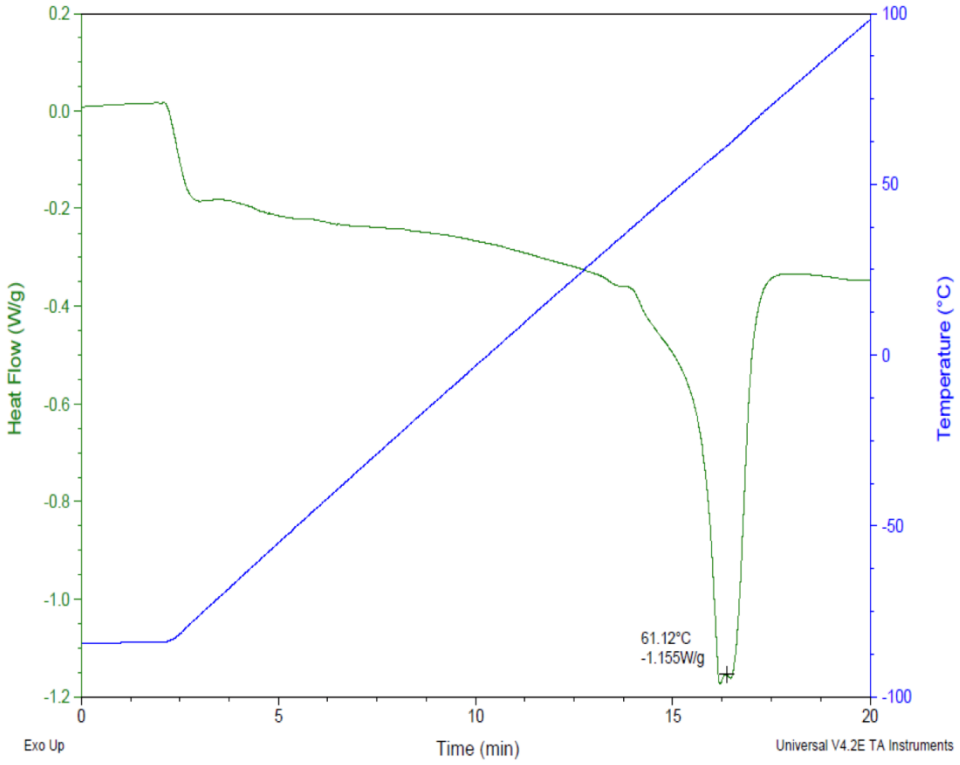

Figure 2.4: Differential scanning calorimetry (DSC) of polycaprolactone displaying the melting temperature of 61.12 °C.

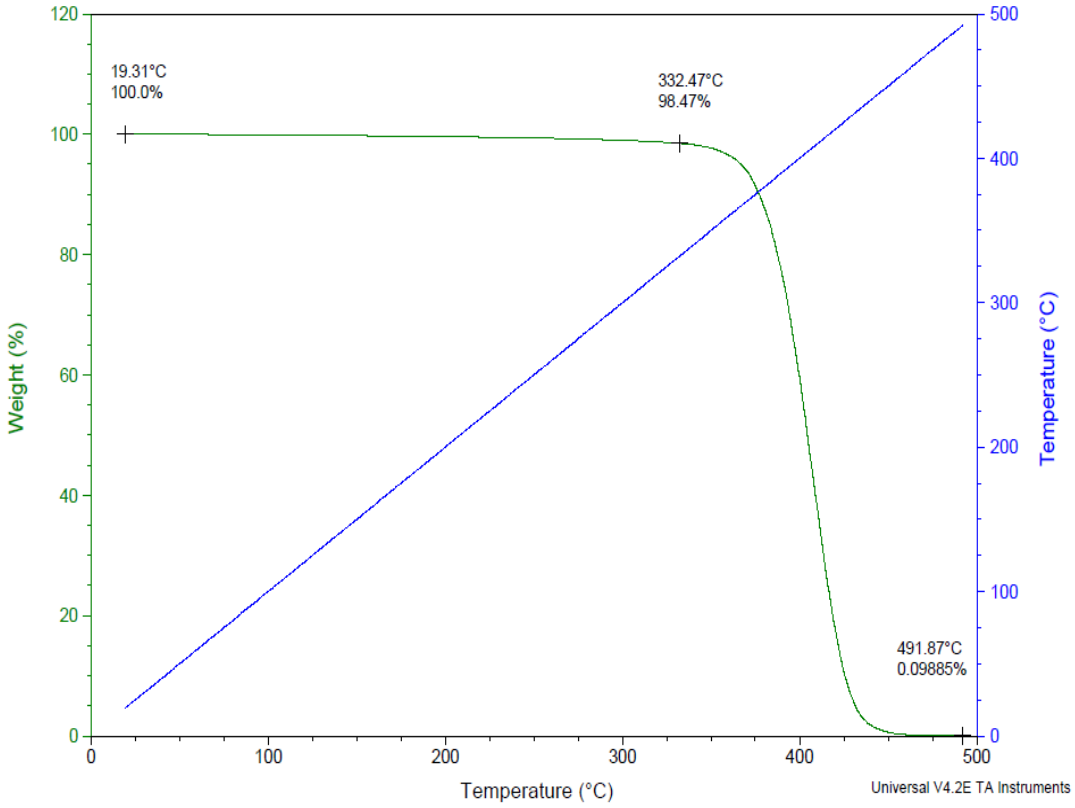

Figure 2.5: Thermogravimetric analysis (TGA) of polycaprolactone displaying a 100% degradation temperature near 500 °C

Results of the contact angle analysis (**Figure 2.6**) show that that PCL and hPCL have the highest contact angles with PCL having an average contact angle of 73.8 degrees and hPCL having an average contact angle of 65.0 degrees. NW and hNW have the lowest contact angles with NW having an average contact angle of 13.9 degrees and hNW having an average contact angle of 13.6 degrees.

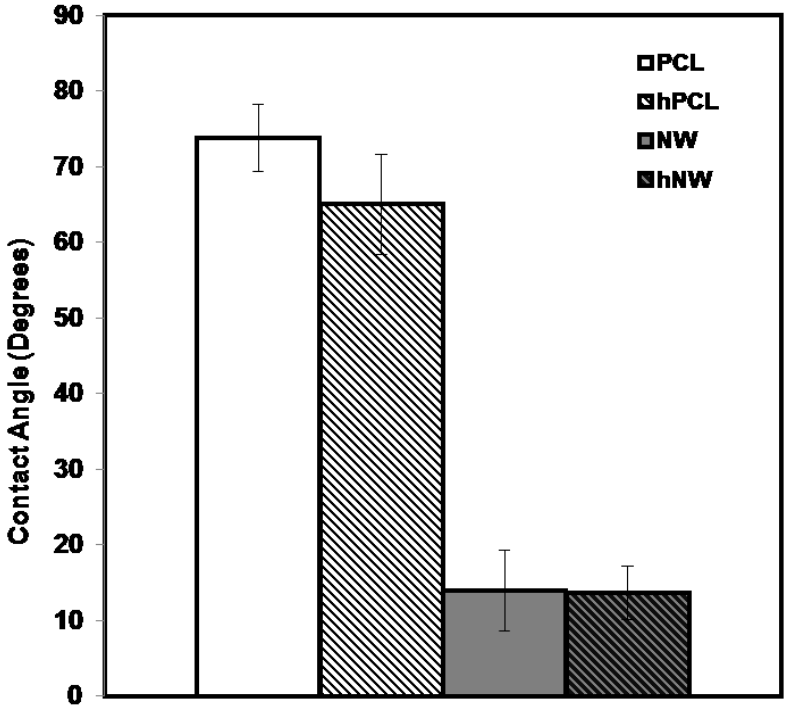

Figure 2.6: Contact Angle measurements of all surfaces

Unaxial tensile testing on PCL (**Figure 2.7**) displayed the average elastic modulus at a 1%/s strain rate was 301.59MPa $\pm$ 42.90MPa. The yield stress and yield strain were 16MPa $\pm$ 1.58MPa and 0.07 respectively. The average elastic modulus of PCL at a 5%/s strain rate was 302.13MPa $\pm$ 67.57MPa. The yield stress and yield strain were 14.56MPa $\pm$ 3.01MPa and 0.07

respectively. From this it was determined that within the range of strain rates used to conduct uniaxial tensile testing, the material did not show strain dependency since the moduli values were not significantly different. In addition, preliminary testing at 0.01%/s and 10%/s strain rates did not show significant difference from the averages mechanical property values obtained from the tests at 1%/s and 5%/s strain rates. **Figure 2.8** shows the force vs. displacement curve for the first 20 seconds of data and **Figure 2.9** is the isolated stress vs. strain curve from the DIC data analysis.

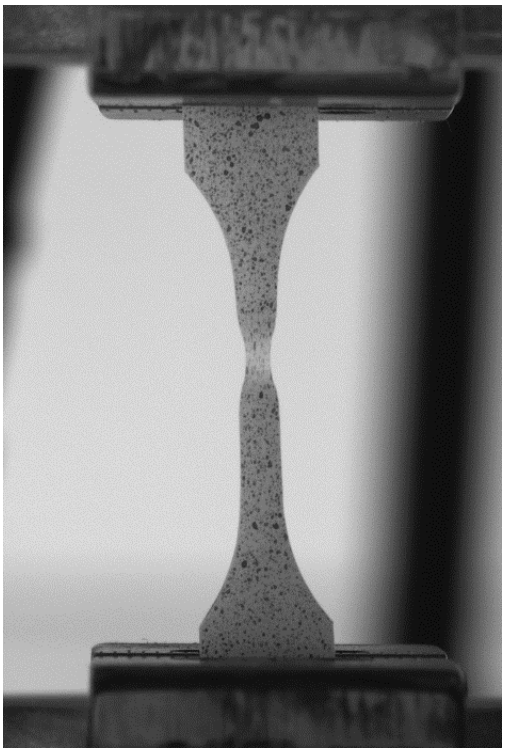

Figure 2.7: Representative image of speckle coated dog-bone PCL samples subjected to uniaxial tensile testing.

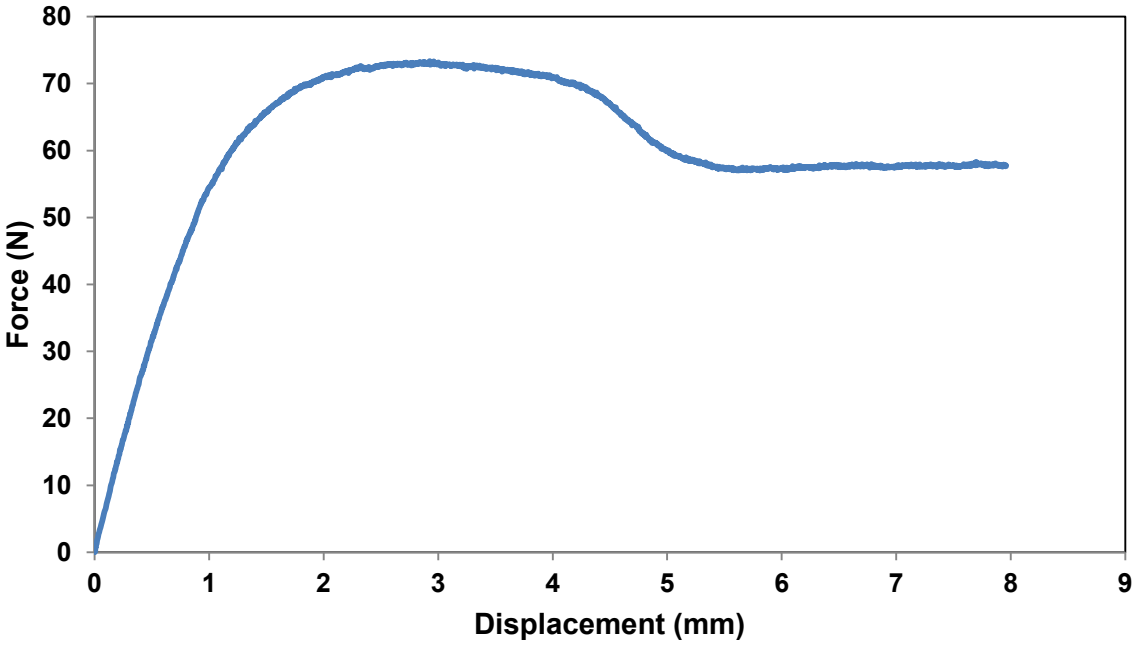

Figure 2.8: First 20 seconds of Force vs. Displacement of uniaxial tensile testing on PCL

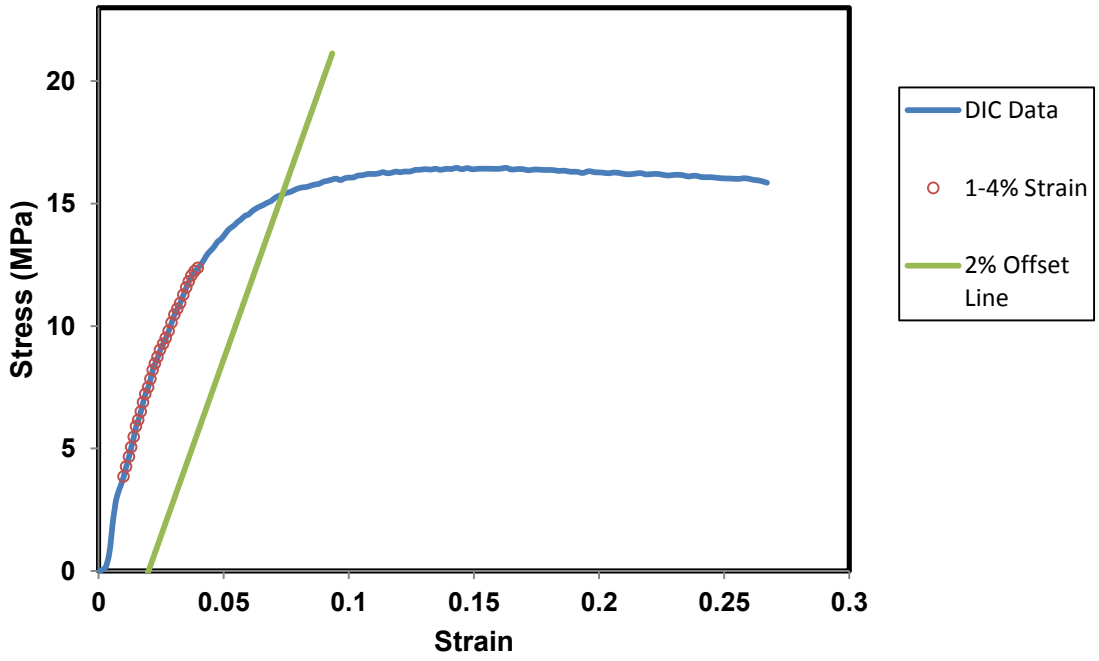

Figure 2.9: First 10 seconds of DIC stress vs. strain data with elastic modulus approximation and 2% offset yield stress/strain on PCL

Unaxial tensile testing on hPCL displayed the average elastic modulus at a 1%/s strain rate was 244.26MPa +/- 104.28MPa. The yield stress and yield strain were 12.91MPa $\pm$ 5.6MPa and 0.07 respectively. The average elastic modulus of hPCL at a 5%/s strain rate was 238.39 MPa +/- 101.01MPa. The yield stress and yield strain were 13.08MPa +/- 5.60MPa and 0.07 respectively. Like the PCL samples, it was determined that within the range of strain rates used to conduct uniaxial tensile testing, the material did not show strain dependency since the moduli values were not significantly different. Even though the elastic moduli and yield stresses are slightly lower for hPCL, the standard deviations are fairly high for both strain rates and there is no statistical significance between PCL and hPCL when the samples are pulled in tension. **Figure 2.10** shows the force vs. displacement curve for the first 20 seconds of data and **Figure 2.11** is the isolated stress vs. strain curve from the DIC data analysis.

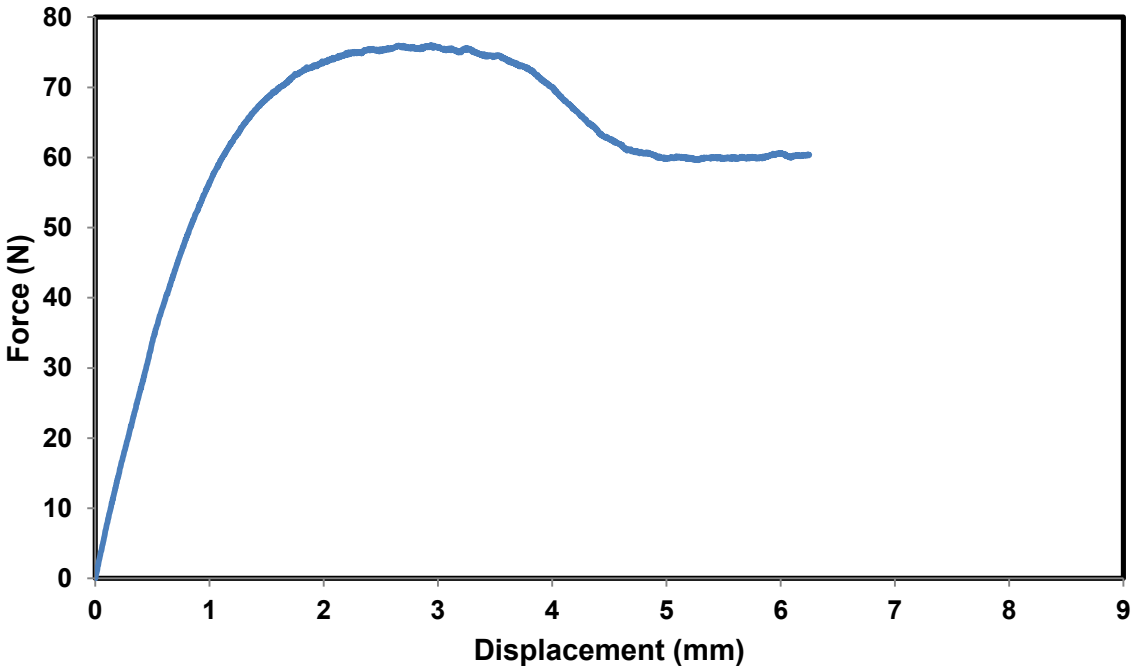

Figure 2.10: First 20 seconds of Force vs. Displacement of uniaxial tensile testing on hPCL

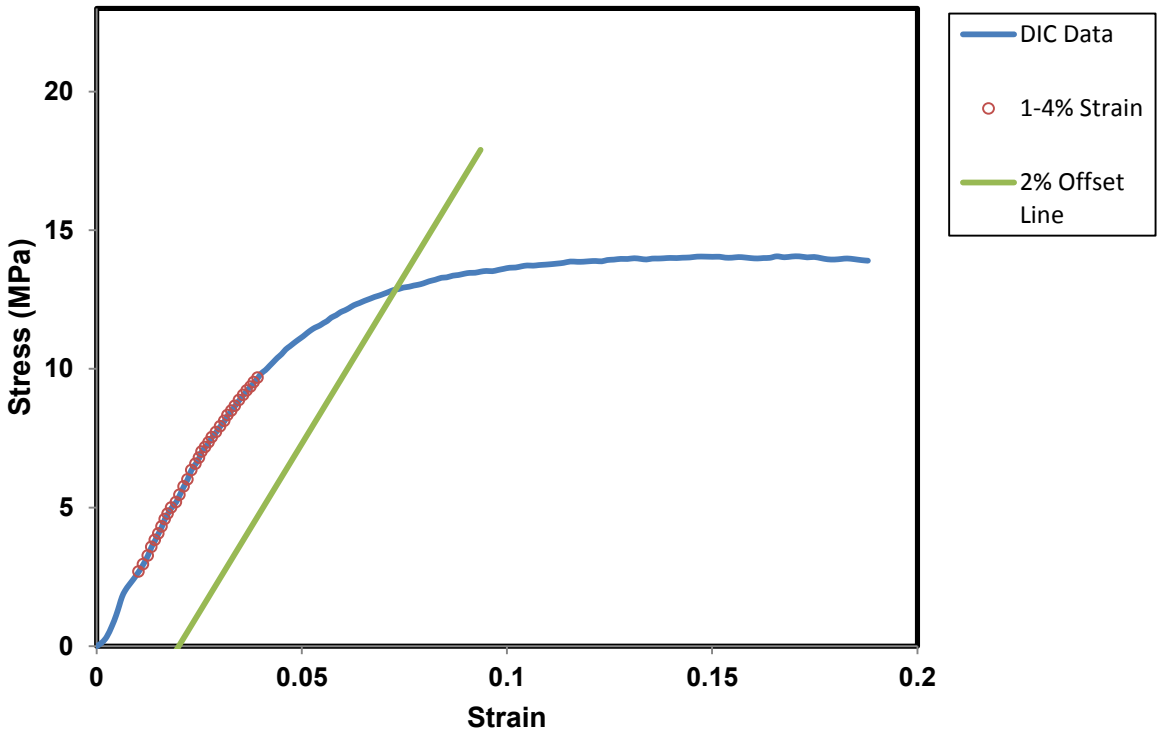

Figure 2.11: First 10 seconds of DIC stress vs. strain data with elastic modulus approximation and 2% offset yield stress/strain on hPCL

The nanoindentation tests were performed to determine the elastic modulus and hardness of PCL, hPCL, NW, and hNW. Load vs Displacment curves show the loading and unloading profiles for each of the 6 loading cycles on each of the samples (**Figure 2.12**). It was determined that the NW and hNW had the highest overall displacements into the surface while PCL and hPCL had lowest displacements. The results of elastic modulus **(Figure 2.13**) showed that hPCL had the highest overall elastic modulus with its true value just settling at 0.68GPa. However, the other surfaces did not have any significant differences between them with hNW, PCL, and NW displaying true values of 0.54GPa, 0.55GPa, and 0.53GPa, respectively. The results of the material hardness (**Figure 2.14**) were much more distinct between the four surfaces. Once again, hPCL had the highest hardness value of 0.053GPa. PCL was significantly lower than hPCL with a hardness value of 0.044GPa. The two nanostructured surfaces, hNW and NW, had the lowest hardness values of 0.021GPa and 0.017GPa, respectively. However, hNW and NW were not significantly different from each other.

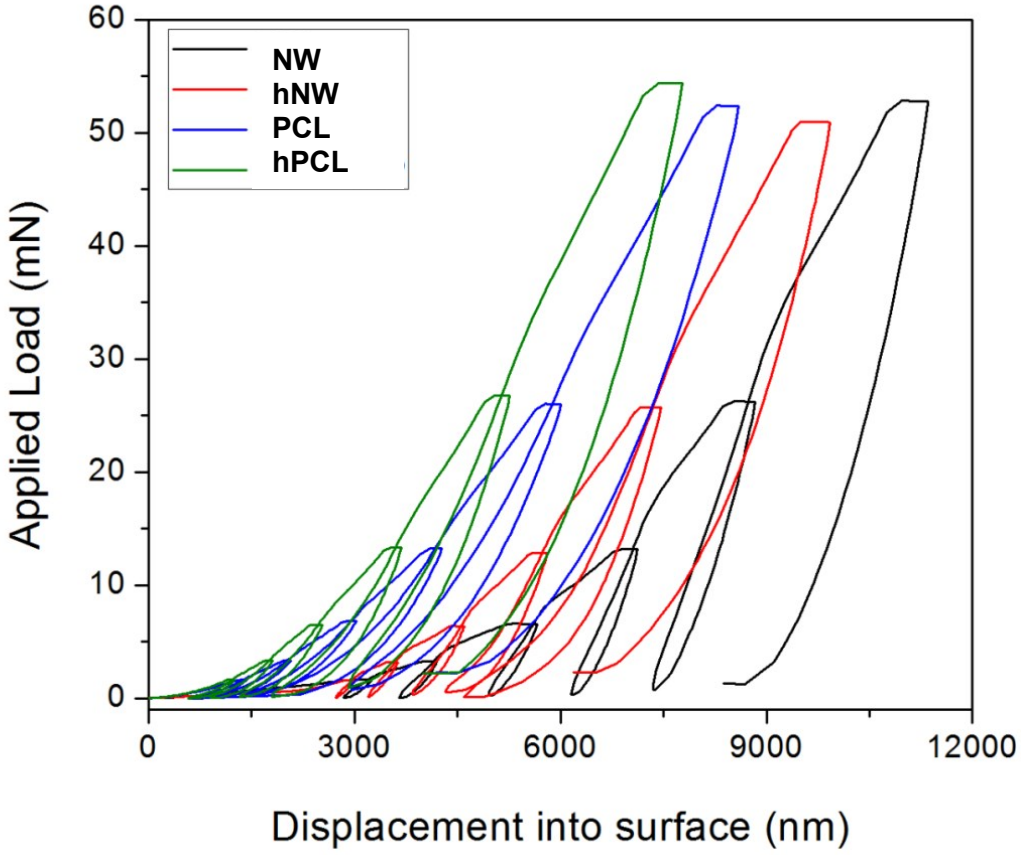

Figure 2.12: Load vs Displacement for all surfaces during nanoindentation analysis

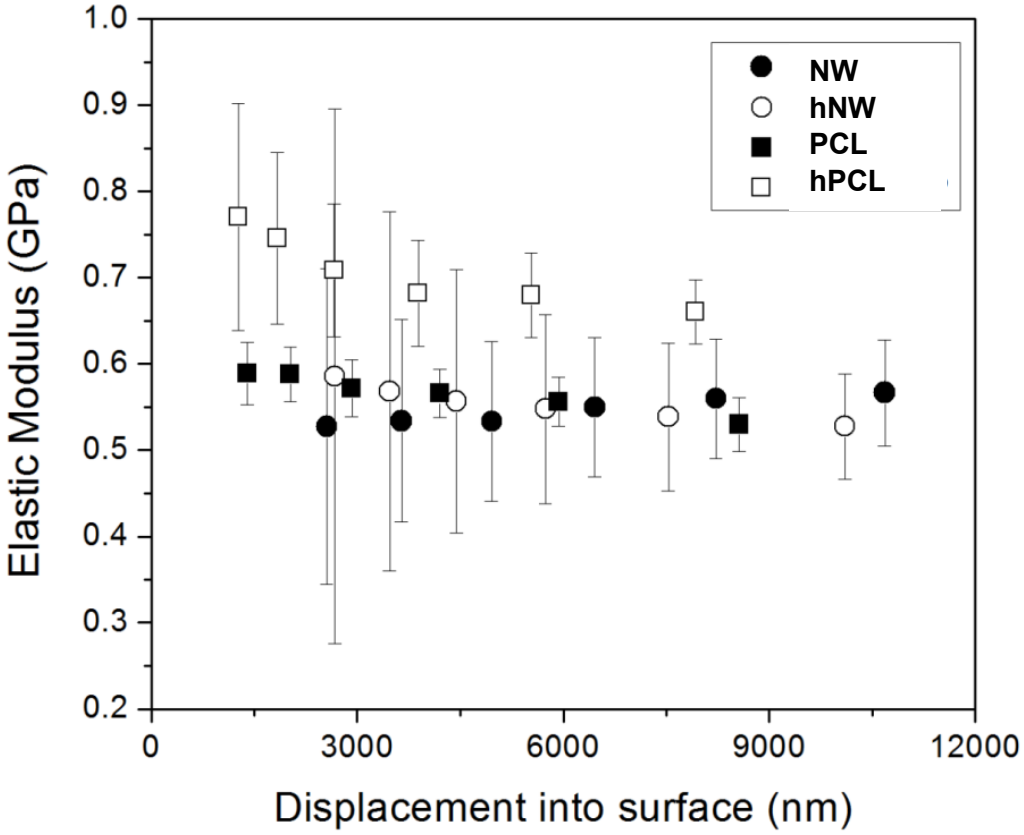

Figure 2.13: Elastic (Young's) Modulus vs Displacement for all surfaces determined using nanoindentation analysis

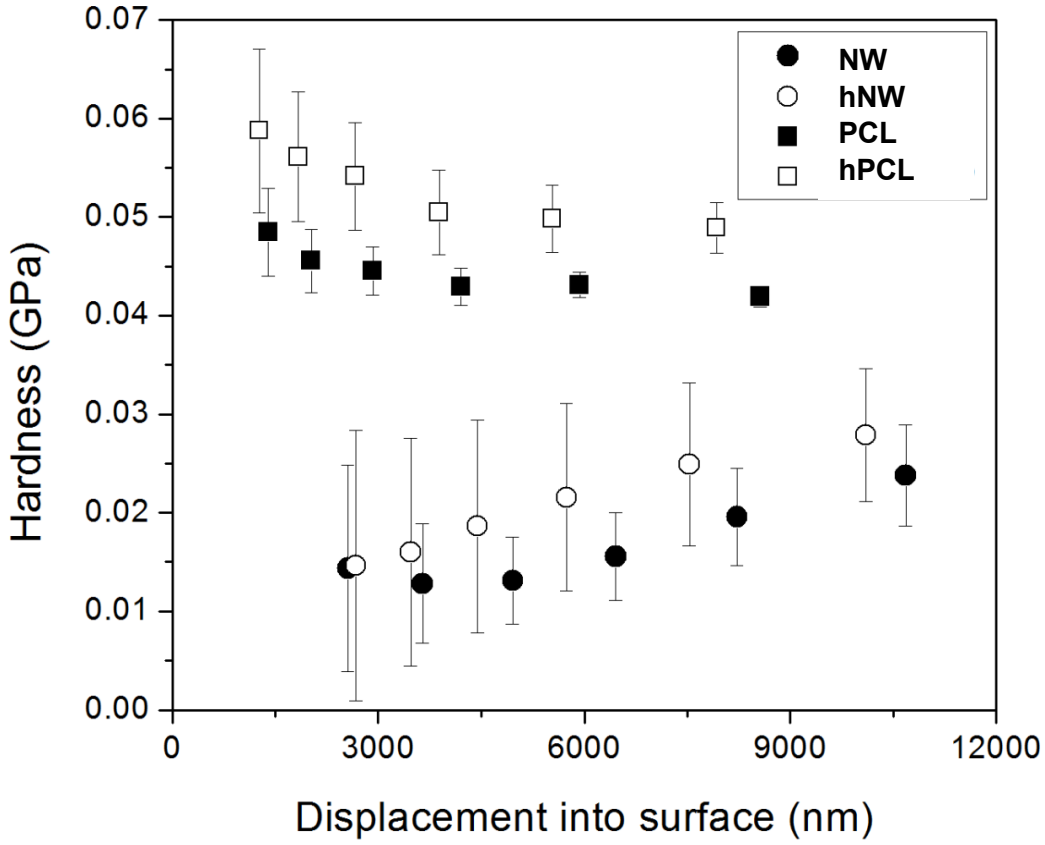

Figure 2.14: Hardness vs Displacement for all surfaces determined using nanoindentation analysis

2.4 Conclusions

Implanted biomedical devices interact with the human physiology at the biomaterial interface. Surface properties of implantable biomaterials are critical for the long-term success of these devices. With the aim of identifying the capabilities of polycaprolactone (PCL) nanowire arrays as interfaces for use in implantable biomedical devices, this research has investigated the characteristics of this specific nanoarchitecture including nanowire morphology, nanoarchitecture, thermal characteristics, hydrophobicity, bulk material tensile mechanical properties, and nanoindentation properties. All of these characteristics were evaluated using SEM/EDS, TGA, DSC, contact angle, uniaxial tensile testing, and nanoindetnation. PCL nanowire arrays were fabricated using a solvent-free thermogravimetric template process using anodized alumina membranes with 100nm pores as the mold. In addition, nanowire arrays were fabricated containing 1 wt% hydroxyapatite nanopowder within the bulk material. The resulting SEM images show the production of vertically oriented, high aspect ratio and uniform array of PCL nanowires. Further, the results of thermal analysis confirm the melting temperature of PCL to be ~61°C and a full degradation (decomposition) temperature of ~500°C. The nanostructured architecture of NW and hNW can be identified as significantly more hydrophilic than the smooth surfaces due to the high surface area of the nanowire arrays. In addition, when testing the mechanical properties of these materials, the elastic modulus and hardness have values in the high megapascal range with NW surface having slightly lower values. The simple fabrication, physiologically relevant architecture, strong mechanical properties, low surface energy and large surface area identify PCL nanowire arrays to be promising interfaces for implantable biomedical devices.

REFERENCES

1. Woodruff, M.A. and D.W. Hutmacher, *The return of a forgotten polymer-Polycaprolactone in the 21st century.* Progress in Polymer Science, 2010. **35**(10): p. 1217-1256.
2. Sinha, V.R., et al., *Poly-epsilon-caprolactone microspheres and nanospheres: an overview.* International Journal of Pharmaceutics, 2004. **278**(1): p. 1-23.
3. Jing, Z., et al., *Biodegradable electrospun fibers for drug delivery.* Journal of Controlled Release, 2003. **92**(3): p. 227-231.
4. Pulkkinen, M., et al., *Effects of block length on the enzymatic degradation and erosion of oxazoline linked poly-epsilon-caprolactone.* European Journal of Pharmaceutical Sciences, 2007. **31**(2): p. 119-128.
5. Sangsanoh, P., et al., *In vitro biocompatibility of schwann cells on surfaces of biocompatible polymeric electrospun fibrous and solution-cast film scaffolds.* Biomacromolecules, 2007. **8**(5): p. 1587-1594.
6. Wutticharoenmongkol, P., P. Pavasant, and P. Supaphol, *Osteoblastic phenotype expression of MC3T3-E1 cultured on electrospun polycaprolactone fiber mats filled with hydroxyapatite nanoparticles.* Biomacromolecules, 2007. **8**(8): p. 2602-2610.
7. Khor, H.L., et al., *Preliminary study of a polycaprolactone membrane utilized as epidermal substrate.* Journal of Materials Science-Materials in Medicine, 2003. **14**(2): p. 113-120.
8. Bezwada, R.S., et al., *Monocryl(R) Suture, a New Ultra-Pliable Absorbable Monofilament Suture.* Biomaterials, 1995. **16**(15): p. 1141-1148.

9. Darney, P.D., et al., *Clinical-Evaluation of the Capronor Contraceptive Implant - Preliminary-Report.* American Journal of Obstetrics and Gynecology, 1989. **160**(5): p. 1292-1295.

10. Pitt, C.G., et al., *Aliphatic Polyesters .2. The Degradation of Poly(Dl-Lactide), Poly(Epsilon-Caprolactone), and Their Copolymers Invivo.* Biomaterials, 1981. **2**(4): p. 215-220.

11. Woodward, S.C., et al., *The Intracellular Degradation of Poly(Epsilon-Caprolactone).* Journal of Biomedical Materials Research, 1985. **19**(4): p. 437-444.

12. Allen, C., et al., *Polycaprolactone-b-poly(ethylene oxide) copolymer micelles as a delivery vehicle for dihydrotestosterone.* Journal of Controlled Release, 2000. **63**(3): p. 275-286.

13. Woei, K., et al., *Evaluation of ultra-thin poly(epsilon-caprolactone) films for tissue-engineered skin.* Tissue Engineering, 2001. **7**(4): p. 441-455.

14. Koshimune, M., et al., *Creating bioabsorbable Schwann cell coated conduits through tissue engineering.* Bio-Medical Materials and Engineering, 2003. **13**(3): p. 223-229.

15. Hutmacher, D.W., et al., *Mechanical properties and cell cultural response of polycaprolactone scaffolds designed and fabricated via fused deposition modeling.* Journal of Biomedical Materials Research, 2001. **55**(2): p. 203-216.

16. Bezwada, R.S., et al., *Monocryl suture, a new ultra-pliable absorbable monofilament suture.* Biomaterials, 1995. **16**(15): p. 1141-8.

17. Cui, W.U., et al., *In situ growth of hydroxyapatite within electrospun poly(DL-lactide) fibers.* Journal of Biomedical Materials Research Part A, 2007. **82A**(4): p. 831-841.

18. Darney, P.D., et al., *Clinical evaluation of the Capronor contraceptive implant: preliminary report.* Am J Obstet Gynecol, 1989. **160**(5 Pt 2): p. 1292-5.

19. Pitt, C.G., et al., *Aliphatic polyesters II. The degradation of poly (DL-lactide), poly (epsilon-caprolactone), and their copolymers in vivo.* Biomaterials, 1981. **2**(4): p. 215-20.

20. Woodward, S.C., et al., *The intracellular degradation of poly(epsilon-caprolactone).* J Biomed Mater Res, 1985. **19**(4): p. 437-44.

21. Oliver, W.C. and G.M. Pharr, *An Improved Technique for Determining Hardness and Elastic-Modulus Using Load and Displacement Sensing Indentation Experiments.* Journal of Materials Research, 1992. **7**(6): p. 1564-1583.

CHAPTER 3

OSTEOGENIC DIFFERENTIAION OF ADIPOSE-DERIVED STEM CELLS ON NANOWIRE SURFACES UNDER OSTEOGENIC CONDITIONS

3.1 Introduction

Orthopedic tissue engineering remains a highly active research area primarily due to complications accompanying challenging healing scenarios [1]. Osteoporosis, traumatic bone fracture, primary bone tumor resection, spinal arthroplasty, orthopedic implant fixation, and total joint arthroplasty are just a few of the many examples of conditions or surgical procedures requiring bone repair or replacement [2]. The most widely used bone graft material for the treatment of critical sized bone defect scenarios are autografts and allografts. Today, this treatment is still considered to be the gold standard of care [3]. However, problems associated with bone grafts include increased scar tissue formation, donor site morbidity, pain, prolonged rehabilitation, increased risk of deep infection, inflammation and restricted availability [4-8].As a result, a promising alternative to conventional treatments for bone defects is the development of synthetic bone tissue engineered scaffolds [9].

The primary intent for synthetic tissue engineering scaffolds for bone regeneration is to enhance bone formation by recruiting bone marrow stromal cells (MSCs) to migrate to the site of the bone defect. MSCs contain a heterogeneous cell population within which exist progenitor cells capable of differentiating into multiple phenotypes including the osteoblasts [10-13]. In order to direct progenitor cell differentiation to a specific phenotype, efforts for biomimetic designs have been aimed toward creating similar signals and conditions that are present in active bone regeneration. Growth factors and cytokines are soluble signals that have been shown to

enhance osteogenesis by activating cell surface receptors [14-17]. An ideal bone regeneration scaffold must be capable of supporting progenitor cell differentiation along the osteogenic line (osteoinduction), promote cell migration and proliferation (osteoconduction), and allow subsequent extracellular matrix production and tissue integration (osseointegration) while simultaneously degrading at a controlled rate as new bone is synthesized [2, 6, 18]. Recently, adipose tissue has received attention and is believed to contain an abundant source of multipotent progenitor cells [19]. With the increased incidence of obesity in the U.S. and abroad, subcutaneous adipose tissue is abundant and readily accessible [20]. Thousands of liposuction surgeries are performed in the U.S. each year and these procedures yield anywhere from 100 ml to >3 L of lipoaspirate tissue [21]. In vitro, adipose derived stem cells (ADSCs), like MSCs, can differentiate into multiple cell lineages including osteogenic, chondrogenic, myogenic, adipogenic and even neuronal pathways [19]. Although it remains to be determined whether ADSCs meet the definition of MSCs, they are multi-potential, are available in large numbers, are easily accessible, and attach and proliferate rapidly in culture, making them an attractive cell source for tissue engineering. In addition, ADSCs demonstrate a substantial *in vitro* bone formation capacity, similar to that of MSCs, but are much easier to culture [22-24].

Human bone is assembled from nanoscale organic and mineral phases into larger hierarchical architectures [25]. Specifically calcium phosphate crystallites that are similar to hydroxyapatite (HAp) compositionally and structurally are nanoscale materials [26-28]. Calcium phosphates such as HAp in biodegradable polymers can potentially enhance the osseoinductivity of the bone scaffold [6]. The inclusion of calcium phosphates in a polymer scaffold may enhance (a) the mineral deposition rate, (b) the mechanical properties, and (c) the protein adsorption, thus improving the overall potential of the bone scaffold [29-31]. HAp ($Ca_5(PO_4)_3OH$) is the primary

the inorganic phase of the bone tissue, and in Haversian bone it resides in gaps at the ends of type I collagen fibrils with a well-controlled crystallographic orientation [32]. Because HAp is an important component of natural bone tissue, it is an attractive design feature for synthetic bone tissue scaffolds as a means of more closely mimicking the natural tissue composition [33-38]. Further, micro- and nanotopographies have also been shown to modulate cell behaviors on metallic [39-41] as well as polymeric implant materials [42-44]. ADSCs and osteoblast functionality is heavily regulated by surface nano- and micro-topography *in vitro* which is not surprising considering the properties and function of bone. In addition to topographical manipulations, the inclusion of bioactive molecules and adhesion factors has been shown to further improve the osteoconduction and osteoinduction of synthetic bone scaffolds [45-50]. It is suggested that nanotopography may result in improved cellular adhesion that in turn may help to increase the matrix deposition.

It is hypothesized that PCL nanowire surfaces will provide a favorable template for adhesion, proliferation and differentiation of ADSCs. Further, HAp nanoparticles were encapsulated within the nanowire architecture since it may directly influence the differentiation of ADSCs into an osteogenic phenotype. In this study, we have evaluated adhesion, proliferation and differentiation of ADSCs on nanowire surfaces with and without HAp nanoparticles.

3.2 Methods

3.2.1 Adipose derived stem cell culture on different surfaces

Adult human ADSCs at passage 2 (Zen-Bio Inc.) were expanded using standard cell culture techniques. All the cells used in this study were below passage 5. Following expansion, cells were detached using 0.25% Trypsin-EDTA and suspended in growth media consisting of

DMEM with 10% fetal bovine serum (FBS, Sigma) and 1% penicillin/streptomycin (Sigma).All the surfaces were sterilized by incubating in 70% ethanol at room temperature followed by exposure to UV light for 30 min. Following sterilization, the surfaces were rinsed twice with warm phosphate buffered saline (PBS). Cells were seeded on all surfaces in 48-well plates at a density of $1x10^4$ cells/well. The surfaces were incubated at 37ºC and 5% CO_2 for the entire duration of the study. Half of the growth media was changed on day 4. On day 7, all the growth media was replaced with an osteogenic differentiation media consisting of growth media plus dexamethasone (10^{-8}M), ascorbic acid (50 mg/ml), and β-glycerophosphate (6mmol). The osteogenic differentiation media was changed every other day for up to 3 weeks of culture.

3.2.2 ADSC adhesion and proliferation on different surfaces

After day 1 and day 7 of initial culture, ADSC adhesion, proliferation, and spatial organization were investigated by staining the adhered cells with 5-Chloromethylfluorescein diacetate (CMFDA – live cells), rhodamine-phalloidin (actin – cytoskeleton), and 4',6-diamidino-2-phenylindole (DAPI – nucleus).At each time point, the surfaces were removed from the growth media, and incubated in the CMFDA stain at a concentration of 10μM for 45 min in a 37°C and 5% CO_2 incubator. Next, the substrates were incubated for another 30 min at 37°C and 5% CO_2 in warm growth medium. The cells were then fixed with 3.7% formaldehyde for 15 min at room temperature. In order to permeabilize the cells, the surfaces were incubated in 1% Triton-X 100 for 3 min. The substrates were then incubated in rhodamine-phalloidin stain at a concentration of 5μL/mL for 30 min. After 25 min of rhodamine-phalloidin staining, DAPI was added at a ratio of 105:1000. The substrates were then rinsed in PBS and imaged using a Zeiss Axioplan 2 fluorescence microscope. The number of adhered cells on all the surfaces was

determined from 10x DAPI stained images by counting the nuclei using "Analyze Particles" feature embedded in the Image J software. The cell shape factor was also determined using ImageJ software with 10x rhodamine-phalloidin stained images. The cell shape factor was approximated by the ratio of cellular length to cellular width. The cellular length was defined by the diameter of the smallest circle that encompassed the entire cell and the cellular width was defined as the diameter of the largest circle that would fit entirely within the cell.

The cell viability was measured after 1 and 4 days of culture (log phase growth) using a commercially available MTT assay kit (Sigma). Adhered cells were incubated at 37ºC for 3 hrs in a (3-[4,5-dimethylthiazol-2-yl]-2,5-diphenyl tetrazolium bromide (MTT) solution. Mitochondrial dehydrogenase of viable cells cleaves the tetrazolium ring leaving behind purple formazan crystals. The formazan crystals were dissolved in the MTT solvent. The optical density (OD) of the resulting solvent was measured at 570nm using a spectrophotometer (FLUOstar Omega; BMG Labtech, Durham, NC). Background absorbance was measured at 690nm and subtracted from the measured absorbance.

The morphology of the adhered ADSCs was investigated using SEM after 1 and 7 days of culture. SEM was done to visualize how cells adhered and proliferated on the surfaces as well as how they interacted with the nanowire morphology. In brief, the cells were fixed in a solution of 3% glutaraldehyde (Sigma), 0.1 M sodium cacodylate (Polysciences), and 0.1M sucrose (Sigma) for 45 min. The surfaces were then incubated in a buffer containing 0.1M sodium cacodylate and 0.1M sucrose. After fixation, the cells were dehydrated by incubating the surfaces in increasing concentrations of ethanol (35%, 50%, 70%, 100%) for 10 min each. The surfaces were further dehydrated by incubating them in hexamethyldisilazane (HMDS, Sigma) for 10

min. The surfaces were stored in a desiccator until examination using SEM. The surfaces were sputter coated with 10 nm of gold and imaged using at a voltage of 7kV.

3.2.3 ADSC differentiation on different surfaces

ADSC responses to the different surfaces were evaluated after providing the cells with osteogenic differentiation media. The surfaces were removed from the culture media and rinsed twice with PBS prior to analysis. Cytoplasmic alkaline phosphatase (ALP) was measured after 1, 2 and 3 weeks of culture. Adhered cells were incubated and shaken at 150 RPM for 20 min at room temperature in 0.2% Triton-X cell lysate solution. A commercially available ALP colorimetric assay kit (Quanticrome BioAssay Systems) was used to quantify ALP concentration in the cell lysate. In brief, ALP catalyzes the reaction of *p*-Nitrophenolphosphate (*p*-NPP) to p-nitrophenol and phosphate. This was detected colorimetrically using a spectrophotometer by measuring the absorbance at 405nm after 1 min and 5 min.

Calcium mineralization on different surfaces was detected using alizarin red staining after 1 and 3 week of culture. All surfaces were rinsed twice in PBS followed by a rinse in cold (4ºC) ringer solution (Sigma). Adhered cells were fixed in 4% paraformaldehyde in cold PBS for 10 min, and then rinsed in cold DI water. The surfaces were incubated in a solution of 2% alizarin red (Sigma) (in PBS adjusted to a pH of 4.0 to 4.2 with 10% ammonium hydroxide) for 15 min at room temperature to stain for calcium. The surfaces were rinsed three times in DI water and digital images of stained surfaces were obtained.

The morphology of adhered ADSCs on surfaces was investigated using SEM after 1 and 3 weeks of culture using the method described in previous section.

After 3 weeks of culture, ADSCs on different surfaces were immuno-labeled for osteocalcin (OC) and osteopontin (OP). Cells were fixed and permeabilized as described earlier. All the surfaces were incubated with 10% bovine serum albumin for 30 min at room temperature to prevent nonspecific binding. After rinsing in PBS, the surfaces were incubated with either anti-osteocalcin primary antibody (1:100 in PBS, V-19 purified goat polyclonal antibody of human origin, Santa Cruz Biotechnology) or anti-osteopontin primary antibody (P-18 purified goat polyclonal antibody of mouse origin, Santa Cruz Biotechnology) for 1 hr at room temperature. Following primary antibody incubation, surfaces were washed three times with PBS at an interval of 5 min each. The surfaces were then incubated in FITC-labeled secondary antibodies for osteocalcin and osteopontin (1:200 donkey antigoatIgG, Santa Cruz Biotechnology) for 45 min in the dark. Finally, the surfaces were rinsed twice in PBS and incubated in rhodamine-phalloidin stain at a concentration of 5uL/mL for 30 min. After 25 min of rhodamine-phalloidin staining, DAPI was added at a ratio of 105:1000. The surfaces were then rinsed in PBS and visualized using a Zeiss Axioplan 2 fluorescence microscope. The number of adhered cells on all the surfaces was determined from 10x DAPI stained images by counting the nuclei using "Analyze Particles" feature embedded in the Image J software. The percentage of area covered with osteocalcin and osteopontin (i.e. percentage of area that was stained with FITC) was also determined using ImageJ software. This percentage was divided by total number of cells that were present in that particular image.

3.2.4 Statistical Analysis

Data within the graphs are expressed as the average count and the standard error of the mean. All the quantitative results were analyzed using one-way analysis of variance (ANOVA)

and multiple comparisons are tested using Tukey's HSD. Statistical significance was considered at $p < 0.05$. All qualitative methods used $n_{min}=3$ and all quantitative methods used $n_{min}=5$.

3.3 Results and Discussion

An ideal bone scaffold should be physically and chemically biomimetic. For bone regeneration, the scaffold must be capable of supporting progenitor cell differentiation along the osteogenic line, promote cell migration and proliferation, and allow subsequent extracellular matrix production and tissue integration while simultaneously degrading. There are two specific components of this work that are significant in terms of its application to orthopedic tissue engineering: fabrication of nanowire surfaces and investigation of ADSC response to nanoscale surface topography. It is well documented that both micro- and nano-scale features are critical for cells to adhere, proliferate and differentiate into specific phenotypes. This study addresses the critical design consideration to develop scaffolds with nanoscale surface topography growth and maintainence of ADSCs.

After 1 and 7 days of initial culture in growth media, the adhered cells on different surfaces were stained using CMFDA, Rhodamine-phalloidin and DAPI (**Figure 3.1**). CMFDA fluorescent probes are freely able to pass through the membranes of viable cells and the probes are converted to cell-impermeant reaction products. These reaction products are present throughout the cytoplasm of living cells and fluoresce. In this study, the CMFDA fluorescent probes are FITC labeled causing them to have green fluorescence. Rhodamine-phalloidin is a high affinity F-actin probe coupled with a red-orange fluorescent dye called tetramethylrhodamine isothiocyanate (TRITC). Phalloidin is a bicycling heptapeptide that binds to F-actin and the TRITC provides very little non-specific staining to it the high selectivity of the

bone between F-actin and phalloidin. DAPI is strictly a nucleus stain because it binds to the adenine-thymine rich regions of the DNA. The fluorescence microscopy images were evaluated to determine the cell adhesion, proliferation, survival, morphology, and spatial organization. The results indicate that PCL and hPCL surfaces supported higher cell adhesion and proliferation as compared to NW and hNW surfaces (**Figure 3.1**).

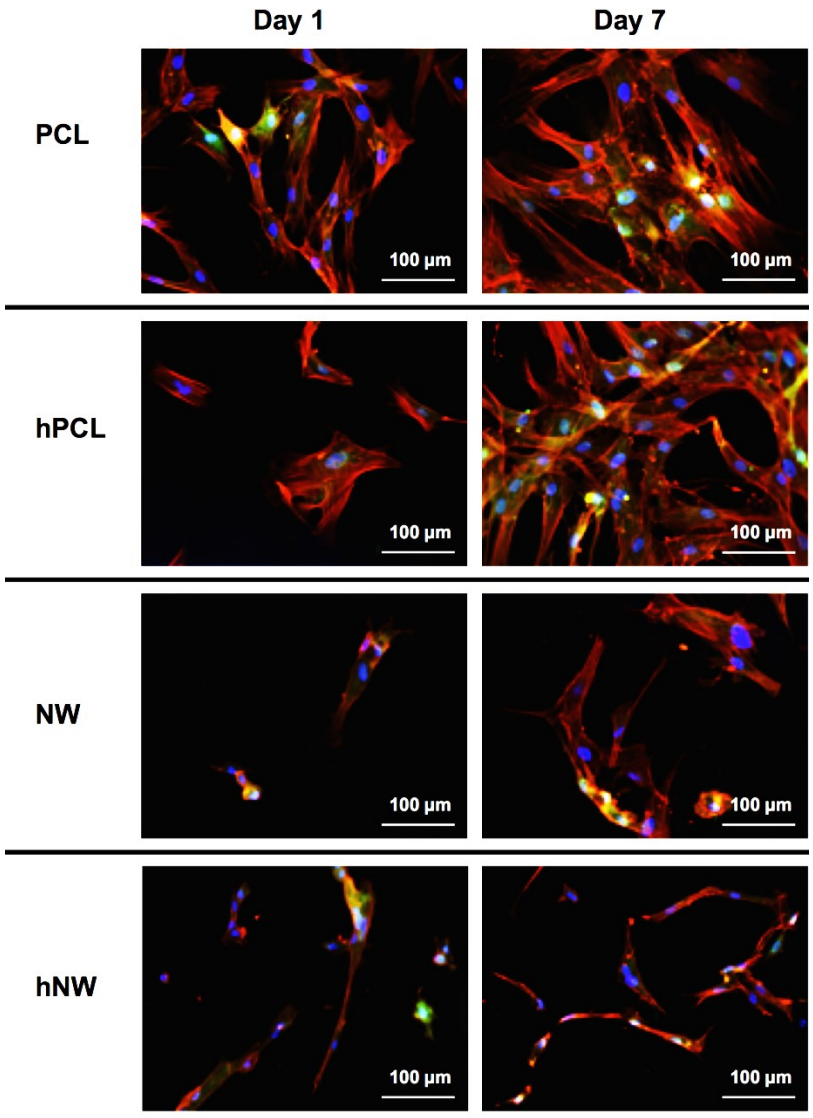

Figure 3.1: Representative fluorescence microscopy images of ADSCs on PCL, hPCL, NW, and hNW surfaces after 1 and 7 days of culture.

After 1 day of culture, the cells on the PCL and hPCL surfaces appear to spread in all directions; however they have very similar shape. On the contrary, after 1 day of culture, the cells on the NW and hNW surfaces have elongated morphologies. After 7 days culture, the cells have proliferated on all the surfaces. However, PCL and hPCL surfaces seem to have higher number of cells compared to NW and hNW surfaces. Further, the cells on PCL and hPCL surface appear to spread in all direction, whereas the cell on NW and hNW surface have elongated morphologies with cellular extensions interaction with each other. The cell adhesion and proliferation was quantified from the 10x DAPI stained images and counting the nuclei using ImageJ software (**Figure 3.2**).

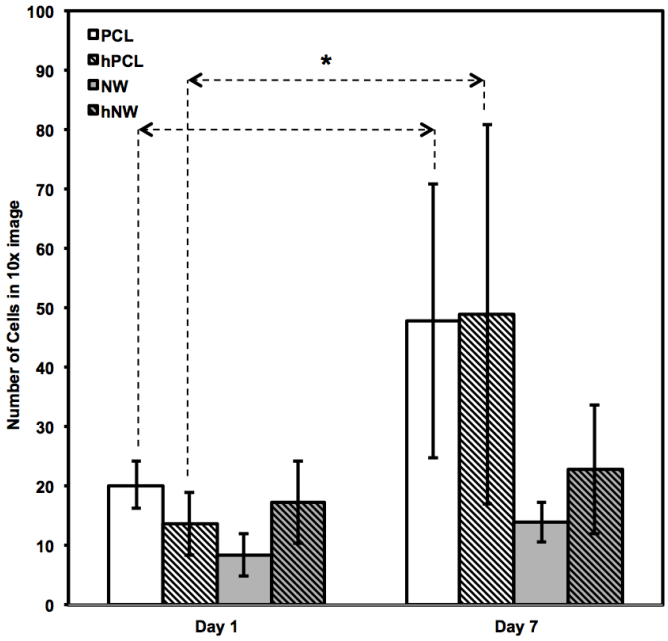

Figure 3.2: Cell counts on PCL, hPCL, NW, and hNW surfaces after 1 and 7 days of culture. Cell nuclei were counted using DAPI fluorescence.

Significantly more cells are present on PCL and hPCL surfaces after 7 days of culture as compared to NW and hNW surfaces, indicating less proliferation. The number of cells on NW and hNW surfaces after 7 days of culture is about the same as that after 1 day of culture. Although the PCL and hPCL surfaces support higher cell adhesion and proliferation, the cells do no exhibit altered morphologies after 1 and 7 days of culture. In contrast, the cells appear to have elongated morphologies on NW and hNW as compared to PCL and hPCL surfaces. Further, the cells appear to be more elongated after 7 days of culture on NW and hNW as compared to after 1 day of culture. This behavior was quantified by calculating the cell shape factor using 10x rhodamine-phalloidin stained images after 7 days of culture (**Figure 3.3**).

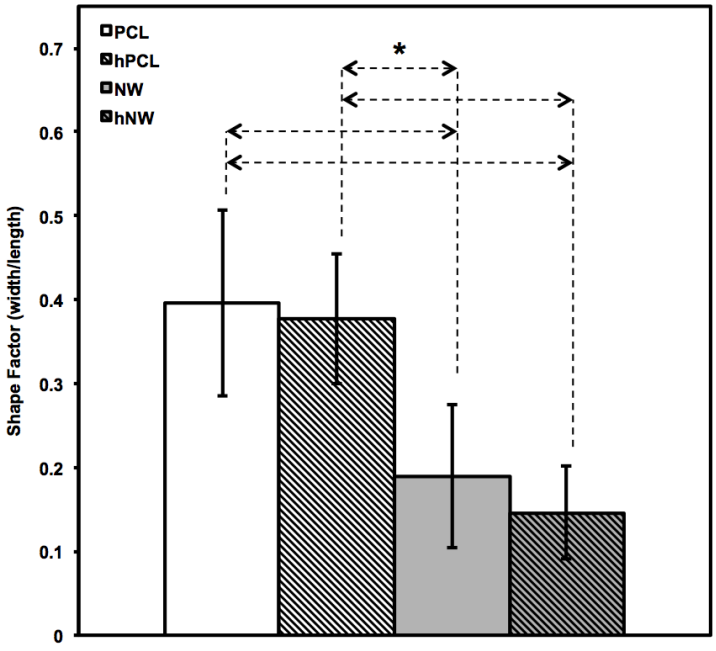

Figure 3.3: Shape factor approximations of ADSCs after 7 days of culture on different surfaces. ADSCs on PCL and hPCL surfaces had higher shape factor values while, ADSCs on NW and hNW surfaces had lower shape factor values indicating elongated cell morphologies.

The shape factor is an important quantitative parameter that indicates the whether the cell is spherical or elongated. A shape factor → 1 indicated that the cell has spherical morphology, whereas shape factor → 0 indicated that the cell has elongated morphology. The shape of the cell is important since it not only affects cell migration and communication, but also the cell differentiation. The results indicate that the cell on PCL and hPCL surfaces had shape factor significantly higher than that for cell on NW and hNW surfaces (**Figure 3.3**).

The cell viability on all the surfaces was investigated using MTT assay after 1 and 4 days of culture (**Figure 3.4**). In brief, MTT activity is the measure of cell viability and is the measure of mitochondrial activity. The results indicate that the cells are viable on all the surfaces after 1 day of culture. However, after 4 days of culture, there was significant increase in the viability for cells on PCL and hPCL surfaces. The cells on NW and hNW surfaces showed slight increase in the viability after 4 days of culture, however it was not significant. These results are in conjunction with results of fluorescence microscopy. The increased viability on PCL and hPCL surfaces is because the surfaces support higher cell adhesion and proliferation. The results from the MTT assay indicate that the cells are viable on all the surfaces after 4 days of culture and there are no cytotoxic effects of the surface on cell functionality.

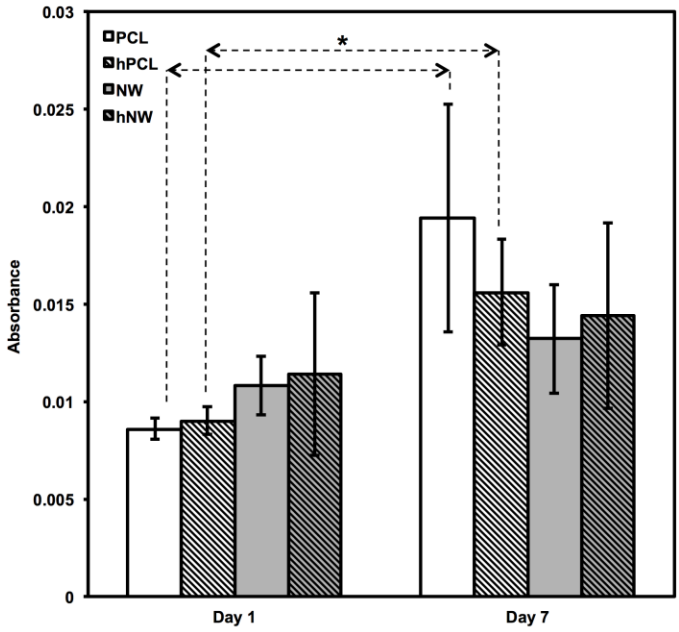

Figure 3.4: ADSC viability after 1 and 7 days of culture using MTT absorbance. Data indicates increased MTT activity on all surfaces with significant increases on PCL and hPCL.

To visualize the morphological changes in the cells on different surfaces, SEM images were taken after 1 and 7 of culture (**Figure 3.5**). In addition to morphology, SEM also allows for visualization of the interaction of the cell processes with the surface nanoarchitecture. The results support the results from fluorescence microscopy indicating higher number of cells on PCL and hPCL surfaces as compared to NW and hNW surfaces, as well as elongated cell morphologies on NW and hNW surfaces as compared to PCL and hPCL surfaces. The cells on PCL and hPCL surfaces seem to have a spreading morphology but do not interact with other cells on the surface. In contrast, the cells on NW and hNW surfaces have longer cellular extensions that seems to be involved in cell communication. High magnification SEM images of cells on NW and hNW surfaces show that the cellular extensions are interacting with the nanowire architecture after 1 day of culture. These extensions seem to be longer after 7 days of culture showing the

interaction of the cell with the nanowire architecture and formation of a complex network on the surface.

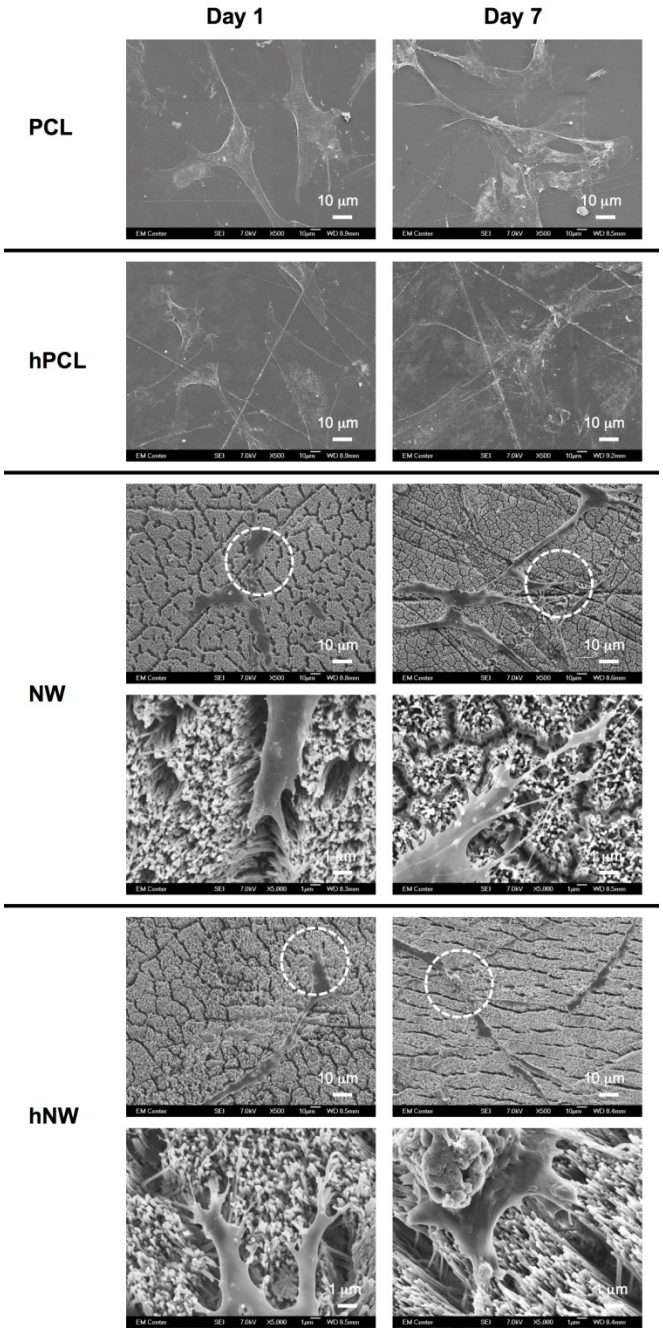

Figure 3.5: Representative SEM images of ADSCs on PCL, hPCL, NW, and hNW surfaces after 1 and 7 days of culture.

A tissue engineering scaffold for bone regeneration relies heavily on its capability to help yield and accelerate the production of extracellular matrix in order for it to be clinically relevant. Thus, it is important to investigate the ability of these surfaces to lead ADSCs towards osteogenic differentiation and also determine if the inclusion of encapsulated HAp nanoparticles either enhances or inhibits osteoblast differentiation. Thus, in this study cellular production of alkaline phosphatase, the mineralization of calcium, and the expression of two marker proteins, OC and OP, were investigated. After 7 days of initial culture, the growth media was supplemented with β-glycerophosphate, L-ascorbic acid, and dexamethasone.

Alkaline phosphatase (ALP) is a ubiquitous enzyme in bone, liver, kidney, placental, and intestinal tissues. It is a key ingredient in matrix vesicles, aids in mineralization by hydrolyzing organic phosphate esters, and is a standard biomarker for osteoblast phenotype. The presence of ALP in matrix vesicles, the site of new bone formation, suggests the role of ALP in mineralization. ALP aids in the mineralization of HAp by hydrolyzing organic phosphate esters which produces an excess of free inorganic phosphate thereby initiating the biomineralization process. ALP plays a direct role in the induction of HAp deposition on extracellular matrix proteins and is known to exhibit cyclic behavior when it is active. ALP activity was measuredafter 1, 2 and 3 weeks of culture (**Figure 3.6**). The results indicate increase in ALP activity on all the surfaces from week 1 to week 2 indicating the initiation of differentiation and calcium phosphate mineralization. However, from week 2 to week 3, the NW and hNW surfaces saw a decrease in ALP activity. Since ALP is an early biomarker of mineralization, the decrease can be associated with mature differentiation of the cells to osteoblasts and the deposition of extracellular matrices that are more characteristic of osteoblasts. As mentioned earlier, ALP is

cyclic enzyme during the mineralization process is activated only when the cells need to produce more extracellular HAp.

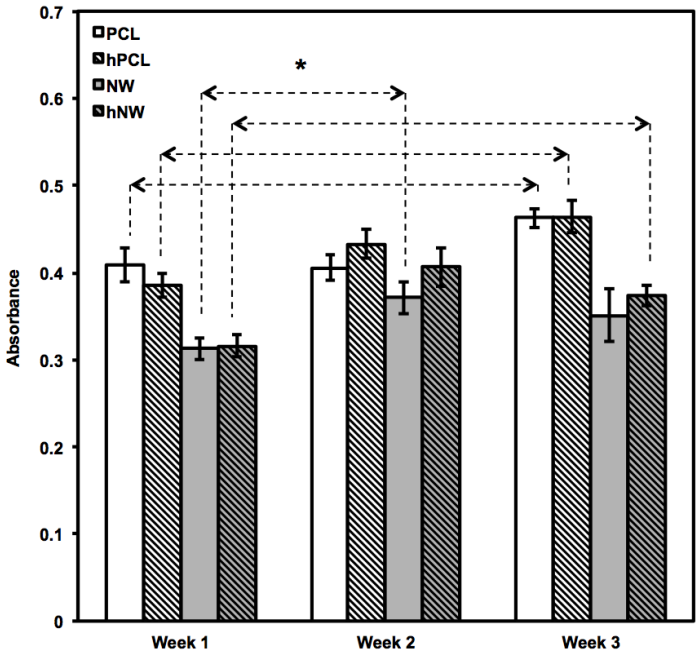

Figure 3.6: ALP activity on PCL, hPCL, NW, and hNW surfaces after 1, 2 and 3 weeks of ADSC culture in osteogenic conditions.

In addition to detecting intracellular ALP concentration for mineralization, alizarin red was used to stain the surfaced deposited calcium (**Figure 3.7**). Alizarin Red S, an anthraquinone derivative, is used to identify calcium in tissue sections. The reaction is not strictly specific for calcium, since magnesium, manganese, barium, strontium, and iron may interfere, but these elements usually do not occur in sufficient concentration to interfere with the staining. Calcium forms an Alizarin Red S-calcium complex in a chelation process, and the end product is birefringent. Alizarin Red staining was also used on surfaces that were not cultured with cells. Both PCL and NW surfaces without cells did not show any red stain, where as hPCL and hNW surfaces showed red stain due to the presence of calcium in HAp (**Figure 3.7**). After 1 week of

culture, PCL and NW surfaces had little to no red stain present on the surface. However, as expected both hPCL and nNW surfaces showed red stain, a slightly more intense then that on surfaces without any cells, due to the presence of HAp on the surface. After 3 weeks of culture, the PCL surfaces showed no signs of red stain in form of spherulites or globules and the surface looked similar to that after 1 week of culture. The hPCL surface showed a little more intense red stain as compared to after 1 week of culture. On the contrary, both NW and hNW surfaces had more intense red stain as compared to after 1 week of culture (as well as compared to hNW surfaces without cells) indication mineralization. Since Alizarin Red stain is a qualitative technique, it is difficult to exactly determine which of either NW or hNW surfaces exhibited highest production of calcium.

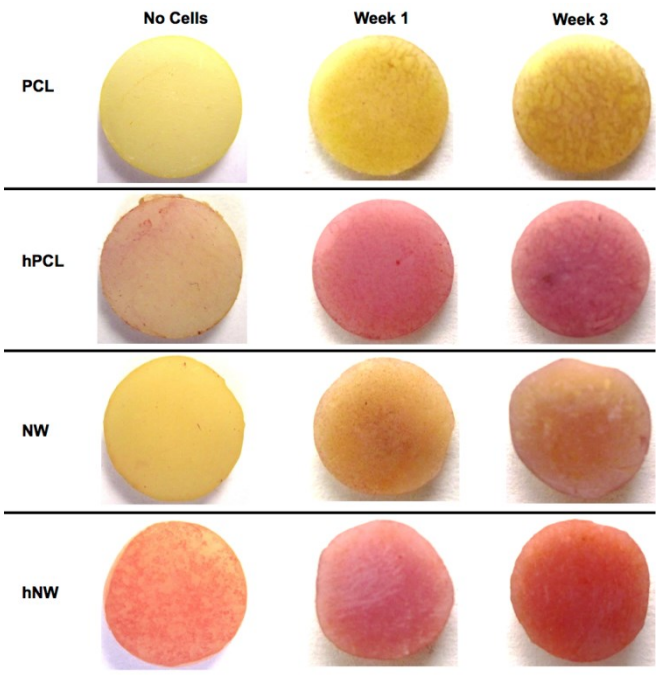

Figure 3.7 Calcium (alizarin red) staining on PCL, hPCL, NW, and hNW surfaces with no cells and after 1 and 3 weeks of ADSC culture in osteogenic conditions.

After 3 weeks of culture, ADSCs on different surfaces were immuno-labeled for OC and OP. OC is a primary biomarker in the bone formation process and is present due to the activity of mature osteoblast phenotypes. It is often known as the bone gamma-carboxyglutamic (Gla) protein. The protein is up-regulated during bone formation and remodeling *in vivo,* and is a HAp and Ca^{2+} binding ECM protein. It is the most abundant and widely studied non-collagenous bone ECM protein. OP is an extracellular structural glycoprotein that is an organic component of bone tissue. It is involved in regulating mineral deposition, cell migration, and is often present at mineralized tissue/implant interfaces. OP is also known as bone sialoprotein 1, secreted phosphoprotein 1, and bone phosphoprotein. Like OC, it is also a HAp and Ca^{2+} binding protein which is also found in other tissues besides bone such as the kidney, placenta, brain. It preferentially aggregates to mineral phase interfaces and is considered to be a "linker" molecule. Intracellular and extracellular OC and OP on different surfaces was detected immunofluorescence imaging. FITC immunolabeling for OC (**Figure 3.8(a)**) and OP (**Figure 3.9(a)**) after 1 and 3 week of culture indicates that all the surfaces are expressing both the proteins, which higher expression on NW surfaces after 3 weeks of culture as compared to other surfaces. Further, it is also evident that there are more number of cells present on PCL and hPCL surfaces as compared to NW and hNW surfaces after 1 and 3 weeks of culture. Thus, in order to partially quantify the amount of proteins expressed on all surfaces, the fluorescence microscopy images were analyzed using ImageJ software to determine the surface area covered with FITC and was normalized with number of cells (by counting nuclei) present in that image. This will give relative expressions of OC (**Figure 3.8(b)**) and OP (**Figure 3.9(b)**) for a group of cells that were visualized. The quantitative analysis shows that all the surfaces had similar expressions of OC and OP after 1 week of culture. However, after 3 weeks of culture, NW surfaces had

significantly higher expressions of OC and OP as compared to hNW, PCL and hPCL surfaces. Even though there are more cells present on PCL and hPCL surfaces as compared to NW surfaces, these cells are probably not differentiated completely to express osteogenic markers. This indicates that the topography of the NW surfaces not only affects the cellular morphology but also influenced the cellular differentiation. Further, it was surprising to see relatively lower expressions of OC and OP on hNW surfaces. This may be due to the fact that the presence of HAp may hinder or delay cellular differentiation since the cells may not have to "work hard" enough to produce their own HAp. However, further studies are required to understand this phenomenon and also effect of different amounts of HAp on the surfaces.

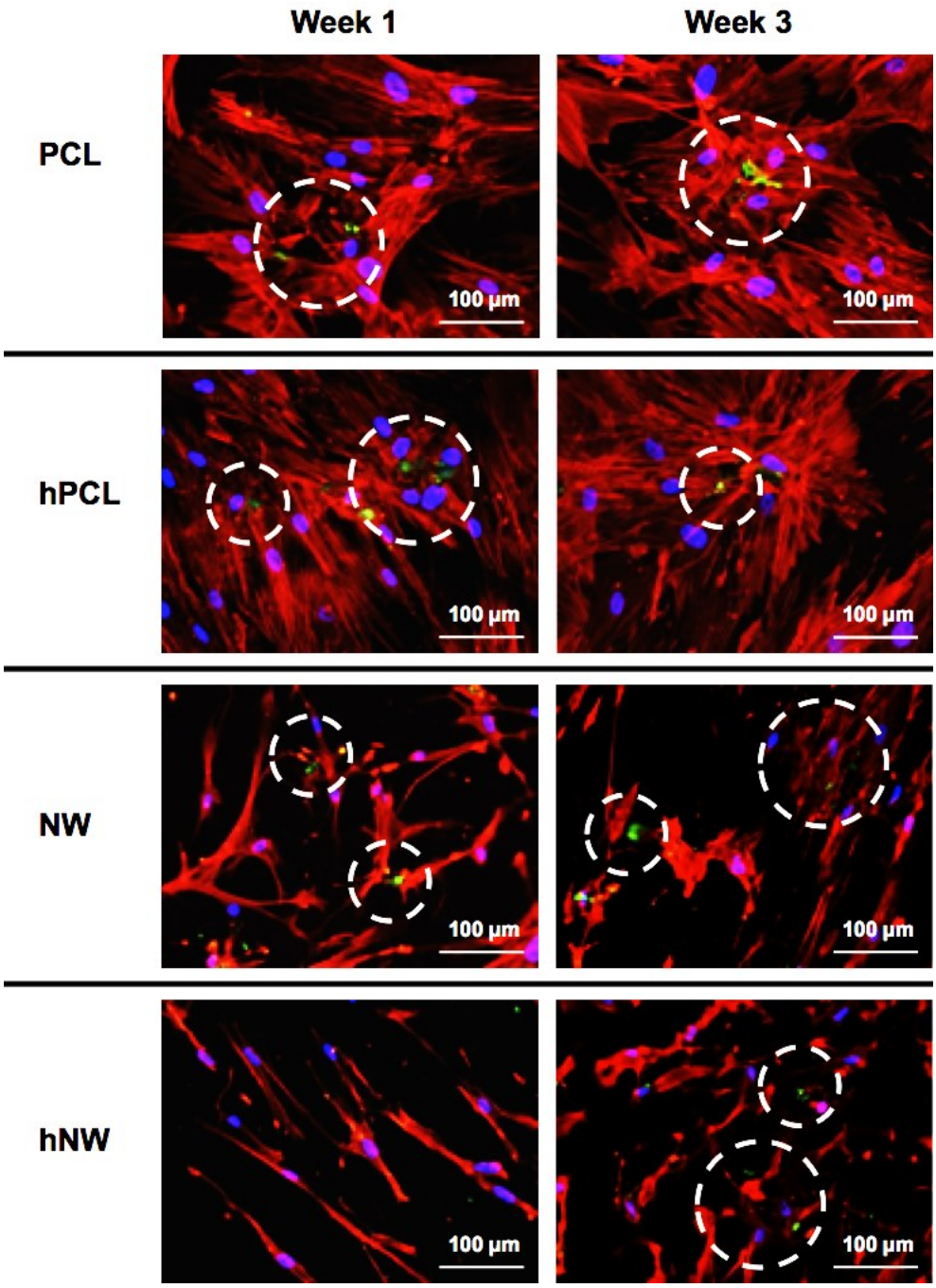

Figure 3.8: (a) Representative fluorescence microscopy images of ADSCs on PCL, hPCL, NW and hNW for Osteocalcin (green), actin (red) and nucleus (blue) after 1 and 3 weeks of culture in osteogenic conditions. Circles indicate the location of FITC-labeled osteocalcin.

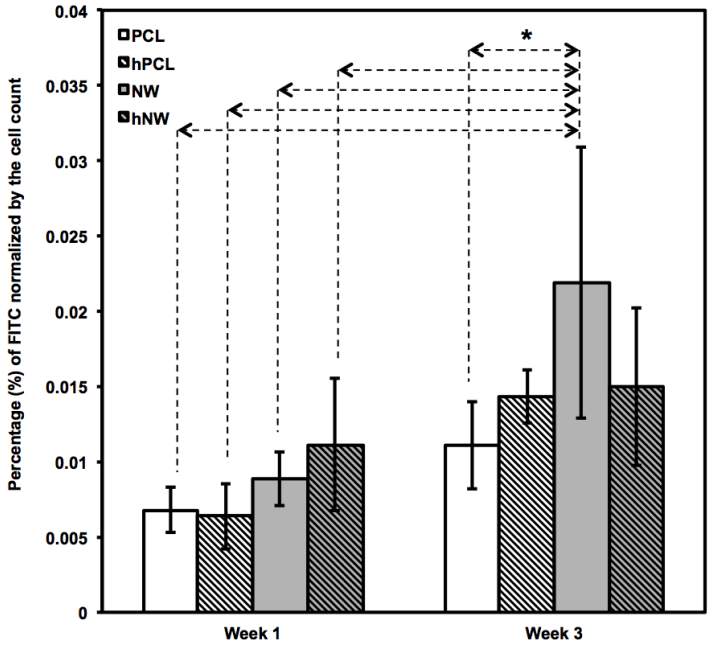

Figure 3.8: (b) Percentage of FITC-labeled osteocalcin normalized by total number of cells in an image.

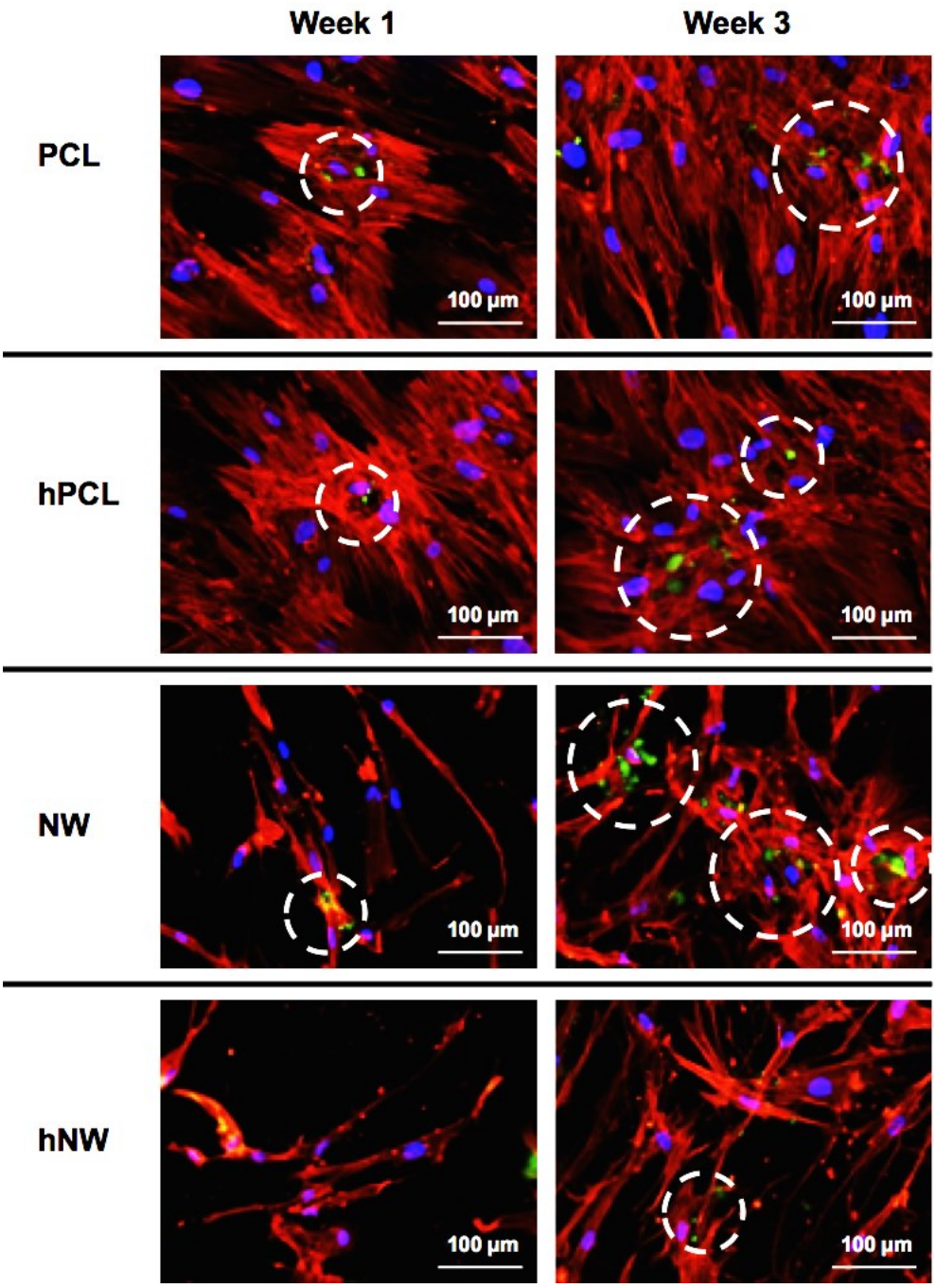

Figure 3.9: (a) Representative fluorescence microscopy images of ADSCs on PCL, hPCL, NW and nNW for osteopontin (green), actin (red) and nucleus (blue) after 1 and 3 weeks of culture in osteogenic conditions. Circles indicate the location of FITC-labeled osteopontin.

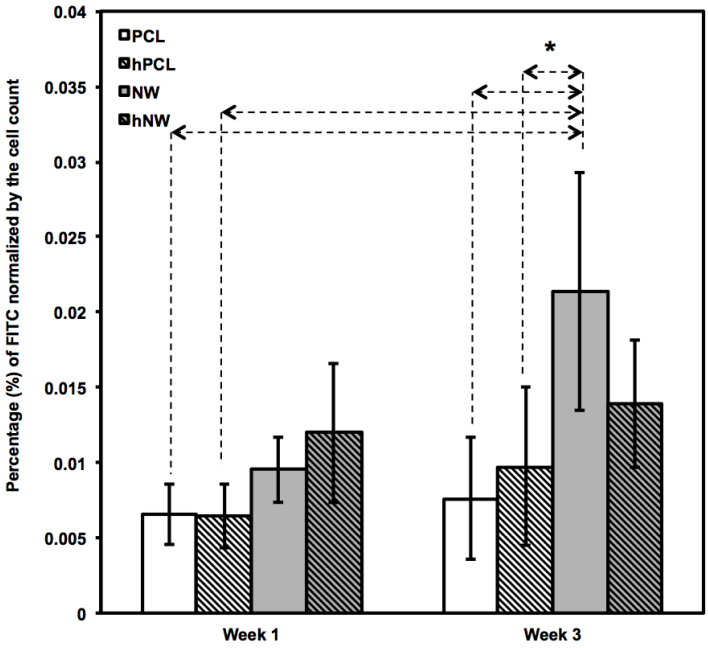

Figure 3.9: (b) Percentage of FITC-labeled osteopontin normalized by total number of cells in an image.

The cell morphology after 1 and 3 weeks of differentiation was investigated using SEM imaging (**Figure 3.10**). The results indicate higher number of cells on both PCL and hPCL surfaces. However, cells on NW and hNW surfaces have extended morphologies. It is evident from high magnification images that the cells on NW and hNW surfaces have many cellular extensions that are interacting with the nanowire morphology. Such interaction of the cells with the nanotopography may aid in cellular differentiation as evident from immunofluorescence imaging.

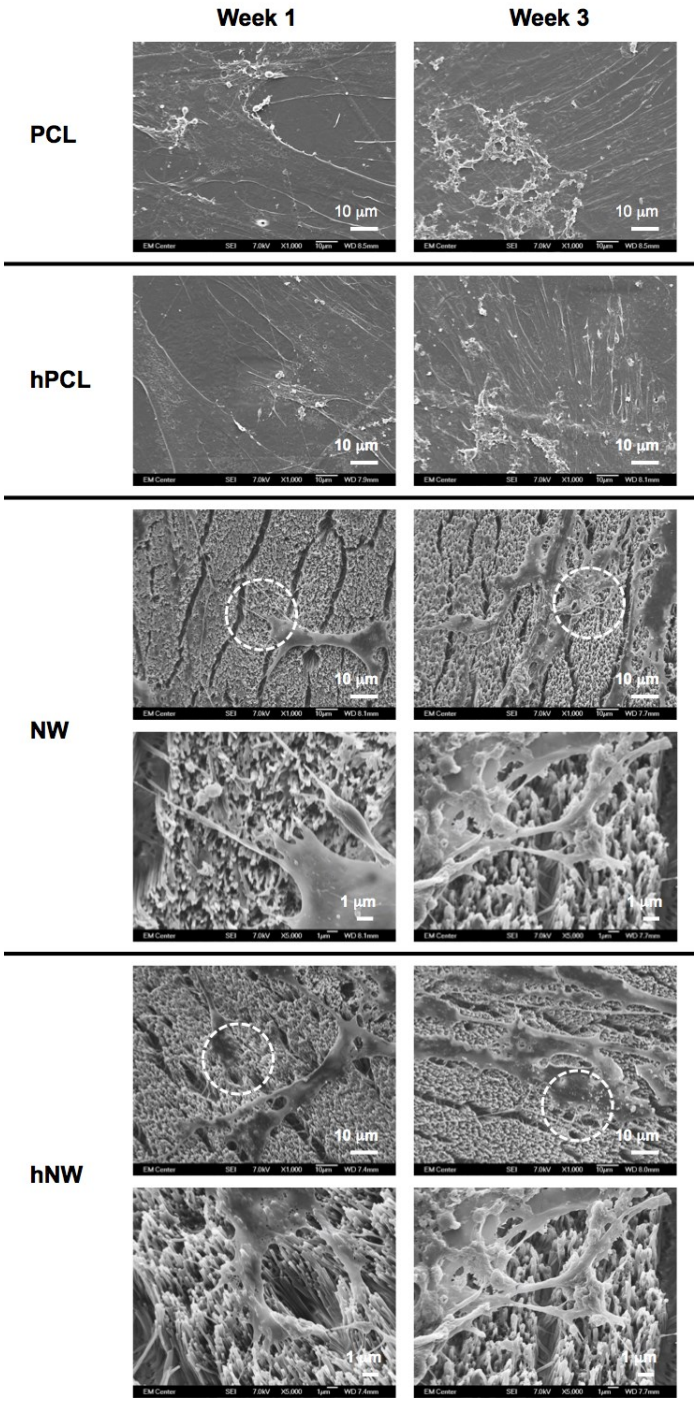

Figure 3.10: Representative SEM images of ADSCs on PCL, hPCL, NW, and hNW surfaces after 1 and 3 weeks of culture in osteogenic conditions. The high magnification images on NW and hNW surfaces show cell extensions and adhesion sites of differentiating ADSCs.

3.4 Conclusion:

The limitations of autografts and allografts for critical-sized defects have proven to be numerous and challenging to overcome. Biodegradable synthetic bone scaffolds hold a lot of promise for future treatment regimens because of their ability to promote cell migration and extracellular matrix production as the scaffold slowly degrades. Stem cells, which are a unique population of cells due to their ability to differentiate down multiple different cell pathways, have been heavily employed to assess bone synthetic scaffolds. Even though the bone marrow stroma has been the most widely used source for obtaining MSCs, there are many complications associated with harvesting these cells because of the invasive nature of the procedure. ADSCs, which are easier to harvest and abundant in the lipoaspirate tissue, were used in this study to evaluate the effect on nanotopography on cellular functionality. A solvent-free, gravimetric template synthesis technique was used to fabricate NW and hNW surfaces. Surface characterization techniques verified the NW surfaces have a uniform morphology, as well as the presence of HApon hNW surfaces. The NW and hNW surfaces both demonstratedlower ADSC adhesion and proliferation as compared to PCL and hPCL surfaces. However, ADSCs on NW and hNW surfaces displayed an elongated morphology with cellular extensions interacting with nanotopography. Further, all the surfaces expressed ALP activity for up to 3 weeks of culture in osteogenic conditions. However, NW surfaces expressed highest OC and OP expression, followed by hNW, PCL and hPCL surfaces. Overall this study has shown that the presence of hydroxyapatite nanoparticles does not have a significant effect on enhancing osteogenic differentiation, however the topography of the PCL nanowire surfaces has the most influence on ADSC behavior.

REFERENCES

1. Drosse, I., et al., *Tissue engineering for bone defect healing: an update on a multi-component approach.* Injury, 2008. **39 Suppl 2**: p. S9-20.
2. Mistry, A.S. and A.G. Mikos, *Tissue engineering strategies for bone regeneration.* Adv Biochem Eng Biotechnol, 2005. **94**: p. 1-22.
3. Khan, S.N., et al., *The biology of bone grafting.* J Am Acad Orthop Surg, 2005. **13**(1): p. 77-86.
4. Silber, J.S., et al., *Donor site morbidity after anterior iliac crest bone harvest for single-level anterior cervical discectomy and fusion.* Spine (Phila Pa 1976), 2003. **28**(2): p. 134-9.
5. Heary, R.F., et al., *Persistent iliac crest donor site pain: independent outcome assessment.* Neurosurgery, 2002. **50**(3): p. 510-6; discussion 516-7.
6. Kretlow, J.D. and A.G. Mikos, *Review: mineralization of synthetic polymer scaffolds for bone tissue engineering.* Tissue Eng, 2007. **13**(5): p. 927-38.
7. Arrington, E.D., et al., *Complications of iliac crest bone graft harvesting.* Clin Orthop Relat Res, 1996(329): p. 300-9.
8. Nakajima, T., et al., *Evaluation of posterolateral spinal fusion using mesenchymal stem cells: differences with or without osteogenic differentiation.* Spine (Phila Pa 1976), 2007. **32**(22): p. 2432-6.
9. Langer, R. and J.P. Vacanti, *Tissue engineering.* Science, 1993. **260**(5110): p. 920-6.
10. Heino, T.J. and T.A. Hentunen, *Differentiation of osteoblasts and osteocytes from mesenchymal stem cells.* Curr Stem Cell Res Ther, 2008. **3**(2): p. 131-45.

11. Haynesworth, S.E., et al., *Characterization of cells with osteogenic potential from human marrow.* Bone, 1992. **13**(1): p. 81-8.

12. Prockop, D.J., *Marrow stromal cells as stem cells for continual renewal of nonhematopoietic tissues and as potential vectors for gene therapy.* Journal of Cellular Biochemistry, 1998: p. 284-285.

13. Jorgensen, N.R., et al., *Dexamethasone, BMP-2, and 1,25-dihydroxyvitamin D enhance a more differentiated osteoblast phenotype: validation of an in vitro model for human bone marrow-derived primary osteoblasts.* Steroids, 2004. **69**(4): p. 219-26.

14. Johnson, M.R., et al., *Sustained release of BMP-2 in a lipid-based microtube vehicle.* Acta Biomater, 2009. **5**(1): p. 23-8.

15. Laflamme, C. and M. Rouabhia, *Effect of BMP-2 and BMP-7 homodimers and a mixture of BMP-2/BMP-7 homodimers on osteoblast adhesion and growth following culture on a collagen scaffold.* Biomedical Materials, 2008. **3**(1).

16. Laurencin, C.T., et al., *Poly(lactide-co-glycolide)/hydroxyapatite delivery of BMP-2-producing cells: a regional gene therapy approach to bone regeneration.* Biomaterials, 2001. **22**(11): p. 1271-1277.

17. Lee, J.Y., et al., *Osteoblastic differentiation of human bone marrow stromal cells in self-assembled BMP-2 receptor-binding peptide-amphiphiles.* Biomaterials, 2009. **30**(21): p. 3532-3541.

18. Albrektsson, T. and C. Johansson, *Osteoinduction, osteoconduction and osseointegration.* Eur Spine J, 2001. **10 Suppl 2**: p. S96-101.

19. Zheng, B., et al., *Mouse adipose-derived stem cells undergo multilineage differentiation in vitro but primarily osteogenic and chondrogenic differentiation in vivo.* Tissue Engineering, 2006. **12**(7): p. 1891-1901.

20. Bunnell, B.A., et al., *Adipose-derived stem cells: isolation, expansion and differentiation.* Methods, 2008. **45**(2): p. 115-20.

21. Katz, A.J., et al., *Emerging approaches to the tissue engineering of fat.* Clin Plast Surg, 1999. **26**(4): p. 587-603, viii.

22. Halvorsen, Y.D.C., et al., *Extracellular matrix mineralization and osteoblast gene expression by human adipose tissue-derived stromal cells.* Tissue Engineering, 2001. **7**(6): p. 729-741.

23. Zuk, P.A., et al., *Human adipose tissue is a source of multipotent stem cells.* Molecular Biology of the Cell, 2002. **13**(12): p. 4279-4295.

24. Zuk, P.A., et al., *Multilineage cells from human adipose tissue: Implications for cell-based therapies.* Tissue Engineering, 2001. **7**(2): p. 211-228.

25. Rho, J.Y., L. Kuhn-Spearing, and P. Zioupos, *Mechanical properties and the hierarchical structure of bone.* Med Eng Phys, 1998. **20**(2): p. 92-102.

26. Sato, M. and T.J. Webster, *Nanobiotechnology: implications for the future of nanotechnology in orthopedic applications.* Expert Rev Med Devices, 2004. **1**(1): p. 105-14.

27. Stevens, M.M. and J.H. George, *Exploring and engineering the cell surface interface.* Science, 2005. **310**(5751): p. 1135-8.

28. Taton, T.A., *Nanotechnology. Boning up on biology.* Nature, 2001. **412**(6846): p. 491-2.

29. Kim, S.S., et al., *Poly(lactide-co-glycolide)/hydroxyapatite composite scaffolds for bone tissue engineering.* Biomaterials, 2006. **27**(8): p. 1399-409.

30. Rezwan, K., et al., *Biodegradable and bioactive porous polymer/inorganic composite scaffolds for bone tissue engineering.* Biomaterials, 2006. **27**(18): p. 3413-3431.

31. Wei, G.B. and P.X. Ma, *Structure and properties of nano-hydroxyapatite/polymer composite scaffolds for bone tissue engineering.* Biomaterials, 2004. **25**(19): p. 4749-4757.

32. Palmer, L.C., et al., *Biomimetic Systems for Hydroxyapatite Mineralization Inspired By Bone and Enamel.* Chemical Reviews, 2008. **108**(11): p. 4754-4783.

33. Lee, J.H., et al., *Control of Osteogenic Differentiation and Mineralization of Human Mesenchymal Stem Cells on Composite Nanofibers Containing Poly [lactic-co-(glycolic acid)] and Hydroxyapatite.* Macromolecular Bioscience, 2010. **10**(2): p. 173-182.

34. Zhang, P.B., et al., *In vivo mineralization and osteogenesis of nanocomposite scaffold of poly (lactide-co-glycolide) and hydroxyapatite surface-grafted with poly(L-lactide).* Biomaterials, 2009. **30**(1): p. 58-70.

35. Cui, W.U., et al., *In situ growth of hydroxyapatite within electrospun poly(DL-lactide) fibers.* Journal of Biomedical Materials Research Part A, 2007. **82A**(4): p. 831-841.

36. Fang, B., et al., *Proliferation and Osteoblastic Differentiation of Human Bone Marrow Stromal Cells on Hydroxyapatite/Bacterial Cellulose Nanocomposite Scaffolds.* Tissue Engineering Part A, 2009. **15**(5): p. 1091-1098.

37. Guarino, V., et al., *The Influence of Hydroxyapatite Particles on In Vitro Degradation Behavior of Poly epsilon-Caprolactone-Based Composite Scaffolds.* Tissue Engineering Part A, 2009. **15**(11): p. 3655-3668.

38. Mei, F., et al., *Improved biological characteristics of poly(L-lactic acid) electrospun membrane by incorporation of multiwalled carbon nanotubes/hydroxyapatite nanoparticles.* Biomacromolecules, 2007. **8**(12): p. 3729-3735.

39. Biggs, M.J.P., et al., *The use of nanoscale topography to modulate the dynamics of adhesion formation in primary osteoblasts and ERK/MAPK signalling in STRO-1+enriched skeletal stem cells.* Biomaterials, 2009. **30**(28): p. 5094-5103.

40. Dalby, M.J., et al., *The control of human mesenchymal cell differentiation using nanoscale symmetry and disorder.* Nature Materials, 2007. **6**(12): p. 997-1003.

41. Olivares-Navarrete, R., et al., *Direct and indirect effects of microstructured titanium substrates on the induction of mesenchymal stem cell differentiation towards the osteoblast lineage.* Biomaterials, 2010. **31**(10): p. 2728-2735.

42. Ruckh, T.T., et al., *Osteogenic differentiation of bone marrow stromal cells on poly(epsilon-caprolactone) nanofiber scaffolds.* Acta Biomaterialia, 2010. **6**(8): p. 2949-2959.

43. Bechara, S., L. Wadman, and K.C. Popat, *Electroconductive polymeric nanowire templates facilitates in vitro C17.2 neural stem cell line adhesion, proliferation and differentiation.* Acta Biomaterialia, 2011. **7**(7): p. 2892-2901.

44. Porter, J.R., A. Henson, and K.C. Popat, *Biodegradable poly(epsilon-caprolactone) nanowires for bone tissue engineering applications.* Biomaterials, 2009. **30**(5): p. 780-788.

45. Bessho, K., et al., *Experimental studies on bone induction using low-molecular-weight poly (DL-lactide-co-glycolide) as a carrier for recombinant human bone morphogenetic protein-2.* J Biomed Mater Res, 2002. **61**(1): p. 61-5.

46. Garcia, A.J. and C.D. Reyes, *Bio-adhesive surfaces to promote osteoblast differentiation and bone formation.* J Dent Res, 2005. **84**(5): p. 407-13.

47. Heckmann, L., et al., *Interactive effects of growth factors and three-dimensional scaffolds on multipotent mesenchymal stromal cells.* Biotechnol Appl Biochem, 2008. **49**(Pt 3): p. 185-94.

48. Liu, S.J., et al., *Novel solvent-free fabrication of biodegradable poly-lactic-glycolic acid (PLGA) capsules for antibiotics and rhBMP-2 delivery.* Int J Pharm, 2007. **330**(1-2): p. 45-53.

49. Ruhe, P.Q., et al., *Bone inductive properties of rhBMP-2 loaded porous calcium phosphate cement implants in cranial defects in rabbits.* Biomaterials, 2004. **25**(11): p. 2123-32.

50. Wilson, C.J., et al., *Mediation of biomaterial-cell interactions by adsorbed proteins: a review.* Tissue Eng, 2005. **11**(1-2): p. 1-18.

CHAPTER 4

CHONDROGENIC DIFFERENTIATION OF ADIPOSE-DERIVED STEM CELLS ON NANOWIRE SURFACES UNDER CHONDROGENIC CONDITIONS

4.1 Introduction

It is important to mimic the *in vivo* environment of cells when designing scaffolds for tissue engineering. The motivation to use nanostructured surfaces as scaffolds for tissue engineering is driven by previous studies that have shown that nanoscale materials affect cell behavior such as morphology, functionality and cell-cell interactions [1-3]. In natural tissues, cells are surrounded by an extracellular matrix which consists of features ranging from nanometers to micrometers. Furthermore, studies have shown that nanoscale surfaces contributed to improving cell behavior such as fibroblast adhesion [4], neuronal differentiation [5], and osteoblast phenotypic activity [6, 7]. Therefore, nanotopography may result in improved cellular adhesion and thus, enhanced matrix deposition on the surface for other cell types such as chondrocytes. It could also be possible that these nanostructured surfaces, which are not able to allow cellular in-growth due to their size, will instead, provide a biomimetic template for matrix deposition.

Cartilage tissue possesses a unique nanostructure rarely duplicated in synthetic materials. Specifically, chondrocytes are naturally accustomed to interacting with a well-organized nanostructured collagen matrix [8]. The unique microarchitecture of extracellular cartilage matrix facilitates the load transfer and provides resistance to tensile, compressive, and shear stresses. Unlike other tissues, in hyaline cartilage, roughly 85% consists of extracellular matrix materials while only 15% are taken by chondrocytes [9]. The extracellular matrix overtakes the

biomechanical function of the cartilage and the small number of cells only responsible for its preservation and regeneration [9]. Similar to osteoblast interaction with surrounding surfaces *in vitro*, chondrocyte functionality is also heavily regulated by surface micro and nano topography *in vitro.* The most common nanostructured materials developed for chondrogenic tissue engineering applications are nanofiber scaffolds. Recent studies have used synthetic polymers such as polycaprolactone and poly (lactic-co-glycolic acid) to develop nanofibrous scaffolds of electropun nanofibers to differentiate MSCs to chondrocytes and maintain their mature functionality [10]. In addition, polycaprolactone nanofiber scaffolds have been used in conjunction with submersion in a dioxane/water mixture and phase separated to create a nanoporous structure [11]. These polycaprolactone nanoporous scaffolds demonstrated higher in vitro expression of chondrogenic markers and had higher histological scored in comparison with commercially available collagen scaffolds typically used for cartilage repair [11].

In this study, we use a solvent-free gravimetric template method to physically modify the surface of polycaprolactone with controlled arrays of high aspect ratio substrate-bound perpendicular nanowires. In this study, these nanowire surfaces were used as templates for growth and maintenance of ADSCs, and their potential to support differentiated states of these cells. Specifically, this study focuses on characterizing the ability of ADSCs to differentiate into chondrogenic phenotypes on nanowire surfaces.

4.2 Methods

4.2.1 ADSC culture on PCL and nanowire surfaces

Adult human ADSCs at passage 2 (Zen-Bio Inc.) were expanded using standard cell culture techniques. All the cells used in this study were at passage 5 or below. Cells were detached using 0.25% Trypsin-EDTA and suspended in growth media consisting of DMEM with 10% fetal bovine serum (FBS, Sigma) and 1% penicillin/streptomycin (Sigma). All the surfaces were sterilized by incubating in 70% ethanol at room temperature followed by exposure to UV light for 30 min. Following sterilization, the surfaces were rinsed twice with warm phosphate buffered saline (PBS). Cells were seeded on all surfaces in 48-well plates at a density of 5,000 cells/well. The surfaces were incubated at 37ºC and 5% CO_2 for the entire duration of the study. Half of the growth media was changed on day 4. On day 7, all the growth media was replaced with chondrogenic differentiation media and the cells were cultured for up to 3 weeks. Chondrogenic differentiation media consisted of growth media plus dexamethasone (10^{-7} M), ascorbic acid (50 mg/ml), ITS+ premix (1%) and TGF-β1 (10 ng/ml). Media was changed every other day for the entire duration of the culture.

4.2.2 ADSC adhesion and proliferation on PCL and nanowire surfaces

After 1, 4 and 7 days of initial culture, ADSC adhesion, proliferation, and spatial organization were investigated by staining the adhered cells with 5-Chloromethylfluorescein diacetate (CMFDA – live cells), rhodamine-phalloidin (actin – cytoskeleton), and 4',6-diamidino-2-phenylindole (DAPI – nucleus). At each time point, the surfaces were removed from the growth media, and incubated in the CMFDA stain at a concentration of 10 μM for 45 min in a 37°C and 5% CO_2 incubator. Next, the substrates were incubated for another 30 min at

37°C and 5% CO_2 in warm growth medium. The cells were then fixed with 3.7% formaldehyde for 15 min at room temperature. In order to permeabilize the cells, the surfaces were incubated in 1% Triton-X 100 for 3 min. The substrates were then incubated in rhodamine-phalloidin stain at a concentration of 5μL/mL for 30 min. After 25min of rhodamine-phalloidin staining, DAPI was added at a concentration of 300mM. The substrates were then rinsed in PBS and imaged using a Zeiss Axioplan 2 fluorescence microscope. The number of adhered cells on all the surfaces was determined from 5x DAPI stained images by counting the individual nuclei using ImageJ software. In addition to cell counts, cell shape factor was also determined using Image J software with 10× rhodamine-phalloidin stained images. The cell shape factor was approximated by the ratio of cellular width to cellular length. The cellular width was defined as the diameter of the largest circle that would fit entirely within the cell and the cellular length was defined by the diameter of the smallest circle that encompassed the entire cell.

Cell viability was measured after 1, 4 and 7 days of initial culture (log phase growth) using a commercially available MTT assay kit (Sigma). Adhered cells were incubated at 37ºC for 3 hrs in a (3-[4,5-dimethylthiazol-2-yl]-2,5-diphenyl tetrazolium bromide (MTT) solution. Mitochondrial dehydrogenase of viable cells cleaves the tetrazolium ring leaving behind purple formazan crystals. The formazan crystals were dissolved in the MTT solvent. The optical density (OD) of the resulting solvent was measured at 570nm using a spectrophotometer (FLUOstar Omega; BMG Labtech, Durham, NC). Background absorbance was measured at 690 nm and subtracted from the measured absorbance.

Material cytotoxicity was characterized after 1, 4 and 7 days of initial culture using a commercially available lactate dehydrogenase (LDH) cytotoxicity assay kit (Cayman Chemical). The protocol provided by the manufacturer was followed. Substrates were rapidly shaken on a

horizontal shaker plate (1000 rpm) for 5 min at room temperature. The manufacturer-provided standards along with the substrate-exposed plasma samples were transferred to a 96 well plate. A reaction solution (96% v/v assay buffer, 1% v/v NAD+, 1% v/v Lactic Acid, 1% v/v INT, and 1% v/v LDH Diaphorase) was added in the amounts equal (1:1) to all standards and samples, and further incubated with gentle shaking on an orbital shaker for 30 min at room temperature. The absorbance of the solution was measured at a wavelength of 490 nm to determine the cytotoxic effects of the smooth PCL and nanowire substrates.

The morphology of the adhered ADSCs was investigated using SEM after 1, 4 and 7 days of culture. SEM was done to visualize how cells adhered and proliferated on the surfaces as well as how they interacted with the nanowire morphology. In brief, the cells were fixed in a solution of 3% glutaraldehyde, 0.1 M sodium cacodylate, and 0.1 M sucrose for 45 min. The surfaces were then incubated in a buffer containing 0.1 M sodium cacodylate and 0.1 M sucrose. After fixation, the cells were dehydrated by incubating the surfaces in increasing concentrations of ethanol (35%, 50%, 70%, 100%) for 10 min each. The surfaces were further dehydrated by incubating them in hexamethyldisilazane for 10 min. The surfaces were stored in a desiccator until examination using SEM. The surfaces were sputter coated with 10 nm of gold and imaged using at a voltage of 7 kV.

4.2.3 ADSC chondrogenic differentiation

ADSC responses to the different surfaces were evaluated after providing the cells with chonodrogenic differentiation media. After 1, 2 and 3 weeks of culture, ADSCs on different surfaces were immuno-labeled for Sox9 and Collagen 2 (Col2). Cells were fixed and permeabilized as described earlier. All the surfaces were incubated with 10% bovine serum albumin for 30 min at room temperature to prevent nonspecific binding. After rinsing in PBS, the surfaces were incubated with either anti-Sox9 primary antibody (1:100 in PBS, purified goat polyclonal antibody of human origin, Santa Cruz Biotechnology) or anti-Col2 primary antibody (1:100 in PBS, purified goat polyclonal antibody of mouse origin, Santa Cruz Biotechnology) for 1 hr at room temperature. Following primary antibody incubation, surfaces were rinsed three times with PBS at an interval of 5 min each. The surfaces were then incubated in FITC-labeled secondary antibodies for Sox9 and Col2 (1:200 donkey antigoat IgG, Santa Cruz Biotechnology) for 45 min in the dark. Finally, the surfaces were rinsed twice in PBS and incubated in rhodamine-phalloidin stain at a concentration of 5µl/ml for 30 min. After 25 min of rhodamine-phalloidin staining, DAPI was added at a concentration of 300 nM. The surfaces were then rinsed in PBS and visualized using a Zeiss Axioplan 2 fluorescence microscope. The number of adhered cells on all the surfaces after 1 and 3 weeks of culture was determined from 5x DAPI stained images by counting the individual nuclei using ImageJ software. Using the cell counts, cell proliferation ratio from day 7 to day 1 and week 3 to week 1 was calculated.

Glycosaminoglycan formation on the surfaces was detected using alcian blue staining after 1, 2, and 3 weeks of culture. All surfaces were rinsed twice in PBS followed by fixation in cold (4ºC) acetone:methanol solution for 3 min. Substrates were transferred to a 1% alcian blue solution in 3% acetic acid. The surfaces were incubated at room temperature in alcian blue for 30

min followed by three rinses in 3% acetic acid for 2 min each. After rinsing in deionized water for 2 minutes, the surfaces were allowed to dry for imaging or placed in a 1% SDS solution for 30 min on a 200 rpm shaker plate to solubilize the alcian blue stain. Absorbance of the solubilized solution was measured at 605nm.

The morphology of adhered ADSCs on surfaces was investigated using SEM after 1, 2 and 3 weeks of culture using the method described in previous section.

4.2.4 Statistical Analysis

Data within the graphs are expressed as the average count and the standard deviation of the mean. All the quantitative results were analyzed using paired t-test or one-way analysis of variance (ANOVA). Multiple comparisons are tested using Tukey's HSD. Statistical significance was considered at $p < 0.05$. All qualitative methods used $n_{min}=3$ and all quantitative methods used $n_{min}=5$. Experiments were repeated at least three times with three different cell culture populations.

4.3 Results and Discussion

Despite many advances in tissue engineering, there are still significant challenges associated with restructuring, repairing, or replacing damaged tissue in the body. Currently, a major obstacle has been trying to develop scaffolds for cartilage tissue engineering that provides the correct mechanical properties to endure the loads associated with articular joints as well as promote cell-scaffold interactions to aid in extracellular matrix deposition. In addition, adipogenic tissue engineering is widely growing due to an increased need for more innovative reconstruction therapies following adipose tissue traumas and cosmetic surgeries. Recently, lipoaspirate tissue has been identified as a viable alternative source for MSCs because it contains a supportive stroma that can easily be isolated. ADSCs can differentiate into a variety of mesodermal lineages including the chondrogenic phenotypes. This study is aimed at determining the effects of substrate bound nanowires surfaces on the viability and differentiation potential of ADSCs into a chondrogenic lineage.

Prior research with polycaprolactone NW surfaces have shown the ability of stem cells to differentiate into osteogenic lineages [12]. In this study, a similar sintering and solvent-free nanotemplating method was used to fabricate both PCL and NW. SEM images confirmed the presence of substrate bound perpendicular nanowires as well as the absence of residual alumina membrane (**Figure 4.1)**. SEM images also indicated randomized microchannels between the groups of nanowires due to static surface charge and surface tension following expansion of the nanowires after membrane dissolution. To ensure there would be adequate extrusion of the polymer through the aluminum oxide membrane during nanowire fabrication, the polymer was melted slightly above the melting temperature at 70°C for 20 min when the formation of a clear melt interface was present between the bulk material and the membrane.

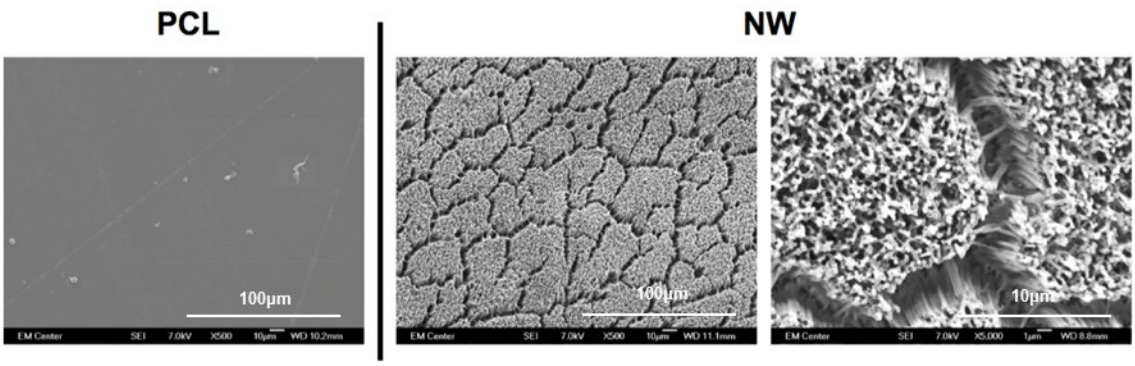

Figure 4.1: Representative SEM images of PCL and NW. The high magnification SEM images of NW show the nanoarchitecture as well as presence of randomized microchannels.

ADSC adhesion and proliferation were investigated for up to 7 days of initial culture in growth media by staining the cells with CellTracker™ Green CMFDA (5-Chloromethylfluorescein diacetate), rhodamine-phalloidin and DAPI (**Figure 4.2**). CMFDA fluorescent probes are FITC labeled which causes them to fluoresce green as they freely pass through the membranes of viable cells. Once these probes reach the cytoplasm, the probes are converted to cell-impermeant reaction products which are present throughout the cell. Once this reaction takes place, the cells can be fixed using a formalin solution. Rhodamine-phalloidin is a high affinity F-actin probe coupled with a red-orange fluorescent dye called tetramethylrhodamine isothiocyanate (TRITC). DAPI is a DNA stain which binds to the adenine-thymine rich regions and causes the nuclei of the cells to fluoresce blue. After 1 day of culture, both surfaces supported similar cell adhesion with different cell morphologies. On PCL, the cells appear to have "round" morphologies due to the actin filaments organizing themselves in all directions. On NW, the cells have elongated morphologies because the actin filaments of each cell appear to align in a specific direction with the nanowires. After 4 and 7 days of culture, both surfaces support cell proliferation with the slightly more cells on PCL as compared to NW

(**Figure 4.2)**. However, although NW have lesser number of cells, their extended morphologies appear to form networks with neighboring cells using cellular extensions.

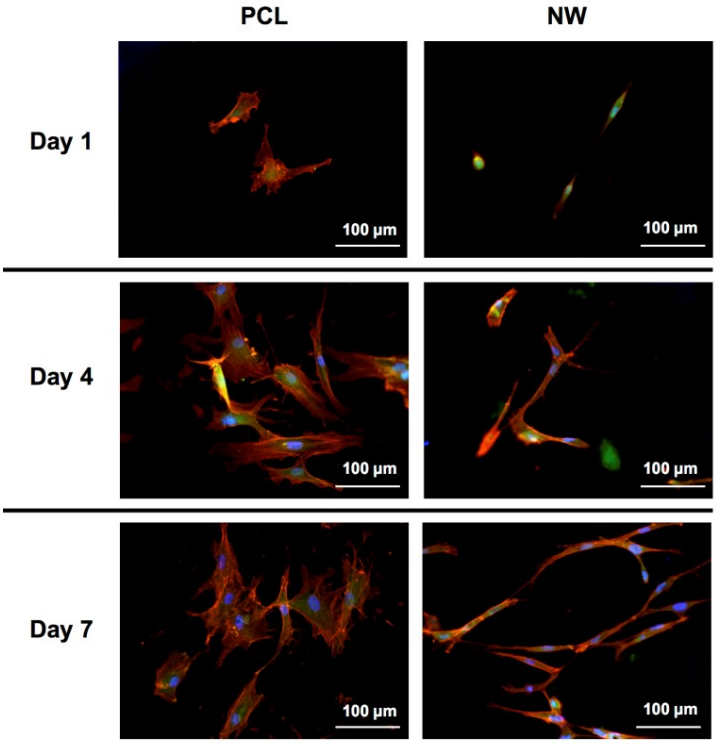

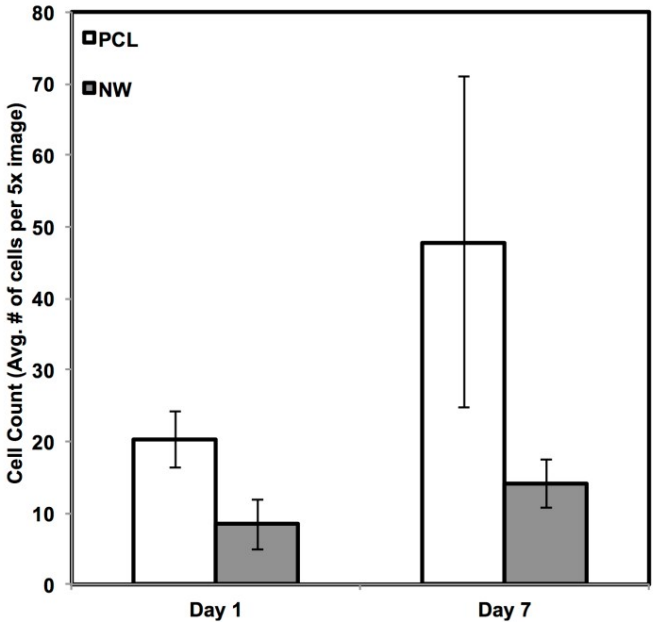

Figure 4.2: Representative fluorescence microscopy images of ADSCs on PCL and NW after 1, 4, and 7 days of culture; cell count after 1 and 7 days of culture. Cell nuclei were counted using DAPI fluorescence and ImageJ software.

The cell morphology was partially quantified by calculating the cell shape factor using 10× rhodamine-phalloidin stained images after 7 days of culture (**Figure 4.3**). The shape factor is an important quantitative parameter that indicates the whether the cell is spherical or elongated. A shape factor → 1 indicated that the cell has spherical morphology, whereas shape factor → 0 indicated that the cell has elongated morphology. The shape of the cell is important since it not only affects cell migration and communication, but also the cell differentiation. The results indicate that the cell on PCL have shape factor higher than that on NW. This indicated that the cells have spherical morphology on PCL compared to elongated morphology on NW.

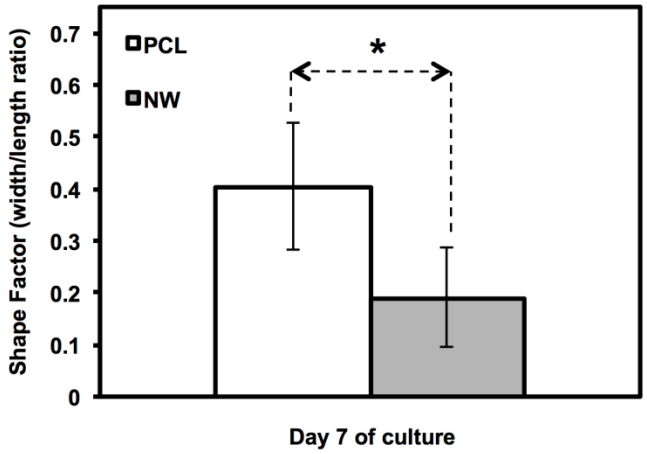

Figure 4.3: Shape factor approximations of ADSCs after 7 days of culture on PCL and NW. Asterisks (*) above the pairs of data indicate statistical significance using p-value less than α=0.05.

The cell viability on all the surfaces was investigated using MTT assay after 1, 4, and 7 days of culture in growth media conditions (**Figure 4.4a**). MTT activity is measure of cell viability by quantifying the absorbance of mitochondrial activity. During the first 4 days of culture, mitochondrial activity is most likely directed at increasing the proliferation of cells across the surfaces. After 1 day of culture, the results indicate approximately an equal amount of MTT activity on both surfaces. Although both surfaces continue to have steady and significant increases from day 1 to day 7, there appears to be more MTT activity on the PCL in comparison with NW which confirms the results from the fluorescence microscopy images and cell counts. The number of cells that initially attach to PCL after one day of culture is double in comparison with NW and this correlates with the MTT results.

In addition to observing cell viability, it is also essential to determine whether the surfaces have any cytotoxic effects that may be inhibiting cell adhesion or proliferation. Material cytotoxicity was determined through an LDH assay (**Figure 4.4b**). LDH is an enzyme located inside the cytoplasm of cells that is released upon cell death. This assay measures the amount of formazan following a two-step reduction, where LDH catalyzes NAD+ to NADH and H+ by oxidation and a subsequent catalyst reaction by diaphorase converting tetrazolium salt to a colored formazan. Measurements using spectrophotometery determine the concentration of LDH released into the culture medium, or in other words, determine the level of cell death due to possible cytotoxic effects from the substrate. From day 1 to day 4, there is an increase in LDH absorbance, due to initial cell death and detachment from the surfaces in the first 4 days of the growth period. However, this absorbance level decreases from day 4 to day 7, which means that both surfaces, PCL and NW, are not cytotoxic to the cells over time.

(a)

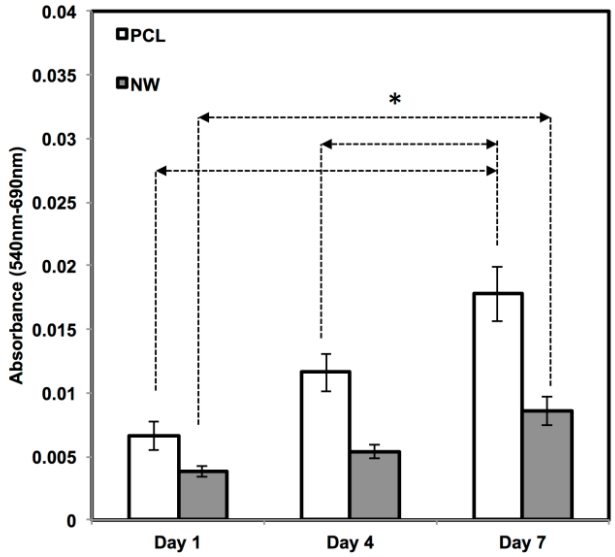

(b)

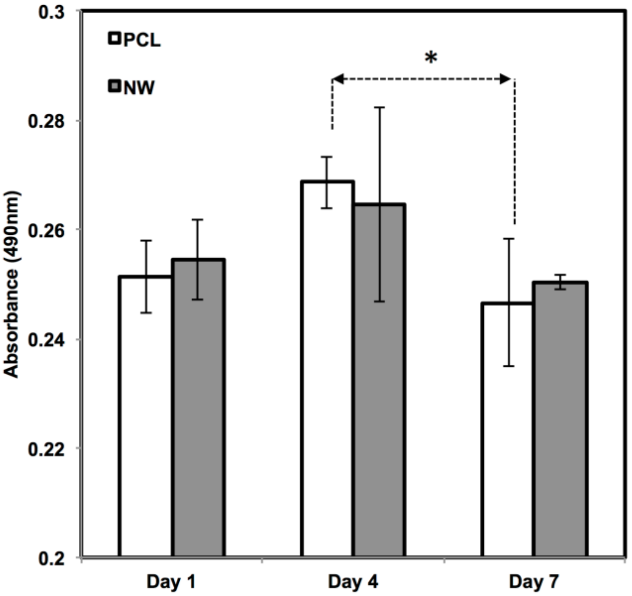

Figure 4.4: (a) ADSC viability after 1, 4, and 7 days of culture using MTT absorbance. Data indicates increased MTT activity on all surfaces with significant increases on PCL. (b) Cytotoxicity of the surfaces after 1, 4, and 7 days of culture using LDH absorbance. Asterisks (*) above the pairs of data indicate statistical significance using p-value less than α=0.05.

To visualize the morphological changes in the cells on different surfaces, SEM images were taken after 1, 4 and 7 of culture (**Figure 4.5**). In addition to morphology, SEM also allows for visualization of the interaction of the cell processes with the surface nanoarchitecture as well as amongst cells. The SEM results support the results from fluorescence microscopy indicating higher number of cells on PCL than NW, as well as elongated cell morphologies on NW. The cells on PCL seem to spread in all directions with limited interaction with other cells. In contrast, the cells on NW have longer cellular extensions that seem to be involved in cell to cell communication. High magnification SEM images of cells on NW show that the cellular extensions are interacting with the nanowire architecture after 1 day of culture. These extensions seem to be longer after 7 days of culture showing the interaction of the cells with the nanowire architecture as well as form a complex cellular network.

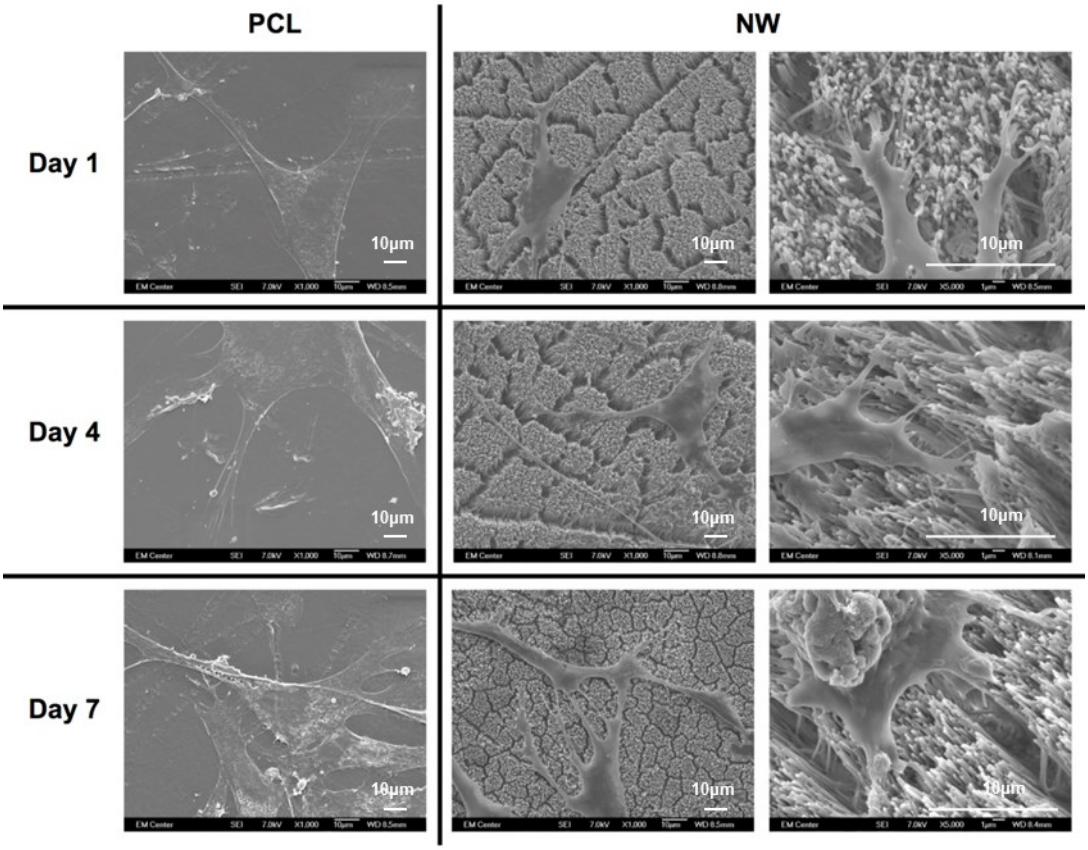

Figure 4.5: Representative SEM images of ADSCs on PCL and NW after 1, 4, and 7 days of culture. The high magnification images on NW show cell extensions and adhesion sites between the ADSCs and the individual nanowires.

For surfaces cultured under chondrogenic differentiation conditions, ADSCs on the different surfaces were immuno-labeled for sox9 and col2 (collagen type II) (**Figure 4.6a** and **Figure 4.6b**). Sox9 is a protein transcribed by the sox9 gene within the nucleus and is an early marker for differentiation as well as a marker for mature chondrocytes. Although sox9 is present during most of the chondrogenic differentiation process, it is not expressed by cells undergoing hypertrophic chondrogenesis. Col2 is the basis for all articular cartilage and is a marker for maturing chondrocytes. Intracellular sox9 and intra/extracellular col2 was detected by FITC-labeled immunofluorescence after 1, 2 and 3 weeks ADSCs culture under chondrogenic conditions.

(a)

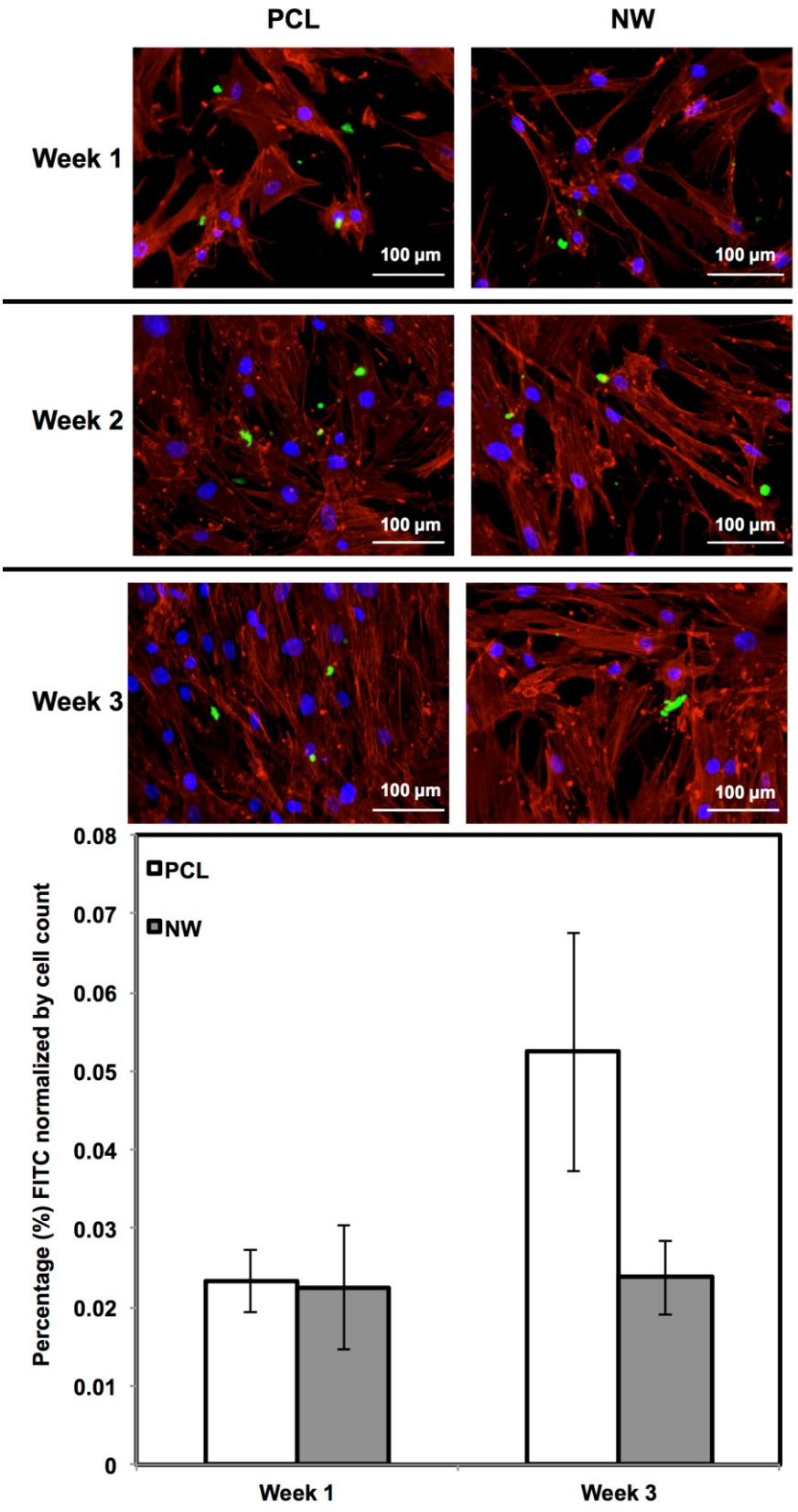
PCL
NW
Week 1
Week 2
Week 3
100 µm
Percentage (%) FITC normalized by cell count
0.08
0.07
0.06
0.05
0.04
0.03
0.02
0.01
0
PCL
NW
Week 1
Week 3

(b)

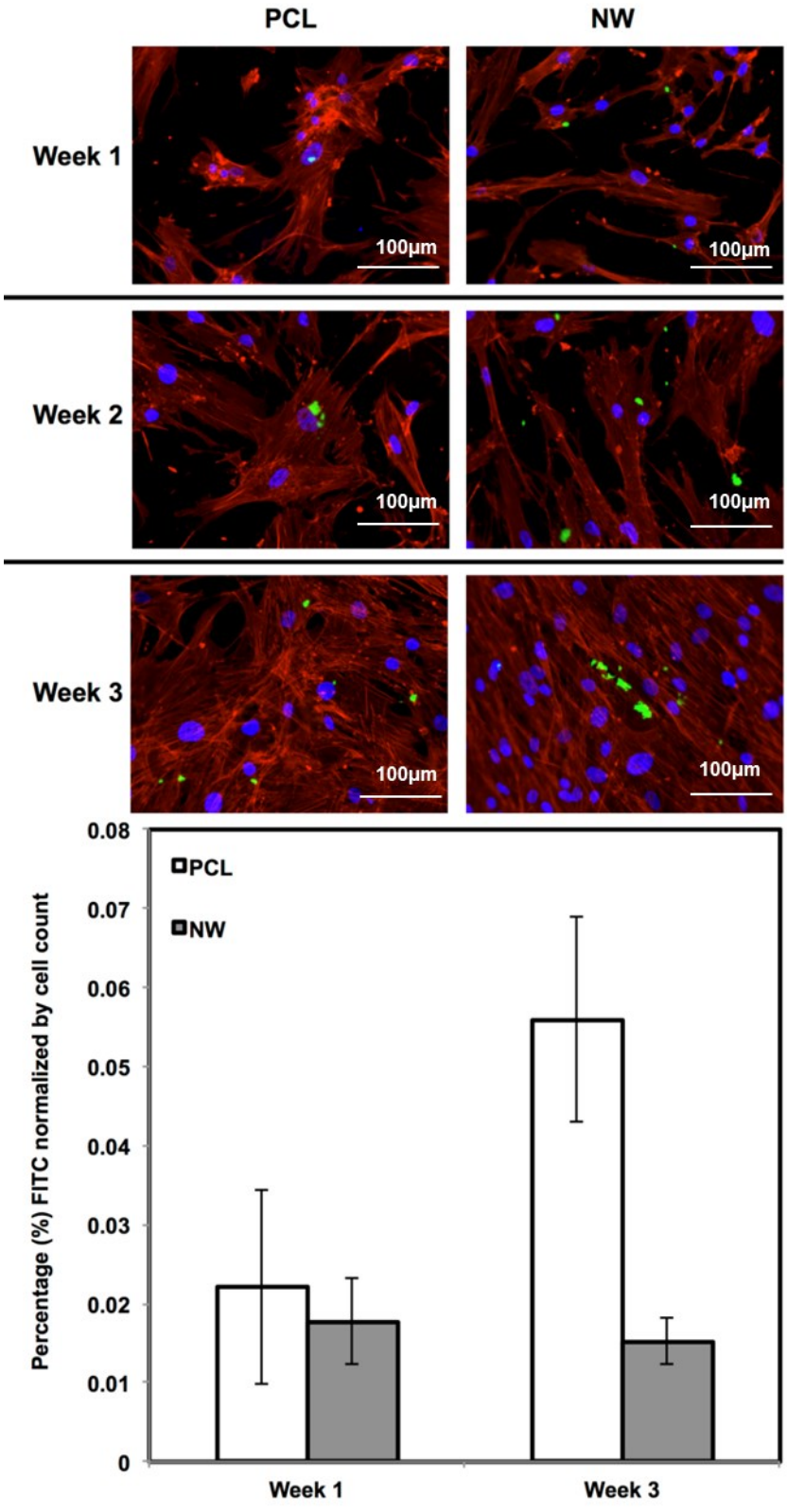
PCL
NW
Week 1
Week 2
Week 3
100μm
Percentage (%) FITC normalized by cell count
0.08
0.07
0.06
0.05
0.04
0.03
0.02
0.01
0
PCL
NW
Week 1
Week 3

Figure 4.6: (a) Representative immunofluorescence images of ADSCs on PCL and NW for sox9 (green), actin (red) and nuclei (blue) after 1, 2, and 3 weeks of culture in chondrogenic conditions. (b) Representative immunofluorescence images of ADSCs on PCL and NW for col2 (green), actin (red) and nuclei (blue) after 1, 2, and 3 weeks of culture in chondrogenic conditions. Percentage of FITC-labeled sox9 (a) and col2 (b) were normalized by total number of cells within a particular image.

The percentage of FITC detected during immunofluorescence was normalized by the number of cells on the particular image (**Figures 4.7a and 4.7b**). For sox9 expression, the protein was present on both surfaces during all three weeks of differentiation. However, ADSCs on PCL saw an increase from week 1 to week 3 whereas ADSCs on NW saw the same amount of expression. Even though the percentage of FITC does not increase from week 1 to week 3 on NW, the amount of sox9 protein increases because the number of cells on the surfaces increased. A similar trend is observed for col2 expression on both surfaces. However, for both sox 9 and collagen 2, this increase protein expression on NW is significantly smaller in comparison to the cells on PCL. It appears that the nanotopography of NW does not have a significant effect on chondrogenic differentiation of ADSCs.

Since the chondrogenic differentiation media was supplemented with a high concentration of TGF-β1, there was increased proliferation on both PCL and NW from week 1 to week 3 (**Figure 4.8a**). The proliferation ratio for PCL during initial growth period (D7/D1) is lower to that during the differentiation period (W3/W1) (**Figure 4.8b**). Further, the proliferation ratio of NW during growth period (D7/D1) is also lower than that during the differentiation

period (W3/W1) (**Figure 4.8b**). This increase in proliferation is due the presence of TGF-β1 in the differentiation media.

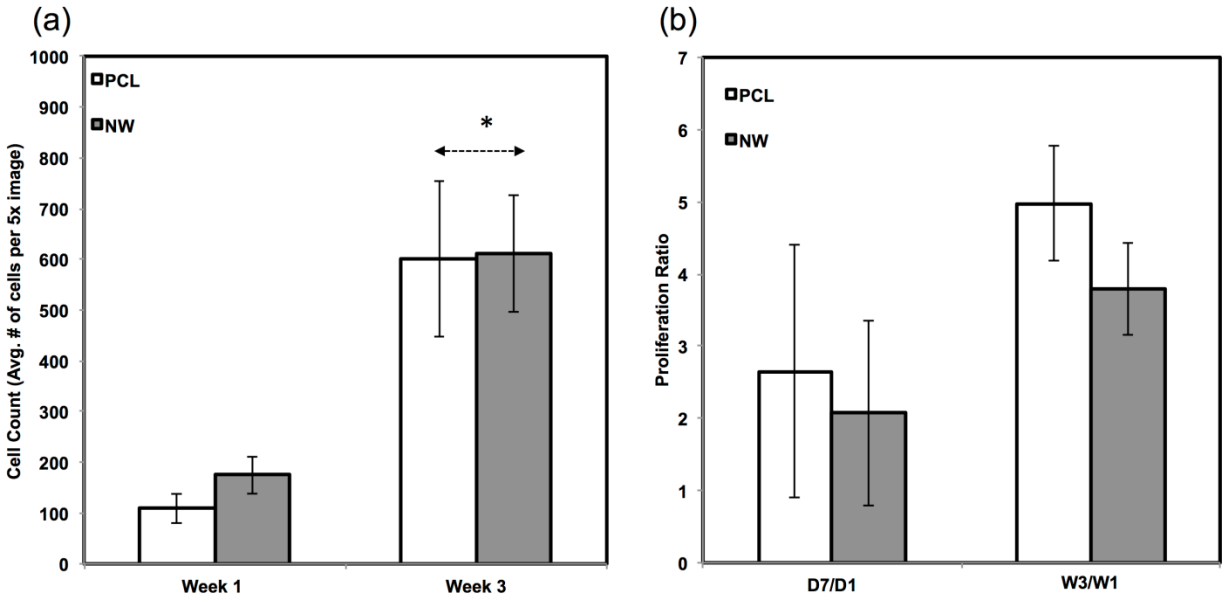

Figure 4.7: (a) Average cell counts on PCL and NW after 1 and 3 weeks of culture in chondrogenic conditions. Cell nuclei were counted using DAPI fluorescence and ImageJ software. (b) Comparisons of proliferation ratios between the growth period (D7/D1) and the differentiation period (W3/W1). Asterisks (*) above data pairs indicate statistical significance using p-value less than α=0.05.

In addition to observing protein expression via immunofluorescence, ADSCs were stained using alcian blue for early differentiation and extracellular matrix production (**Figure 4.8**). Alcian blue is a polyvalent dye that is used to stain for acidic polysaccharides such as glycosaminoglycans (GAGs) and sulfated glycosaminoglycans (sGAGs). These polysaccharides are widely present in all connective tissues and especially in both articular and hyaline cartilage tissue. After 1 week in chondrogenic differentiation conditions, both surfaces had little to no

staining of alcian blue, however it is evident after 3 weeks in chondrogenic differentiation conditions, both surfaces showed alcain blue staining indicating that GAGs were expressed on the surface. Alcian blue staining followed the same trend that was observed during sox 9 and col2 immunofluoresnce. Although both surfaces showed that GAGs were present, the PCL had much more alcian blue absorption than NW and therefore, more GAG production. Although the photos give a comparable qualitative measure of the stain, the alcian blue was solubilized in 1% SDS to give a quantitative measure of the dye using spectrophotometry. As expected, both surfaces saw an increase in alcian blue absorption from week 1 to week 3, but the adsorption on NW was less than PCL.

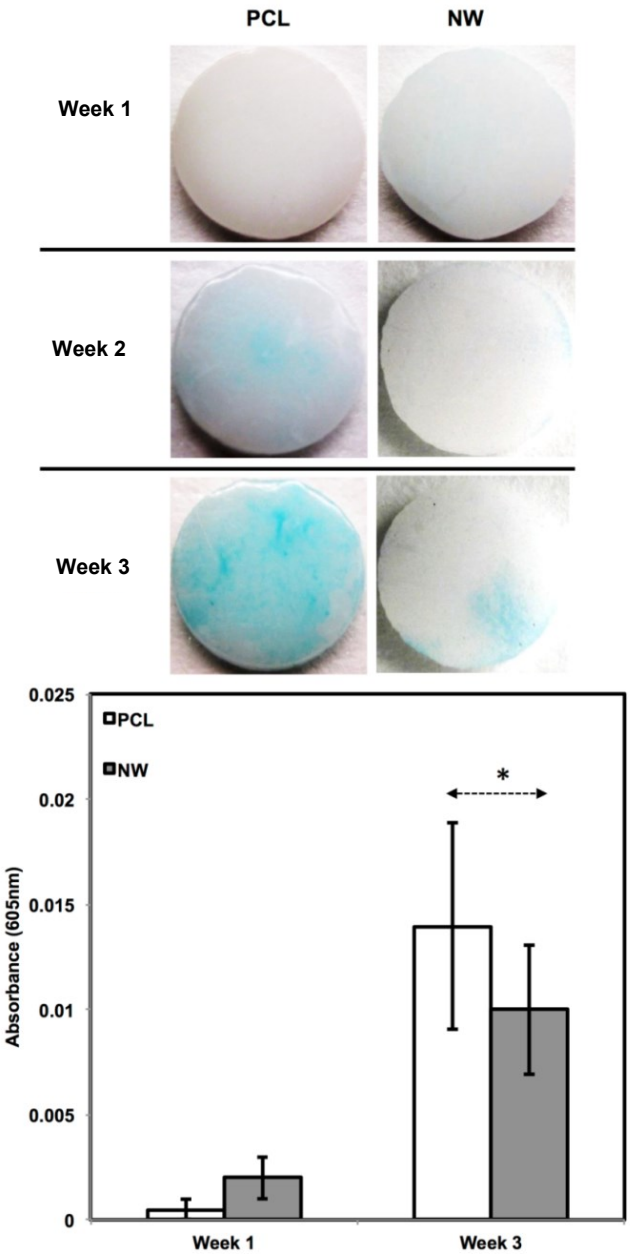

Figure 4.8: Alcian blue (GAG) staining of PCL and NW after 1, 2 and 3 weeks of culture in chondrogenic conditions as well as quantification of alcian blue absorbance after 1 and 3 weeks of culture. Asterisk (*) above Week 3 indicates statistical significance from Week1 using p-value less than α=0.05

To further understand the behavior of the ADSCs as they are subjected to chondrogenic differentiation, it is important to look at the role of cytoskeletal organization and cytoskeletal stress. Although spreading and aligning of the actin filaments of cells on NW and within the NW microgrooves is advantageous for osteogenesis to occur [12, 13], typical culture methods for inducing chondrogenic differentiation are done in suspension which involves little stress on the cells [14, 15]. Unlike the method used in this study, the cells pellets do not endure high cytoskeletal tensile stresses like they do on NW surfaces. Since the cells are more isotropic on the PCL, there is more chondrogenic differentiation than the cells that have aligned filaments on the NW.

The cell morphology after 1 and 3 weeks of chondrogenic differentiation was investigated using SEM imaging (**Figure 4.9)**. The results indicate higher number of cells on both PCL and NW, however, cells on NW have extended morphologies with cellular extension that interact with the individual nanowires. In the higher magnification images of cells on NW, it is evident that the cells were attaching with individual nanowires that allows them to stretch long distances as they migrate across the surface. In addition, some of the ADSCs interact with the nanowires by embedding themselves between the grooves of grouped nanowires.

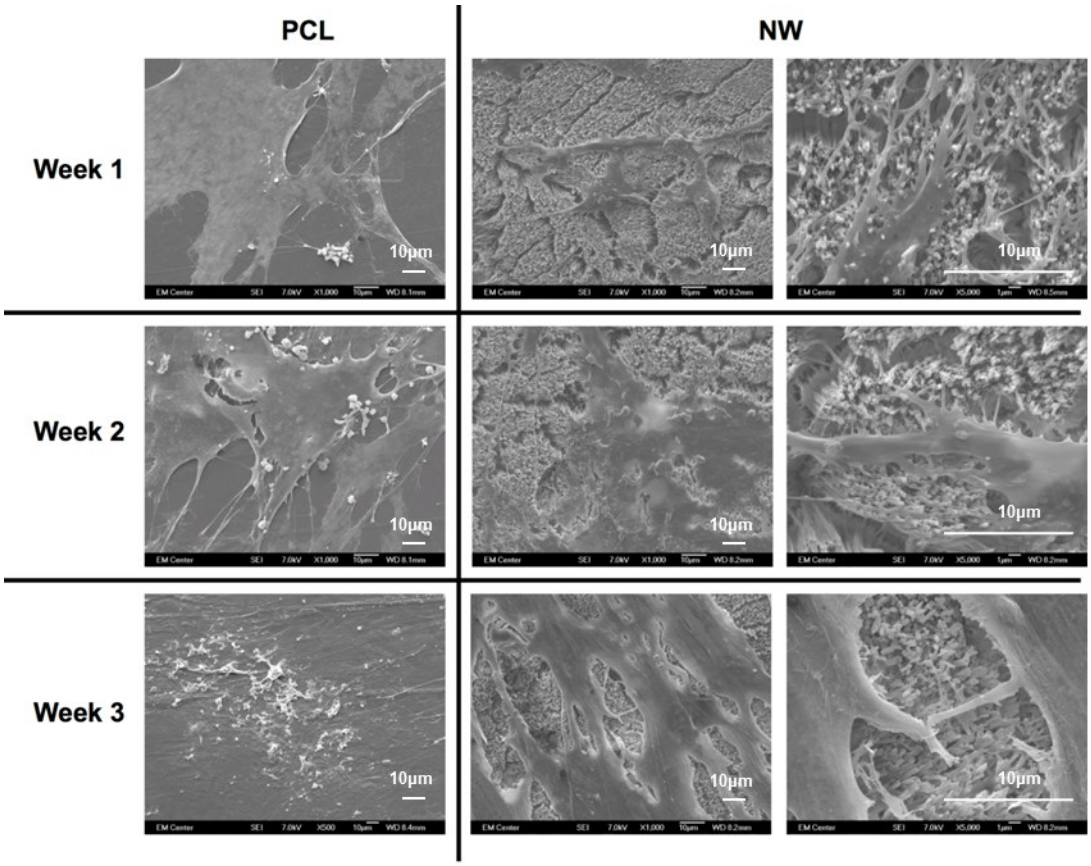

Figure 4.9: Representative SEM images of ADSCs on PCL and NW after 1, 2, and 3 weeks of culture in chondrogenic conditions.

4.4 Conclusions

This study investigated the differentiation potential of ADSCs on polycaprolactone nanowire into a chondrogenic phenotype. ADSC adhesion, proliferation, viability, and morphology were investigated for up to 7 days of culture using fluorescence microscopy imaging, a cell viability assay, and SEM. The results show that the cells on both surfaces, PCL and NW, promote adhesion and proliferation, however the cells on NW have much more elongated morphologies. Differentiation was investigated after the 7 day growth period for up to 3 weeks of culture using immunofluorescence imaging, histological staining, and SEM. On NW,

fewer cells appear to have differentiated into chondrogenic phenotypes as compared to cells on PCL. Chondrogenic marker proteins, sox9 and col2, had no change in expression of over the 3 weeks of culture on the NW, however both seemed to increase on PCL. In addition, chondrogenic histological staining using alcian blue, indicated lower GAG presence on NW as compared to PCL. Therefore, the results indicate that the nanowire architecture may provide a less favorable template for chondrogenic differentiation of ADSCs.

REFERENCES

1. Cao, H., et al., *The topographical effect of electrospun nanofibrous scaffolds on the in vivo and in vitro foreign body reaction.* Journal of Biomedical Materials Research Part A, 2010. **93A**(3): p. 1151-1159.
2. Bechara, S., L. Wadman, and K.C. Popat, *Electroconductive polymeric nanowire templates facilitates in vitro C17.2 neural stem cell line adhesion, proliferation and differentiation.* Acta Biomaterialia, 2011. **7**(7): p. 2892-2901.
3. McMurray, R.J., et al., *Nanoscale surfaces for the long-term maintenance of mesenchymal stem cell phenotype and multipotency.* Nat Mater, 2011. **10**(8): p. 637-644.
4. Park, K., et al., *Surface modification of biodegradable electrospun nanofiber scaffolds and their interaction with fibroblasts.* J Biomater Sci Polym Ed., 2007. **18**(4): p. 369-82.
5. Seidlits, S.K., J.Y. Lee, and C.E. Schmidt, *Nanostructured scaffolds for neural applications.* Nanomedicine, 2008. **3**(2): p. 183-199.
6. Werner, C., M.F. Maitz, and C. Sperling, *Current strategies towards hemocompatible coatings.* Journal of Materials Chemistry, 2007. **17**(32): p. 3376-3384.
7. Bechara, S.L., A. Judson, and K.C. Popat, *Template synthesized poly(epsilon-caprolactone) nanowire surfaces for neural tissue engineering.* Biomaterials, 2010. **31**(13): p. 3492-3501.
8. Burns, K., C. Yao, and T.J. Webster, *Increased chondrocyte adhesion on nanotubular anodized titanium.* Journal of Biomedical Materials Research Part A, 2009. **88A**(3): p. 561-568.

9. Brandt, J., et al., *Nanostructured Materials for Skeletal Repair.* Layered Nanostructures - Polymers with Improved Properties, 2010. **294-I**: p. 109-119.

10. von der Mark, K., et al., *Nanoscale engineering of biomimetic surfaces: cues from the extracellular matrix.* Cell and Tissue Research, 2010. **339**(1): p. 131-153.

11. Christensen, B.B., et al., *A novel nano-structured porous polycaprolactone scaffold improves hyaline cartilage repair in a rabbit model compared to a collagen type I/III scaffold: in vitro and in vivo studies.* Knee Surgery Sports Traumatology Arthroscopy, 2012. **20**(6): p. 1192-1204.

12. Porter, J.R., A. Henson, and K.C. Popat, *Biodegradable poly(epsilon-caprolactone) nanowires for bone tissue engineering applications.* Biomaterials, 2009. **30**(5): p. 780-8.

13. Trujillo, N.A. and K.C. Popat, *Osteogenic Differentiation of Adipose Derived Stem Cells on Polycaprolactone Nanowire Surfaces.* Journal of Biomaterials and Tissue Engineering, 2013. **3**(5): p. 542-553.

14. Mackay, A.M., et al., *Chondrogenic differentiation of cultured human mesenchymal stem cells from marrow.* Tissue Engineering, 1998. **4**(4): p. 415-428.

15. Charles Huang, C.Y., et al., *Chondrogenesis of human bone marrow-derived mesenchymal stem cells in agarose culture.* The Anatomical Record Part A: Discoveries in Molecular, Cellular, and Evolutionary Biology, 2004. **278**(1): p. 428-436.

CHAPTER 5

ADIPOGENIC DIFFERENTIATION OF ADIPOSE-DERIVED STEM CELLS ON NANOWIRE SURFACES UNDER ADIPOGENIC CONDITIONS

5.1 Introduction

Stem cells possess three unique characteristics: self-renewal capacity, long-term viability, and multilineage potential [1, 2]. There are two types of stem cells that exist in the body: somatic stem cells and embryonic stem cells. The ability of somatic stem cells and embryonic stem cells to differentiate into various cell phenotypes has been studied extensively. Embryonic stem cells are pluripotent cells which have the ability to differentiate into all derivatives of the three germ layers. Although they possess great multilineage potential, research associated with embryonic stem cells is accompanied with many ethical and political issues [1, 2]. Due to that fact, mulitpotent somatic stem cells from the bone marrow stroma have been proposed as the best alternative source for research in the past few decades. These adult stem cells from the bone marrow stroma are classified into two groups: hematopoietic stem cells (HSCs) and mesenchymal stem cells (MSCs). Originally, MSCs were identified as a source of osteoprogenitor cells, however it has been shown that they can also differentiate into adipocytes, chondrocytes, osteoblasts, and myoblasts [3-8]. Their ability to differentiate into different phenotypes makes them promising candidates for mesodermal defect repair and disease management. However, clinical use of MSCs in regards to tissue repair has presented problems including pain due to the invasiveness of the procedure of isolation, morbidity, and low cell number upon harvest. This has led many researchers to investigate alternate sources for MSCs

Recently, studies have shown that adipose tissue is believed to contain an abundant source of multipotent progenitor cells [9]. Subcutaneous adipose tissue is a highly abundant and readily accessible tissue source in the body [10]. Thousands of liposuction surgeries are performed in the U.S. each year and these procedures yield anywhere from 100 ml to >3 L of lipoaspirate tissue [11]. Adipose tissue, like bone marrow, is derived from the mesenchyme and contains a supportive stroma that can be easily isolated. Although it remains to be determined whether adipose derived stem cells (ADSCs) meet the same potential as that of MSCs, it is known that ADSCs are multipotent, available in large numbers from the adipose tissue, and proliferate rapidly in culture, making them an attractive cell source for tissue engineering. *In vitro*, adipose derived stem cells (ADSCs), like MSCs, can differentiate into multiple cell lineages including osteogenic, chondrogenic, myogenic, adipogenic and even neuronal pathways [9]. In addition, ADSCs have also demonstrated a substantial *in vitro* bone formation capacity, similar to that of MSCs from bone marrow, with much ease of culture [2, 12, 13].

In addition to osteogenic and chondrogenic differentiation, adipocyte differentiation is a complex process regulated by many transcriptional cascades and hormonal stimuli. [14-18]. One important aspect of adipocyte differentiation is the role of extracellular matrix proteins and cytoskeleton proteins [19]. Because these proteins have a unique structure, it is very likely that extracellular matrix micro and nanoscale topography would affect adipogenesis in *in vitro* culture conditions on a biomimetic scaffold. Previous studies have demonstrated that adipogenic differentiation can be upregulated to a certain extent by changing the geometry to the scaffold to features such as nanogrooves [20]. Cells seeded on nanogroove surfaces penetrated into the grooves with the actin cytoskeleton being more aligned along the grooves, suggesting that cell-to-surface interactions as characterized by contact guidance are closely related to the

adipogenesis [20]. In addition, studies have shown that tailored electroactive nanorods and hydrophobic nanopillars have been successful in not only differentiating MSCs into adipocytes, but actually increasing the rate of differentiation in comparison with flat surfaces [21, 22].

In this study, we use a solvent-free gravimetric template method to physically modify the surface of polycaprolactone with controlled arrays of high aspect ratio substrate-bound perpendicular nanowires. In this study, these nanowire surfaces were used as templates for growth and maintenance of ADSCs, and their potential to support differentiated states of these cells. Specifically, this study focuses on characterizing the ability of ADSCs to differentiate into adipogenic phenotypes on nanowire surfaces.

5.2 Methods

5.2 1 ADSC culture on PCL and nanowire surfaces

Adult human ADSCs at passage 2 (Zen-Bio Inc.) were expanded using standard cell culture techniques. All the cells used in this study were at passage 5 or below. Cells were detached using 0.25% trypsin-EDTA and suspended in growth media consisting of DMEM with 10% fetal bovine serum (FBS, Sigma) and 1% penicillin/streptomycin (Sigma). All the surfaces were sterilized by incubating in 70% ethanol at room temperature followed by exposure to UV light for 30 min. Following sterilization, the surfaces were rinsed twice with warm phosphate buffered saline (PBS). Cells were seeded on all surfaces in 48-well plates at a density of 5,000 cells/well. The surfaces were incubated at 37ºC and 5% CO_2 for the entire duration of the study. Half of the growth media was changed on day 4. On day 7, all the growth media was replaced with adipogenic differentiation media and the cells were cultured for up to 3 weeks.

Adipogenic differentiation media consisted of growth media plus dexamethasone (10^{-7} M), isobutylmethylxanthine (500 μM), biotin (33 μM), calcium pantothenate (17 μM) and human insulin (1μM). Media was changed every other day for up to 7 days. After 7 days, the differentiation media was replaced with adipogenic maintenance media consisted of differentiation media without isobutylmethylxanthine and was changed every other day for the rest of duration of the culture.

5.2.2 ADSC adhesion and proliferation on PCL and nanowire surfaces

After 1, 4 and 7 days of initial culture, ADSC adhesion, proliferation, and spatial organization were investigated by staining the adhered cells with 5-Chloromethylfluorescein diacetate (CMFDA – live cells), rhodamine-phalloidin (actin – cytoskeleton), and 4',6-diamidino-2-phenylindole (DAPI – nucleus). At each time point, the surfaces were removed from the growth media, and incubated in the CMFDA stain at a concentration of 10 μM for 45 min in a 37°C and 5% CO_2 incubator. Next, the substrates were incubated for another 30 min at 37°C and 5% CO_2 in warm growth medium. The cells were then fixed with 3.7% formaldehyde for 15 min at room temperature. In order to permeabilize the cells, the surfaces were incubated in 1% Triton-X 100 for 3 min. The substrates were then incubated in rhodamine-phalloidin stain at a concentration of 5μL/mL for 30 min. After 25 min of rhodamine-phalloidin staining, DAPI was added at a concentration of 300mM. The substrates were then rinsed in PBS and imaged using a Zeiss Axioplan 2 fluorescence microscope. The number of adhered cells on all the surfaces was determined from 5x DAPI stained images by counting the individual nuclei using ImageJ software. In addition to cell counts, cell shape factor was also determined using Image J software with 10× rhodamine-phalloidin stained images. The cell shape factor was approximated by the

ratio of cellular width to cellular length. The cellular width was defined as the diameter of the largest circle that would fit entirely within the cell and the cellular length was defined by the diameter of the smallest circle that encompassed the entire cell.

Cell viability was measured after 1, 4 and 7 days of initial culture (log phase growth) using a commercially available MTT assay kit (Sigma). Adhered cells were incubated at 37ºC for 3 hrs in a (3-[4,5-dimethylthiazol-2-yl]-2,5-diphenyl tetrazolium bromide (MTT) solution. Mitochondrial dehydrogenase of viable cells cleaves the tetrazolium ring leaving behind purple formazan crystals. The formazan crystals were dissolved in the MTT solvent. The optical density (OD) of the resulting solvent was measured at 570nm using a spectrophotometer (FLUOstar Omega; BMG Labtech, Durham, NC). Background absorbance was measured at 690 nm and subtracted from the measured absorbance.

Material cytotoxicity was characterized after 1, 4 and 7 days of initial culture using a commercially available lactate dehydrogenase (LDH) cytotoxicity assay kit (Cayman Chemical). The protocol provided by the manufacturer was followed. Substrates were rapidly shaken on a horizontal shaker plate (1000 rpm) for 5 min at room temperature. The manufacturer-provided standards along with the substrate-exposed plasma samples were transferred to a 96 well plate. A reaction solution (96% v/v assay buffer, 1% v/v NAD+, 1% v/v Lactic Acid, 1% v/v INT, and 1% v/v LDH Diaphorase) was added in the amounts equal (1:1) to all standards and samples, and further incubated with gentle shaking on an orbital shaker for 30 min at room temperature. The absorbance of the solution was measured at a wavelength of 490 nm to determine the cytotoxic effects of the smooth PCL and nanowire substrates.

The morphology of the adhered ADSCs was investigated using SEM after 1, 4 and 7 days of culture. SEM was done to visualize how cells adhered and proliferated on the surfaces as well

as how they interacted with the nanowire morphology. In brief, the cells were fixed in a solution of 3% glutaraldehyde, 0.1 M sodium cacodylate, and 0.1 M sucrose for 45 min. The surfaces were then incubated in a buffer containing 0.1 M sodium cacodylate and 0.1 M sucrose. After fixation, the cells were dehydrated by incubating the surfaces in increasing concentrations of ethanol (35%, 50%, 70%, 100%) for 10 min each. The surfaces were further dehydrated by incubating them in hexamethyldisilazane for 10 min. The surfaces were stored in a desiccator until examination using SEM. The surfaces were sputter coated with 10 nm of gold and imaged using at a voltage of 7 kV.

5.2.3 ADSC Adipogenic Differentiation

ADSC responses to the different surfaces were evaluated after providing the cells with adipogenic differentiation media followed by adipogenic maintenance media. After 1, 2 and 3 weeks of culture, ADSCs on different surfaces were immuno-labeled for PPARγ and adiponectin (Acrp30). Cells were fixed and permeabilized as described earlier. All the surfaces were incubated with 10% bovine serum albumin for 30 min at room temperature to prevent nonspecific binding. After rinsing in PBS, the surfaces were incubated with either anti-PPARY primary antibody (1:100 in PBS, purified goat polyclonal antibody of human origin, Santa Cruz Biotechnology) or anti-Acrp30 primary antibody (1:100 in PBS, purified goat polyclonal antibody of mouse origin, Santa Cruz Biotechnology) for 1 hr at room temperature. Following primary antibody incubation, surfaces were rinsed three times with PBS at an interval of 5 min each. The surfaces were then incubated in FITC-labeled secondary antibodies for PPARγ and Acrp30 (1:200 donkey antigoat IgG, Santa Cruz Biotechnology) for 45 min in the dark. Finally, the surfaces were rinsed twice in PBS and incubated in rhodamine-phalloidin stain at a

concentration of 5µl/ml for 30 min. After 25 min of rhodamine-phalloidin staining, DAPI was added at a concentration of 300 nM. The surfaces were then rinsed in PBS and visualized using a Zeiss Axioplan 2 fluorescence microscope. The number of adhered cells on all the surfaces after 1 and 3 weeks of culture was determined from 5x DAPI stained images by counting the individual nuclei using ImageJ software. Using the cell counts, cell proliferation ratio from day y to day 1 and week 7 to week 1 was calculated.

Lipid formation on the surfaces was detected using Oil Red O staining after 1, 2, and 3 weeks of culture. All surfaces were rinsed twice in PBS followed by fixation in 10% formalin for 1 hr. Surfaces were rinsed in 60% isopropanol and transferred to a 0.5% Oil Red O solution in 60% isopropanol. The surfaces were incubated at room temperature in Oil Red O for 15 min followed by three rinses in DI water for 2 min each. After rinsing, the surfaces were placed in a 100% ispropanol for 30 min on a 200 rpm shaker plate to solubilize the Oil Red O stain. Absorbance of the solubilized solution was measured at 500nm.

The morphology of adhered ADSCs on surfaces was investigated using SEM after 1, 2 and 3 weeks of culture using the method described in previous section.

5.2.4 Statistical Analysis

Data within the graphs are expressed as the average count and the standard deviation of the mean. All the quantitative results were analyzed using paired t-test or one-way analysis of variance (ANOVA). Multiple comparisons are tested using Tukey's HSD. Statistical significance was considered at $p < 0.05$. All qualitative methods used $n_{min}=3$ and all quantitative methods used $n_{min}=5$. Experiments were repeated at least three times with three different cell culture populations.

5.3 Results and Discussion

Results of ADSC culture, adhesion, proliferation, and viability are included in Chapter 4 since the initial growth period on PCL and NW surfaces was conducted simultaneously for chondrogenic and adipogenic differentiation studies. Please refer to Figures 1-6 in Chapter 4 for material characterization, fluorescence images, cell counts, shape factor, MTT assay, LDH assay, and SEM cell morphology.

For surfaces cultured under adipogenic differentiation conditions, ADSCs on different surfaces were immuno-labeled for PPARγ and adiponectin (**Figure 5.1a** and **Figure 5.1b**). PPARγ is a regulator of fatty acid storage and glucose metabolism. It also is known to stimulate lipid uptake and adipogenesis by fat cells. Adiponectin is a protein hormone secreted by mature adipocytes that regulates the metabolism of lipids. Adiponectin is also involved in regulating glucose metabolism and the breakdown of fatty acids. PPARγ and adiponectin were detected by FITC-labeled immunofluorescence during the 3 weeks ADSCs were cultured under adipogenic conditions.

(a)

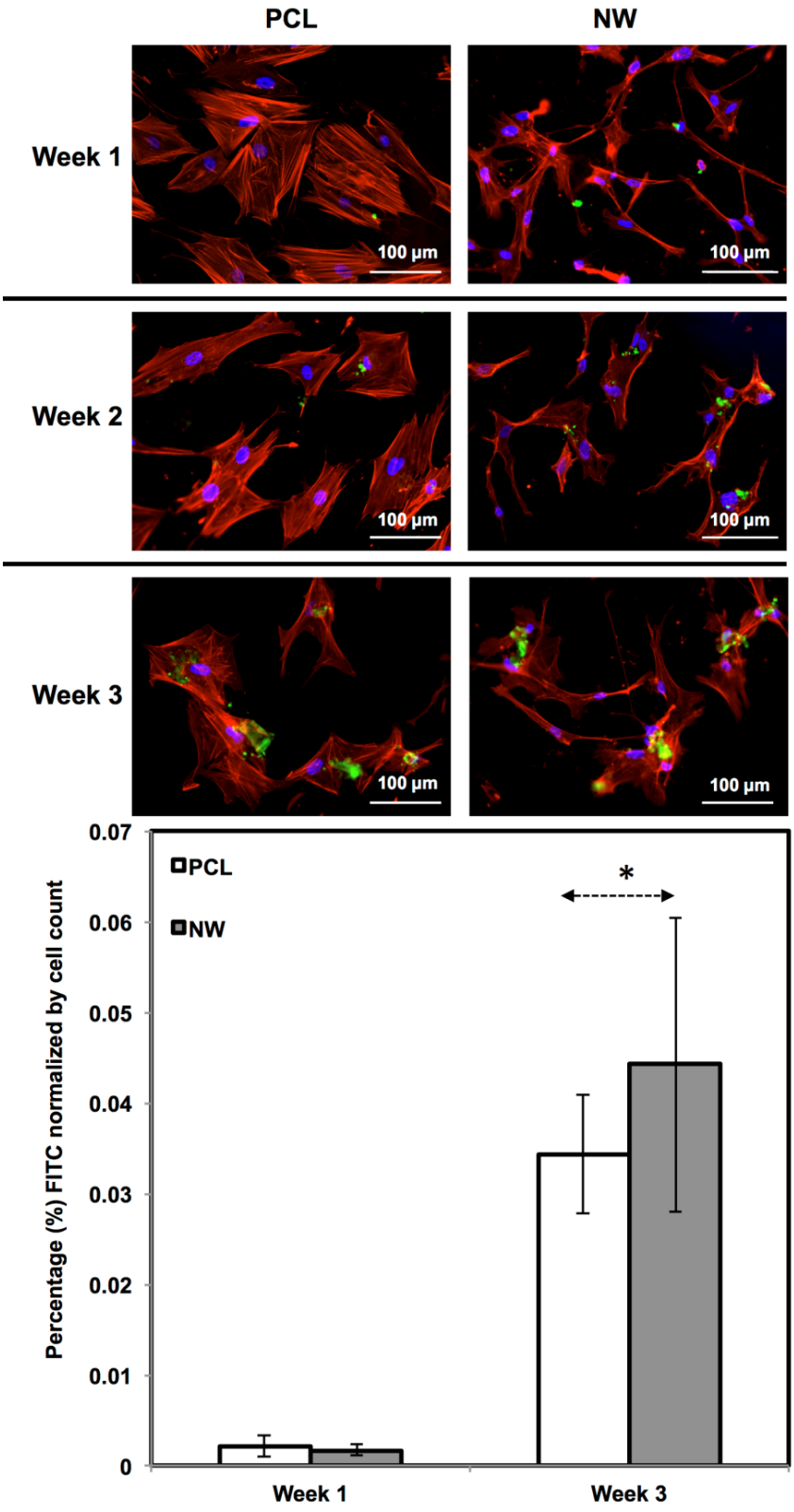
PCL
NW
Week 1
Week 2
Week 3
100 μm
PCL
NW
*
Percentage (%) FITC normalized by cell count
0.07
0.06
0.05
0.04
0.03
0.02
0.01
0
Week 1
Week 3

(b)

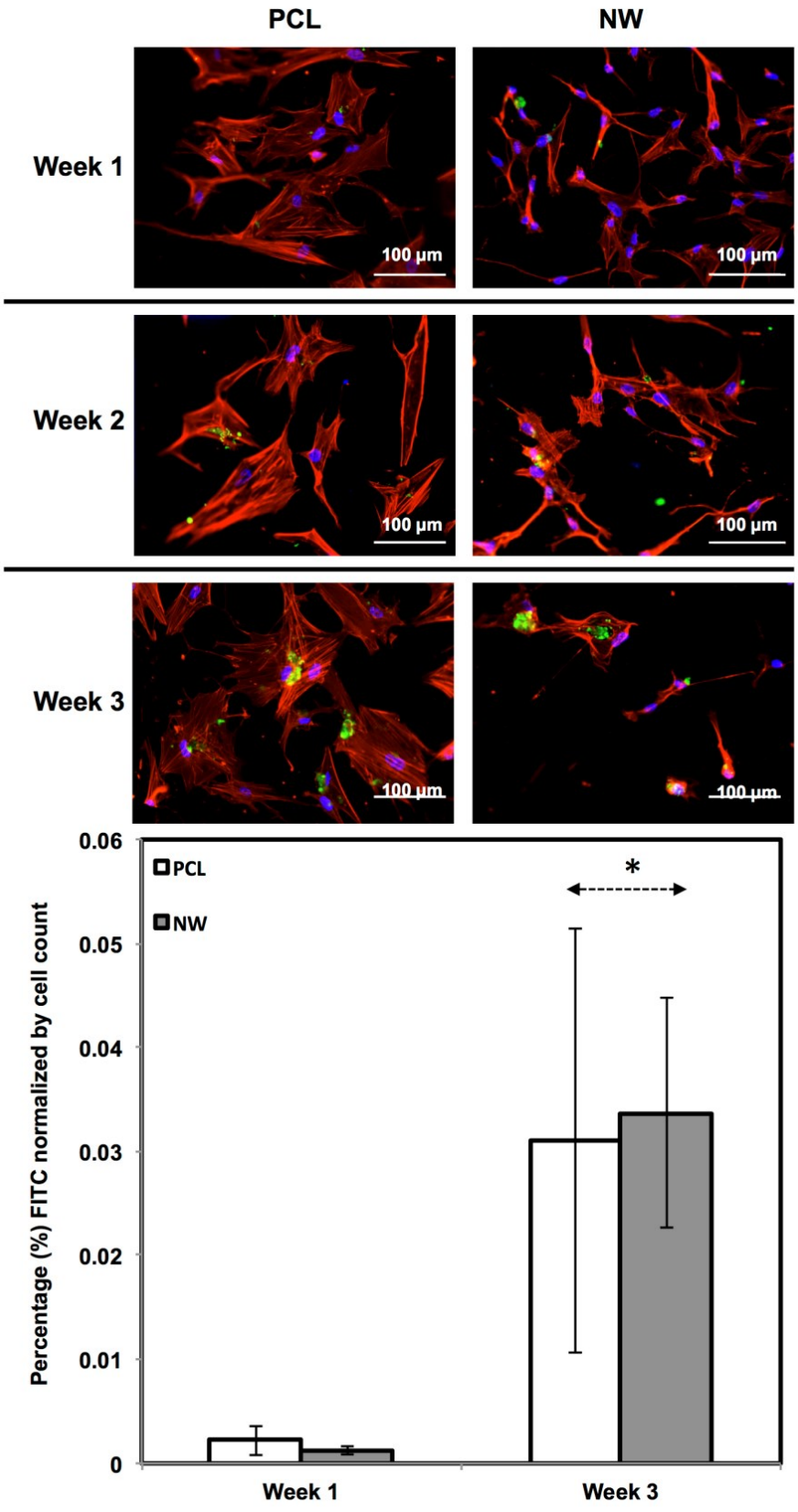
PCL
NW
Week 1
Week 2
Week 3
100 µm
Percentage (%) FITC normalized by cell count
0.06
0.05
0.04
0.03
0.02
0.01
0
PCL
NW
*
Week 1
Week 3

Figure 5.1: (a) Representative immunofluorescence images of ADSCs on PCL and NW for PPARγ (green), actin (red) and nuclei (blue) after 1, 2, and 3 weeks of culture in adipogenic conditions. (b) Representative fluorescence images of ADSCs on PCL and NW for adiponectin (green), actin (red) and nuclei (blue) after 1, 2, and 3 weeks of culture in adipogenic conditions. Percentage of FITC-labeled PPARγ (a) and adiponectin (b) were normalized by total number of cells within a particular image. Asterisks above Week 3 indicate statistical significance from Week 1 using p-value less than α=0.05

The percentage of FITC detected during immunofluorescence was normalized by the number of cells on the particular image (**Figures 5.1a and 5.1b**). It was determined that for PPARγ expression, the protein was present on both surfaces during all three weeks of differentiation with very low levels on the first week. Both surfaces saw a significant increase in PPARγ from week 1 to week 3 with slightly more average expression on NW, however, not enough for it to be statistically different from PCL. Adiponectin had a very similar behavior to PPARγ. Adiponectin expression was detected on both surfaces during the first week even though the amount of FITC-labeled adiponectin is relatively low. After the third week of culture, both surfaces displayed a significant increase in adiponectin with slightly more on NW even though PCL and NW are not statistically different.

The amount of proliferation from week 1 to week 3 did not differ on NW, but increased significantly on PCL under adipogenic conditions (**Figure 5.2a**). The proliferation ratio for PCL during initial growth period (D7/D1) is similar to that during the differentiation period (W3/W1) (**Figure 5.2b**). However, the proliferation ratio of NW during growth period (D7/D1) is higher

than that during the differentiation period (W3/W1) (**Figure 5.2b**). This indicated that the cells on NW are differentiating into adipogenic cells rather than proliferation unlike the cells on PCL.

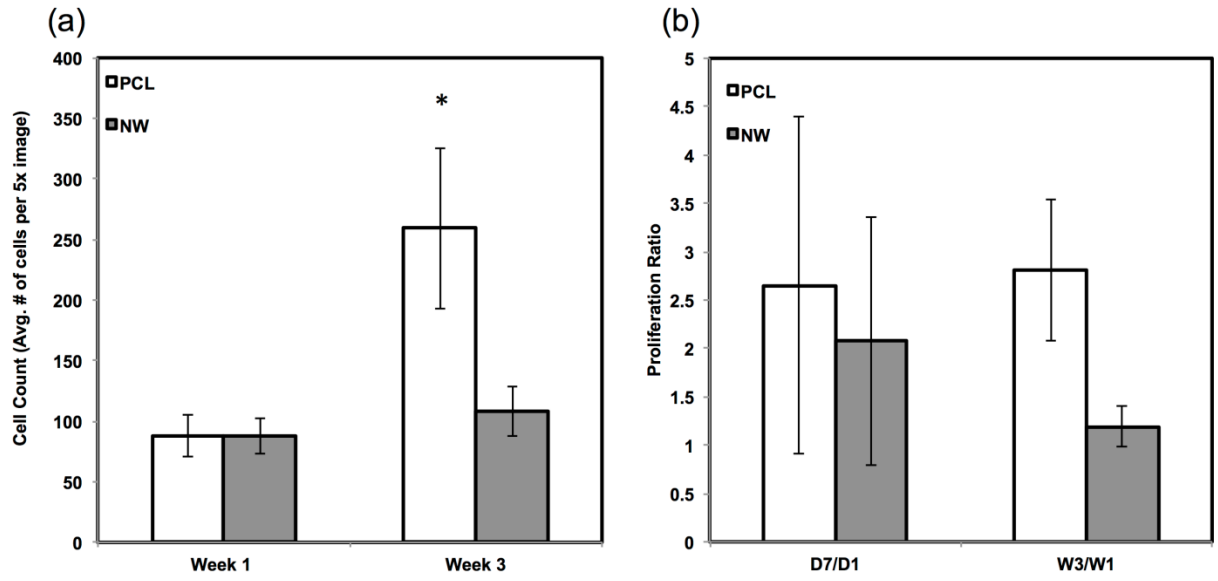

Figure 5.2: (a) Average cell counts on PCL and NW after 1 and 3 weeks of culture in adipogenic conditions. Cell nuclei were counted using DAPI fluorescence and ImageJ software. (b) Comparisons of proliferation ratios between the growth period (D7/D1) and the differentiation period (W3/W1).

ADSCs on both surfaces were also stained using Oil Red O to detect for adipogenic differentiation and extracellular matrix production of lipids (**Figure 5.3**). Oil Red O is a fat-soluble diazo dye that stains for triglycerides and lipids predominantly in frozen tissue sections and paraffin sections. However, it was more recently been used in cell culture and is becoming an increasingly common technique to detect for mature adipocytes during induced adipogenesis. After one week in adipogenic differentiation conditions, both surfaces stained for Oil Red O with more stain detected on NW in comparison with PCL. It is evident after three weeks of

differentiation conditions that lipid production was increasing from the differentiating cells on both surfaces and trend continued with slightly more Oil Red O stain on NW. Oil Red O results seemed to follow immunofluorescence which showed slightly more adipogenic expression on NW even though the number of cells and the rate of proliferation was lower than PCL.

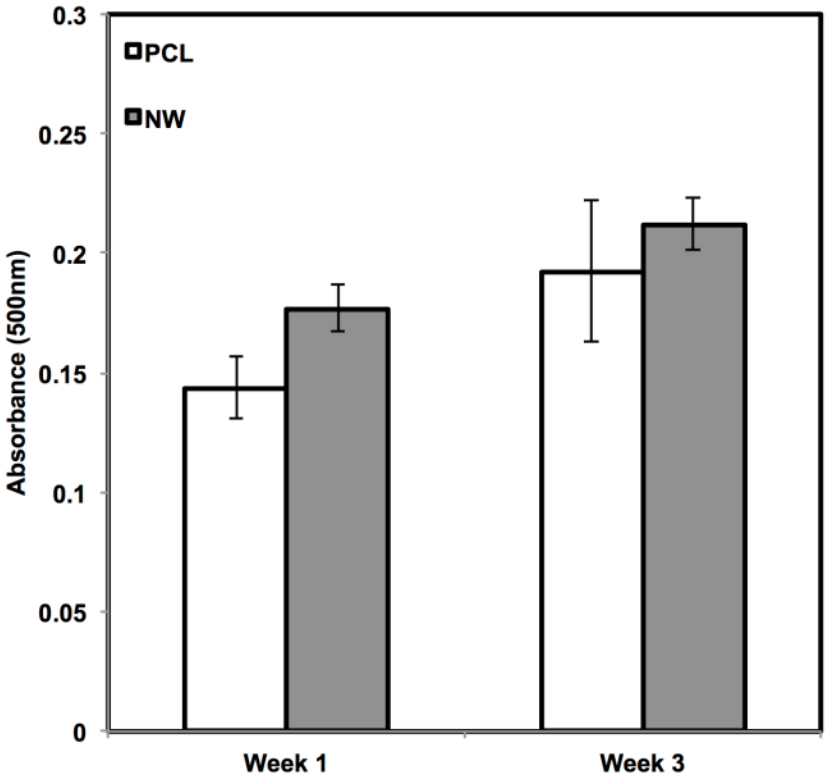

Figure 5.3: Oil red O (lipid) staining of PCL and NW after 1, 2 and 3 weeks of culture in adipogenic conditions as well as quantification of oil red O absorbance after 1 and 3 weeks of culture.

The cell morphology after 1, 2 and 3 weeks of differentiation was investigated using SEM imaging (**Figure 5.4**). As with fluorescence imaging, the results from the images indicate higher number of cells on PCL with very little increase in the number of cells on NW. However,

cells on NW have extended morphologies with cellular extension that interact with the individual nanowires.

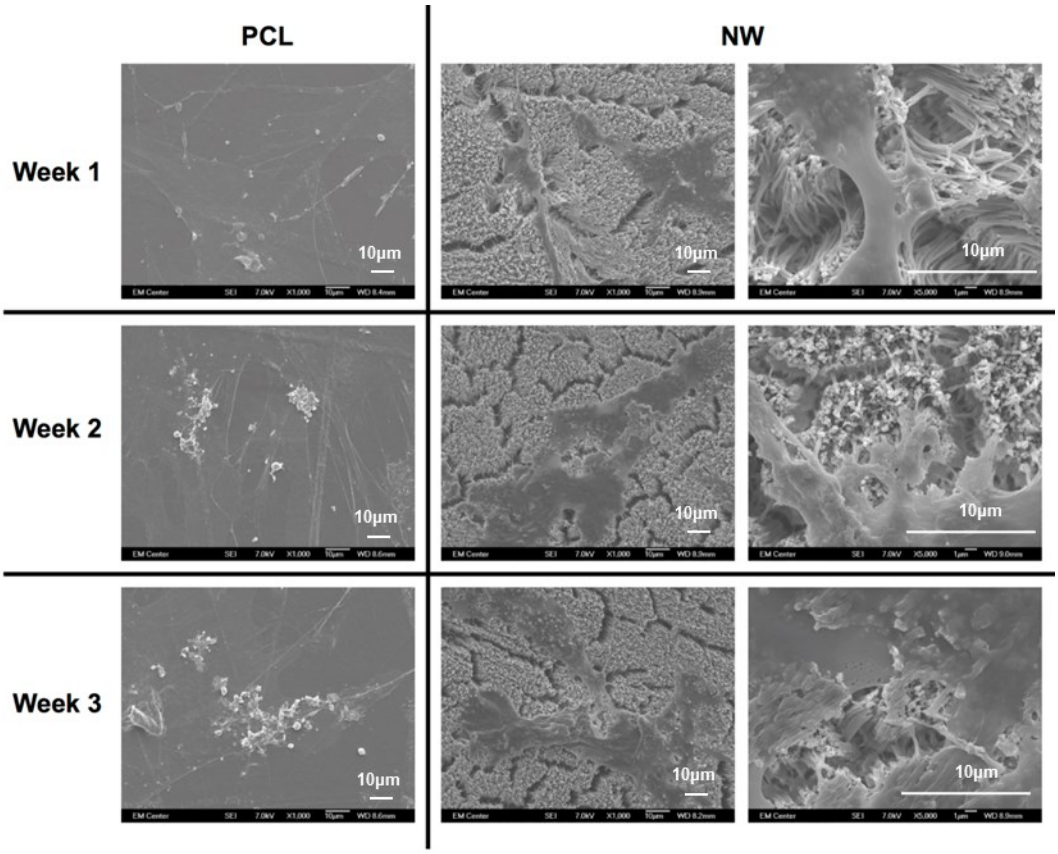

Figure 5.4: Representative SEM images of ADSCs on PCL and NW after 1, 2, and 3 weeks of culture in adipogenic conditions.

5.4 Conclusions

The differentiation potential of ADSCs on polycaprolactone nanowire into adipogenic phenotypes was investigated in this study. Similar to the osteogenic and chondogenic studies in chapter 3 and chapter 4, ADSC adhesion, proliferation, viability, and morphology were investigated for up to 7 days of culture using fluorescence microscopy imaging, a cell viability

assay, and SEM. The results show that the cells on both surfaces, PCL and NW, promote adhesion and proliferation, however the cells on NW have much more elongated morphologies. Differentiation was investigated after the 7 day growth period for up to 3 weeks of culture using immunofluorescence imaging, histological staining, and SEM. On NW, more cells appear to have differentiated into adipogenic phenotypes, and expression of adipogenic marker proteins, PPARγ and adiponectin, increased over the 3 weeks of culture on the NW. In addition, adipogenic histological staining using Oil red O, indicated a moderately higher lipid accumulation and presence on NW compared to PCL. Therefore, the results indicate that the nanowire architecture may provide a more favorable template for adipogenic differentiation of ADSCs.

REFERENCES

1. Rodriguez, A.M., et al., *The human adipose tissue is a source of multipotent stem cells.* Biochimie, 2005. **87**(1): p. 125-128.
2. Zuk, P.A., et al., *Human adipose tissue is a source of multipotent stem cells.* Molecular Biology of the Cell, 2002. **13**(12): p. 4279-4295.
3. Ferrari, G., et al., *Muscle regeneration by bone marrow-derived myogenic progenitors.* Science, 1998. **279**(5356): p. 1528-30.
4. Grigoriadis, A.E., J.N.M. Heersche, and J.E. Aubin, *Differentiation of Muscle, Fat, Cartilage, and Bone from Progenitor Cells Present in a Bone-Derived Clonal Cell-Population - Effect of Dexamethasone.* Journal of Cell Biology, 1988. **106**(6): p. 2139-2151.
5. Hauner, H., P. Schmid, and E.F. Pfeiffer, *Glucocorticoids and Insulin Promote the Differentiation of Human Adipocyte Precursor Cells into Fat-Cells.* Journal of Clinical Endocrinology & Metabolism, 1987. **64**(4): p. 832-835.
6. Johnstone, B., et al., *In vitro chondrogenesis of bone marrow-derived mesenchymal progenitor cells.* Exp Cell Res, 1998. **238**(1): p. 265-72.
7. Pittenger, M.F., et al., *Multilineage potential of adult human mesenchymal stem cells.* Science, 1999. **284**(5411): p. 143-7.
8. Wakitani, S., T. Saito, and A.I. Caplan, *Myogenic cells derived from rat bone marrow mesenchymal stem cells exposed to 5-azacytidine.* Muscle Nerve, 1995. **18**(12): p. 1417-26.

9. Zheng, B., et al., *Mouse adipose-derived stem cells undergo multilineage differentiation in vitro but primarily osteogenic and chondrogenic differentiation in vivo.* Tissue Engineering, 2006. **12**(7): p. 1891-1901.

10. Bunnell, B.A., et al., *Adipose-derived stem cells: isolation, expansion and differentiation.* Methods, 2008. **45**(2): p. 115-20.

11. Katz, A.J., et al., *Emerging approaches to the tissue engineering of fat.* Clin Plast Surg, 1999. **26**(4): p. 587-603, viii.

12. Halvorsen, Y.D.C., et al., *Extracellular matrix mineralization and osteoblast gene expression by human adipose tissue-derived stromal cells.* Tissue Engineering, 2001. **7**(6): p. 729-741.

13. Zuk, P.A., et al., *Multilineage cells from human adipose tissue: Implications for cell-based therapies.* Tissue Engineering, 2001. **7**(2): p. 211-228.

14. Rosen, E.D., et al., *C/EBPalpha induces adipogenesis through PPARgamma: a unified pathway.* Genes Dev, 2002. **16**(1): p. 22-6.

15. Rosen, E.D., et al., *PPAR gamma is required for the differentiation of adipose tissue in vivo and in vitro.* Mol Cell, 1999. **4**(4): p. 611-7.

16. Tanaka, T., et al., *Defective adipocyte differentiation in mice lacking the C/EBPbeta and/or C/EBPdelta gene.* EMBO J, 1997. **16**(24): p. 7432-43.

17. Tontonoz, P., E. Hu, and B.M. Spiegelman, *Stimulation of adipogenesis in fibroblasts by PPAR gamma 2, a lipid-activated transcription factor.* Cell, 1994. **79**(7): p. 1147-56.

18. Wu, Z., et al., *Cross-regulation of C/EBP alpha and PPAR gamma controls the transcriptional pathway of adipogenesis and insulin sensitivity.* Mol Cell, 1999. **3**(2): p. 151-8.

19. Kilian, K.A., et al., *Geometric cues for directing the differentiation of mesenchymal stem cells.* Proc Natl Acad Sci U S A, 2010. **107**(11): p. 4872-7.

20. Kim, M.S., et al., *Effect of nanogroove geometry on adipogenic differentiation.* Nanotechnology, 2011. **22**(49).

21. Luo, W. and M.N. Yousaf, *Tailored electroactive nanorods for biospecific cell adhesion and differentiation.* Chemical Communications, 2009(10): p. 1237-1239.

22. Brammer, K.S., et al., *Hydrophobic nanopillars initiate mesenchymal stem cell aggregation and osteo-differentiation.* Acta Biomater, 2011. **7**(2): p. 683-90.

CHAPTER 6

NANOWIRE TOPOGRAPHY INDUCED DIFFERENTIATION OF ADIPOSE-DERIVED STEM CELLS

6.1 Introduction:

As shown in the previous chapters, ADSCs have the ability to differentiate down multiple cell lineage pathways including osteogenic, chondrogenic, and adipogenic pathways under the influence of biochemical cues from the media conditions. However, not only it is essential for the biomaterial to promote cell adhesion, proliferation, and sustain cell viability, it is also important that it provides additional influence for ADSC differentiation. In this study, osteogenic, chondrogenic, and adipogenic differentiation of ADSCs is investigated on the nanowire surface topography using only minimal essential growth media to maintain cell viability.

As biomaterials for tissue engineering begin moving into a new generation, they must follow specific prerequisites from previous generations. First and second generation biomaterials have proven to be able to support the healing site, be bioactive, have biodegradable properties, and stimulate cell behavior in a defined manner at the molecular level [1]. A biomaterial serves two important roles in regards to stem cell behavior. One purpose is to maintain a population of undifferentiated proliferating stem cells and the second purpose is to non-invasively promote differentiation down a specific phenotypic pathway without the need to induce differentiation with biochemical cues [2]. Surface topography at the microscale and nanoscale levels has been shown to have an essential role in the induction of cell adhesion and subsequent changes in cellular function whether created intentionally or unintentionally on the material. [3-5] The

natural environment for cells in vivo has very complex topographical cues with features that range from the microscale (such as morphology and projections of neighboring cells) to the nanoscale levels (such as protein conformation and small molecule presence). Each of these features has a significant effect on the cell behavior and functionality [6]. The importance of fabricating nanoscale topographies on biomaterial surfaces has been driven by the abundance of nanoscale features within the extra-cellular matrix in addition to the nanoscale protein interactions at the interface of the material and the cell membrane. The interaction of cells with nanotopographies can alter the effect of several cellular aspects including proliferation [7, 8], cell morphology [9-11]), adhesion [12-14], protein expression [15, 16], and gene expression [17-19]. The use of topographically patterned substrates for culturing stem cells has a very clear advantage over the use of defined media in that it allows cell growth, development, and differentiation to be tailored without the need to use potentially harmful chemicals [20].

6.2 Methods:

6.2.1 Adipose derived stem cell culture on different surfaces

Adult human ADSCs at passage 2 (Zen-Bio Inc.) were expanded using standard cell culture techniques. All the cells used in this study were below passage 5. Following expansion, cells were detached using 0.25% Trypsin-EDTA and suspended in growth media consisting of DMEM with 10% fetal bovine serum (FBS, Sigma) and 1% penicillin/streptomycin (Sigma).All the surfaces were sterilized by incubating in 70% ethanol at room temperature followed by exposure to UV light for 30 min. Following sterilization, the surfaces were rinsed twice with warm phosphate buffered saline (PBS). Cells were seeded on all surfaces in 48-well plates at a density of $5x10^3$ cells per well. The surfaces were incubated at 37ºC and 5% CO_2 for the entire

duration of the study. Half of the growth media was changed on day 4. After day 7, growth media was changed every other day for the duration of the study.

6.2.2 ADSC adhesion and proliferation on different surfaces

After day 7 of initial culture, ADSC adhesion and spatial organization were investigated by staining the adhered cells with 5-Chloromethylfluorescein Diacetate (CMFDA – live cells), rhodamine-phalloidin (actin – cytoskeleton), and 4',6-diamidino-2-phenylindole (DAPI – nucleus). The surfaces were removed from the growth media, and incubated in the CMFDA stain at a concentration of 10μM for 45 min in a 37°C and 5% CO_2 incubator. Next, the substrates were incubated for another 30 min at 37°C and 5% CO_2in warm growth medium. The cells were then fixed with 3.7% formaldehyde for 15 min at room temperature. In order to permeabilize the cells, the surfaces were incubated in 1% Triton-X 100 for 3 min. The substrates were then incubated in rhodamine-phalloidin stain at a concentration of 5μL/mL for 30 min. After 25 min of rhodamine-phalloidin staining, DAPI was added at a ratio of 105:1000. The substrates were then rinsed in PBS and imaged using a Zeiss Axioplan 2 fluorescence microscope.

The morphology of the adhered ADSCs was investigated using SEM after 7 days of culture. SEM was done to visualize how cells adhered and proliferated on the surfaces as well as how they interacted with the nanowire morphology. In brief, the cells were fixed in a solution of 3% glutaraldehyde (Sigma), 0.1 M sodium cacodylate (Polysciences), and 0.1M sucrose (Sigma) for 45 min. The surfaces were then incubated in a buffer containing 0.1M sodium cacodylate and 0.1 M sucrose. After fixation, the cells were dehydrated by incubating the surfaces in increasing concentrations of ethanol (35%, 50%, 70%, 100%) for 10 min each. The surfaces were further dehydrated by incubating them in hexamethyldisilazane (HMDS, Sigma) for 10 min. The

surfaces were stored in a desiccator until examination using SEM. The surfaces were sputter coated with 10 nm of gold and imaged using at a voltage of 7kV.

6.2.3 Detection of Osteogenic Differentiation

ADSC osteogenic responses to the different surfaces were evaluated after 14, 28, and 42 days of culture on both surfaces in growth media conditions. The surfaces were removed from the culture media and rinsed twice with PBS prior to analysis. Cytoplasmic alkaline phosphatase (ALP) was measured after 14, 28 and 42 days of culture. Adhered cells were incubated and shaken at 150 RPM for 20 min at room temperature in 0.2% Triton-X cell lysate solution. A commercially available ALP colorimetric assay kit (Quanticrome BioAssay Systems) was used to quantify ALP concentration in the cell lysate. In brief, ALP catalyzes the reaction of *p*-Nitrophenolphosphate (*p*-NPP) to p-nitrophenol and phosphate. This was detected colorimetrically using a spectrophotometer by measuring the absorbance at 405nm after 1 min and 5 min.

Calcium mineralization on different surfaces was detected using Von Kossa staining. All surfaces were rinsed twice in PBS. Adhered cells were fixed in 0.1% glutaraldehyde in PBS for 15 min at room temperature, and then rinsed twice in DI water to fully remove the glutaraldehyde solution. The surfaces were incubated 5% solution of silver nitrate (i.e. 0.5g of silver nitrate in 10ml of DI water) (Sigma) for 30 min at room temperature in the dark. After 30 min, the silver nitrate solution was removed and surfaces were rinsed twice in DI water. The surfaces were allowed to air dry and placed under UV light for approximately 4 hours to monitor the development of brownish/blue spots from the Von Kossa stain. The reaction was stopped by rinsing in DI water.

The morphology of adhered ADSCs on surfaces was investigated using SEM after 14, 28, and 42 days of culture using the method described in previous section.

At each time point, ADSCs on different surfaces were immuno-labeled for osteopontin (OP). Osteocalcin was not detected in this study due to limitations of fluorescent labels and microscope filters. Cells were fixed and permeabilized as described earlier. All the surfaces were incubated with 10% bovine serum albumin for 30 min at room temperature to prevent nonspecific binding. After rinsing in PBS, the surfaces were incubated with anti-OP primary antibody (1:100 AKm2A1 purified mouse monoclonal antibody of mouse origin, Santa Cruz Biotechnology) overnight at 4°C temperature. Following primary antibody incubation, surfaces were washed three times with PBS at an interval of 5 min each. The surfaces were then incubated in FITC-labeled secondary antibodies for osteopontin (1:200 chicken anti-mouse IgG FITC, Santa Cruz Biotechnology) for 45 min in the dark. Following immunofluorescence staining, the surfaces were rinsed twice in PBS and incubated in DAPI for 5 minutes at a concentration of 300 nM. The surfaces were then rinsed in PBS and visualized using a Zeiss Axioplan 2 fluorescence microscope. The number of adhered cells on all the surfaces after 14, 28, and 42 days of culture was determined from 10x DAPI stained images by counting the individual nuclei. In addition, the percentage of area covered with osteopontin in a 20x image (i.e. percentage of area that was stained with FITC) was determined using the "Analyze Particles" feature in ImageJ software. This percentage of osteopontin on each image was divided by total number of cells that were present in that particular image to normalize the value.

6.2.4 Detection of Chondrogenic Differentiation

ADSC chondrogenic responses to the different surfaces were evaluated after 14, 28, and 42 days of culture on both surfaces in growth media conditions. Glycosaminoglycan formation on the surfaces was detected using alcian blue staining. All surfaces were rinsed twice in PBS followed by fixation in cold (4ºC) acetone:methanol solution for 3 min. Substrates were transferred to a 1% alcian blue solution in 3% acetic acid. The surfaces were incubated at room temperature in alcian blue for 30 min followed by three rinses in 3% acetic acid for 2 min each. After rinsing in deionized water for 2 minutes, the surfaces were allowed to dry for imaging or placed in a 1% SDS solution for 30 min on a 200 rpm shaker plate to solubilize the alcian blue stain. Absorbance of the solubilized solution was measured at 605 nm.

The morphology of adhered ADSCs on surfaces was investigated using SEM after 14, 28 and 42 days of culture using the method described in previous section.

At each time point, ADSCs on different surfaces were immuno-labeled for collagen 2 (Col2). Sox9 was not detected in this study due to limitations of fluorescent labels and microscope filters. Cells were fixed and permeabilized as described earlier. All the surfaces were incubated with 10% bovine serum albumin for 30 min at room temperature to prevent nonspecific binding. After rinsing in PBS, the surfaces were incubated with anti-col2 primary antibody (1:100 in PBS, purified goat polyclonal antibody of mouse origin, Santa Cruz Biotechnology) overnight at 4°C temperature. Following primary antibody incubation, surfaces were rinsed three times with PBS at an interval of 5 min each. The surfaces were then incubated in texas-red-labeled secondary antibodies Col2 (1:200 donkey anti-goat IgG, Santa Cruz Biotechnology) for 45 min in the dark. Following immunofluorescence staining, the surfaces were rinsed twice in PBS and incubated in DAPI for 5 minutes at a concentration of 300nM. The

surfaces were then rinsed in PBS and visualized using a Zeiss Axioplan 2 fluorescence microscope. The number of adhered cells on all the surfaces after 14, 28, and 42 days of culture was determined from 10x DAPI stained images by counting the individual nuclei. In addition, the percentage of area covered with collagen 2 in a 20x image (i.e. percentage of area that was stained with FITC) was determined using the "Analyze Particles" feature in ImageJ software. This percentage of collagen 2 on each image was divided by total number of cells that were present in that particular image to normalize the value.

6.2.5 Detection of Adipogenic Differentiation

ADSC adipogenic responses to the different surfaces were evaluated after 14, 28, and 42 days of culture on both surfaces in growth media conditions. Lipid formation on the surfaces was detected using Oil Red O staining. All surfaces were rinsed twice in PBS followed by fixation in 10% formalin for 1 hr. Surfaces were rinsed in 60% isopropanol and transferred to a 0.5% Oil Red O solution in 60% isopropanol. The surfaces were incubated at room temperature in Oil Red O for 15 min followed by three rinses in DI water for 2 min each. After rinsing, the surfaces were placed in a 100% ispropanol for 30 min on a 200 rpm shaker plate to solubilize the Oil Red O stain. Absorbance of the solubilized solution was measured at 500nm.

The morphology of adhered ADSCs on surfaces was investigated using SEM after 14, 28, and 42 days of culture using the method described in previous section.

At each time point, ADSCs on different surfaces were immuno-labeled for adiponectin (Acrp30). PPAR-γ was not detected in this study due to limitations of fluorescent labels and microscope filters. Cells were fixed and permeabilized as described earlier. All the surfaces were incubated with 10% bovine serum albumin for 30 min at room temperature to prevent

nonspecific binding. After rinsing in PBS, the surfaces were incubated with anti-Acrp30 primary antibody (1:100 in PBS, purified goat polyclonal antibody of human origin, Santa Cruz Biotechnology) overnight at 4°C temperature. Following primary antibody incubation, surfaces were rinsed three times with PBS at an interval of 5 min each. The surfaces were then incubated in Texas Red-labeled secondary antibodies Acrp30 (1:200 donkey anti-goat IgG, Santa Cruz Biotechnology) for 45 min in the dark. Following immunofluorescence staining, the surfaces were rinsed twice in PBS and incubated in DAPI for 5 minutes at a concentration of 300 nM. The surfaces were then rinsed in PBS and visualized using a Zeiss Axioplan 2 fluorescence microscope. The number of adhered cells on all the surfaces after 14, 28, and 42 days of culture was determined from 10x DAPI stained images by counting the individual nuclei. In addition, the percentage of area covered with adiponectin in a 20x image (i.e. percentage of area that was stained with FITC) was determined using the "Analyze Particles" feature in ImageJ software. This percentage of adiponectin on each image was divided by total number of cells that were present in that particular image to normalize the value.

6.2.6 Double Immunofluorescence - Simultaneous Staining

For surfaces and at all three time points (14, 28, and 42 days after initial culture), immunofluorescence staining was conducted simultaneously in pairs. Cells were incubated in one of two mixtures of primary antibodies: anti-OP primary mixed with anti-Col2 primary or anti-OP primary mixed with anti-Acrp30 primary. Secondary antibodies for OP were FITC-labeled and secondary antibodies for Col2 and Acrp30 were both Texas Red-labeled. Following double immunofluorescent staining, the surfaces were incubated in DAPI at a concentration of

300nM for 5 min at room temperature. This allowed for detection of two marker protein on one surface with visualization of the cell nuclei.

6.2.7 Statistical Analysis

Data within the graphs are expressed as the average count and the standard deviation of the mean. All the quantitative results were analyzed using one-way analysis of variance (ANOVA) and multiple comparisons are tested using Tukey's HSD. Statistical significance was considered at $p < 0.05$. All qualitative methods used $n_{min}=3$ and all quantitative methods used $n_{min}=5$.

6.3 Results and Discussion

After 7 days of initial culture in growth media, the adhered cells on different surfaces were stained using CMFDA, rhodamine-phalloidin and DAPI (**Figure 6.1**). CMFDA fluorescent probes are freely able to pass through the membranes of viable cells and the probes are converted to cell-impermeant reaction products. These reaction products are present throughout the cytoplasm of living cells and fluoresce. In this study, the CMFDA fluorescent probes are FITC labeled causing them to have green fluorescence. Rhodamine-phalloidin is a high affinity F-actin probe coupled with a red-orange fluorescent dye called tetramethylrhodamine isothiocyanate (TRITC). Phalloidin is a heptapeptide that binds to F-actin and the TRITC provides very little non-specific staining to it the high selectivity of the bone between F-actin and phalloidin. DAPI is strictly a nucleus stain because it binds to the adenine-thymine rich regions of the DNA. After 7 days of culture, results appear similar to that of previous studies. PCL and NW surfaces appear to support ADSC adhesion and proliferation with slightly more cells present on PCL. However,

as previously shown, the cell on the NW surfaces have much more elongated morphologies and appear to form interconnected networks with neighboring cells on the surface. In this study, the representative fluorescent images of day 7 were split to show DAPI, CMFDA, and actin individually as well as combined (**Figure 6.1**).

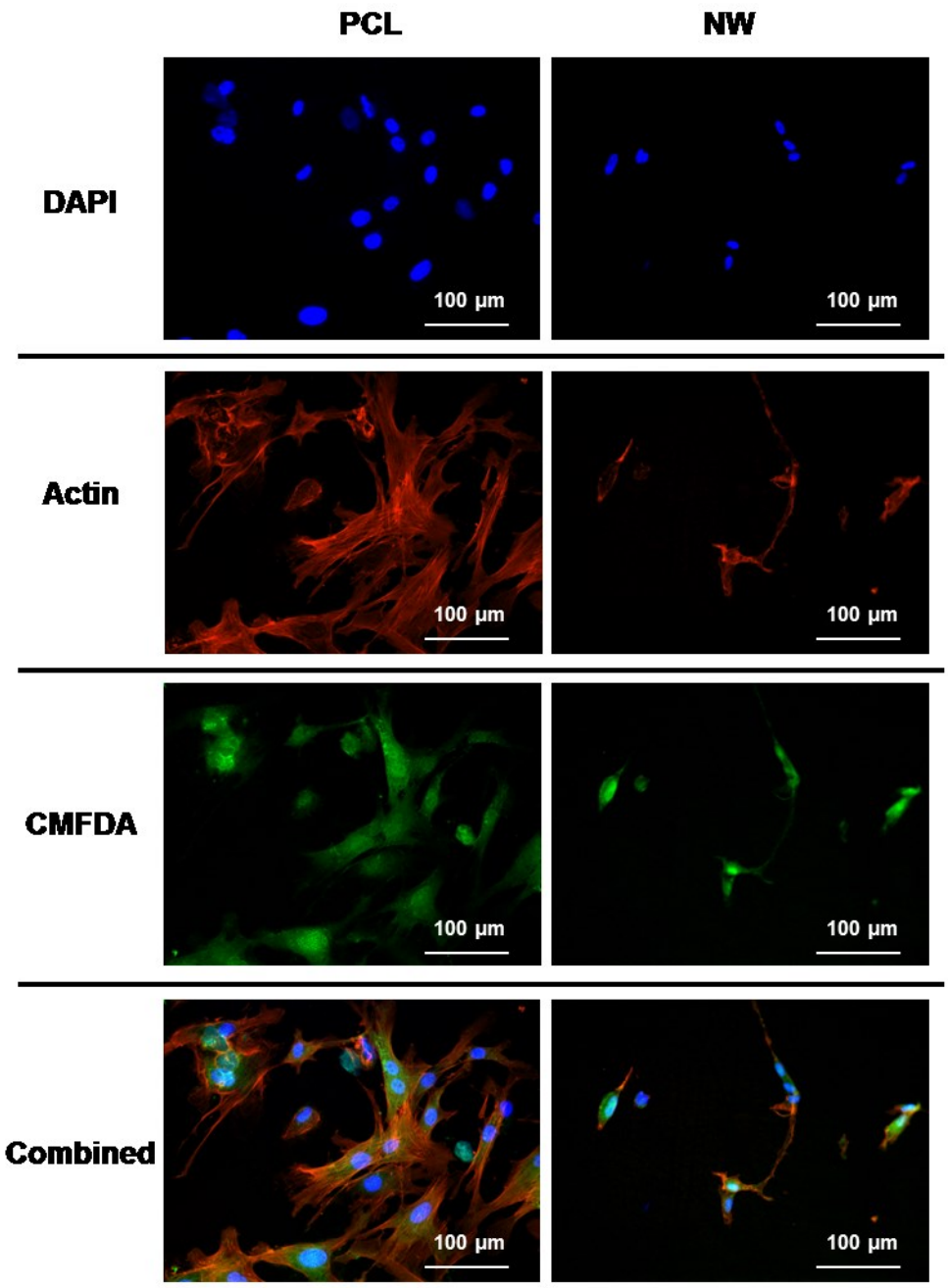

Figure 6.1: Representative fluorescence microscopy images of ADSCs on PCL and NW surfaces after 7 days of culture

It appears after 14 and 28 days of culture, both surfaces support cell proliferation with significantly more cells on PCL as compared to NW (**Figure 6.2)**. The drop in average cell counts on both surfaces at day 42 can be attributed to delamination of most of the cell population as they reached 100% confluency.

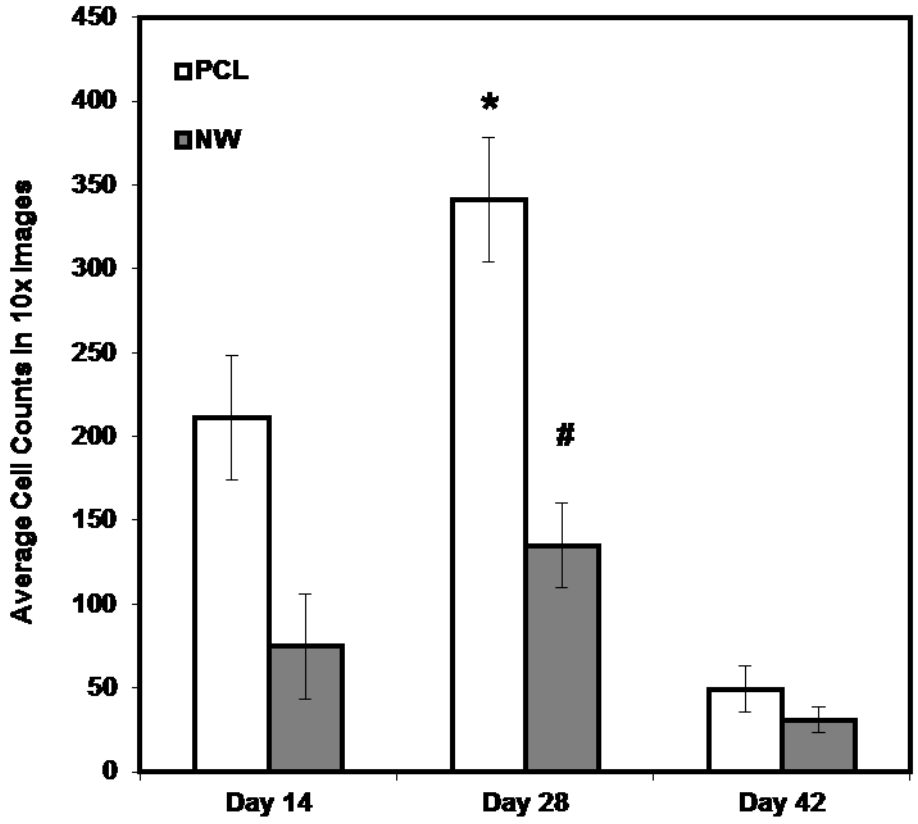

Figure 6.2: Average cell counts on 10x fluorescent images

As stated earlier, alkaline phosphatase (ALP) is a ubiquitous enzyme in bone, liver, kidney, placental, and intestinal tissues. It is a key ingredient in matrix vesicles, aids in mineralization by hydrolyzing organic phosphate esters, and is a standard biomarker for osteoblast phenotype. The presence of ALP in matrix vesicles, the site of new bone formation, suggests the role of ALP in mineralization. ALP aids in the mineralization of HAp by hydrolyzing organic phosphate esters which produces an excess of free inorganic phosphate thereby initiating the biomineralization process. ALP plays a direct role in the induction of HAp deposition on extracellular matrix proteins and is known to exhibit cyclic behavior when it is active. ALP activity was measured after 14, 28 and 42 days of culture (**Figure 6.3**). Increase in ALP activity is occurring on all the surfaces on day 14 indicating the initiation of differentiation and calcium phosphate mineralization. However, from day 14 to day 28, both surfaces saw a decrease in ALP activity with a significant drop in ALP on the NW surfaces. Since ALP is an early biomarker of mineralization, the decrease can be associated with mature differentiation of the cells to osteoblasts and the deposition of extracellular matrices that are more characteristic of osteoblasts. As mentioned earlier, ALP is cyclic enzyme during the mineralization process is activated only when the cells need to produce more extracellular HAp. During the matrix maturation phase of osteogenesis, ALP activity is at its maximum until the beginning of matrix mineralization. This explains why the ALP activity appears to go down on day 28 because mineralization is occurring, especially the NW surfaces. Since the cells are delaminating off of the surfaces due to 100% confluency on day 42, ALP activity goes up because the cells that are left behind are beginning to re-deposit a new extracellular matrix that will eventually lead to mineralization.

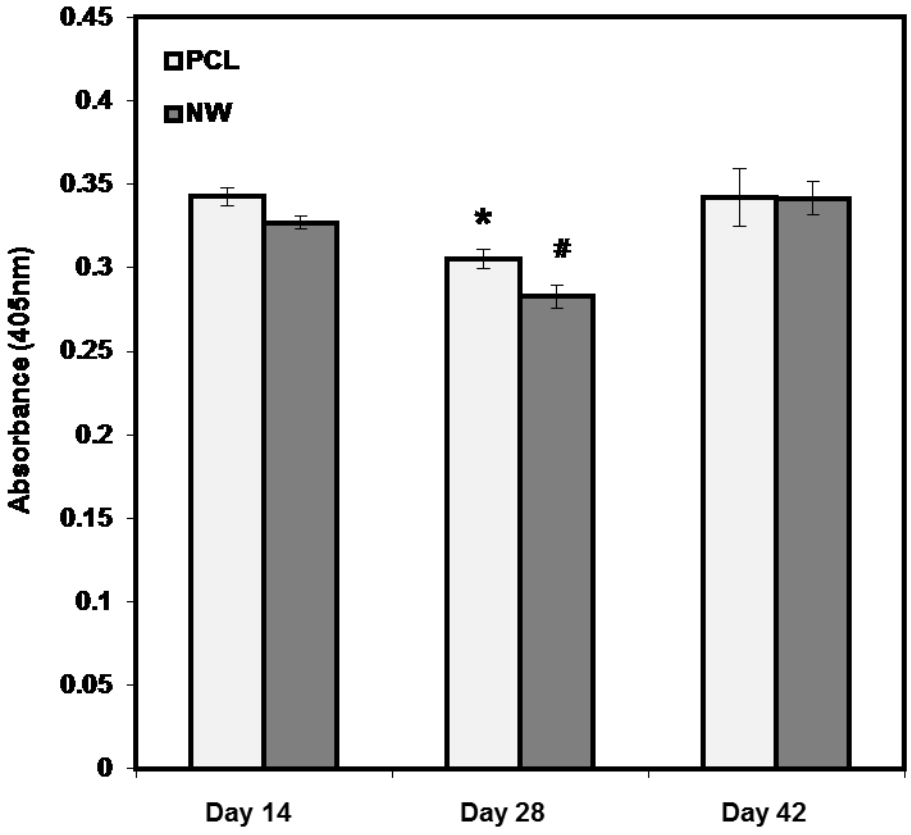

Figure 6.3: Alkaline phosphatase activity after 14, 28, and 42 days after initial culture

Von Kossa staining was used to determine the ability of NW surfaces to induce mineralization. Digital images of the stained surfaces after 14 and 28 days of culture clearly indicate that the cells seeded on the NW surfaces display accelerated mineralization in comparison with the PCL surfaces. Although, mineralization is occurring on the control surfaces, it appears that phosphate detection is minimal in comparison with NW surfaces which have a darker coverage of brown from the silver nitrate stain. This mineral morphology is supported in the literature as an early phase of biomineralization. After 28 days of culture, NW surfaces are almost completely calcified. Day 42 is not shown for Von Kossa since the cells reached 100% confluence and began delaminating off the surface.

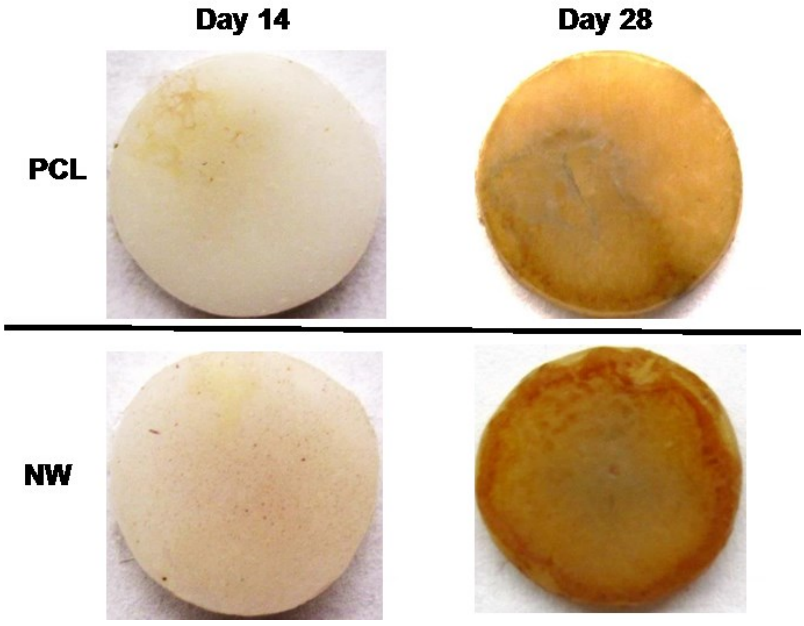

Figure 6.4: Von Kossa (Silver Nitrate) staining of phosphate groups

Additionally, ADSCs were stained using alcian blue for early differentiation and extracellular matrix production of chondrogenic products (**Figure 6.5a**). Alcian blue is a polyvalent dye that is used to stain for acidic polysaccharides such as glycosaminoglycans (GAGs) and sulfated glycosaminoglycans (sGAGs). These polysaccharides are widely present in all connective tissues and especially in both articular and hyaline cartilage tissue. After 14 days of culture both surfaces had little to no staining of alcian blue with slightly more on PCL surfaces. However after 28 days of culture both surfaces displayed the presence of GAGs with PCL having much more alcian blue absorption than NW and therefore, more GAG production. Although the photos give a comparable qualitative measure of the stain, the alcian blue was solubilized in 1% SDS to give a quantitative measure of the dye using spectrophotometry. As

expected, both surfaces saw an increase in alcian blue absorption from day 14 to day 42, but the adsorption on NW was significantly less than PCL (**Figure 6.5b**).

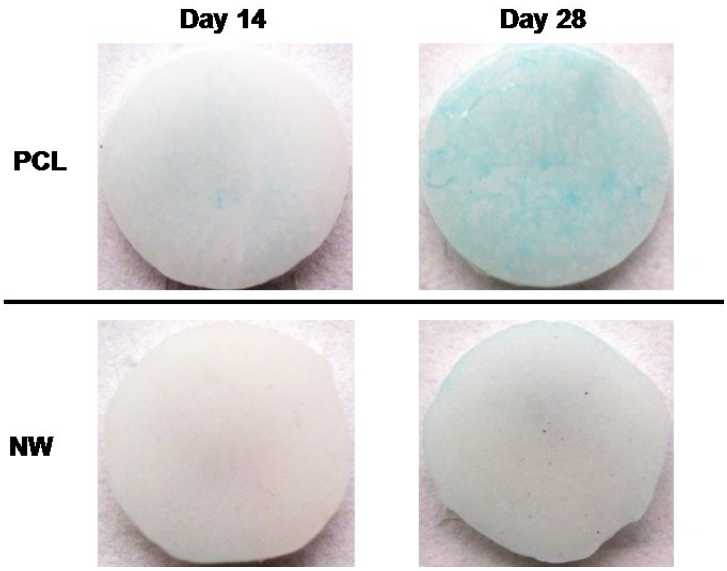

Figure 6.5: (a) Alcian blue staining for the presence of glycosaminoglycans (GAGs)

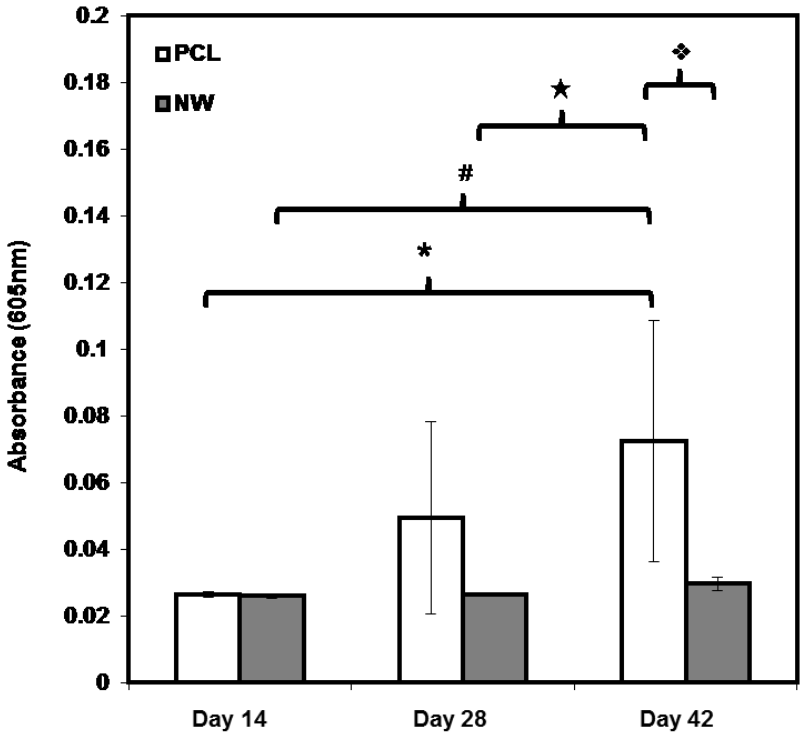

Figure 6.5: (b) Solubilized alcian blue stain to quantify the presence of GAGs on the surfaces

ADSCs on both surfaces were also stained using Oil Red O to detect for adipogenic differentiation and extracellular matrix production of lipids (**Figure 6.6**). As stated before, Oil Red O is a fat-soluble diazo dye that stains for triglycerides and lipids predominantly in frozen tissue sections and paraffin sections. However, it was more recently been used in cell culture and is becoming an increasingly common technique to detect for mature adipocytes during induced adipogenesis. After one 14 days of culture, both surfaces stained for Oil Red O with no significant differences between the two surfaces. However, after 28 days of culture, NW surfaces had a significantly higher level of lipid presence than the PCL surfaces which seemed to decrease from day 14 to day 28. It can assumed that the cells on the PCL surfaces are

differentiating more towards the chondrogenic or osteogenic pathways since von kossa and alcian blue stains were both present. On day 42, since the cells were becoming too confluent and beginning to lift off of the both surfaces, this can explain the drop in Oil Red O absorbance.

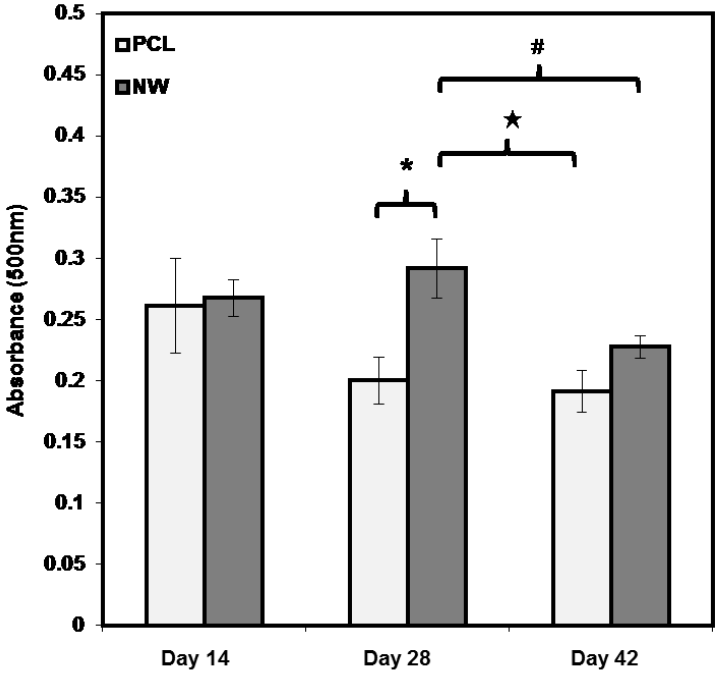

Figure 6.6: Solubilized Oil Red O stain to quantify the presence of lipids on both surfaces

After 14 and 28 days of culture, ADSCs on different surfaces were simultaneously immuno-labeled for OP and COL2 as well as DAPI for the nucleus visualization (**Figure 6.7a**). As previously mentioned in earlier, OP is an extracellular structural glycoprotein that is an organic component of bone and is involved in the process of mineral deposition, cell migration and usually present at the interface between the implant and the mineralized tissue. This important protein is found in many other tissues but plays an important role in binding HAp and Ca^{2+} ions. Col2 is a marker for maturing chondrocytes as the cells continue down the chondrogenic pathway and provides the basis for articular cartilage. The percentage of FITC and Texas Red detected during simultaneous immunofluorescence were normalized by the number of

cells within each particular image (**Figures 6.7b and 6.7c**). For OP expression, the marker protein was present on both surfaces during both time points. However, ADSCs on the NW surfaces had a significant increase in the amount of OP expression when normalized to the number of nuclei. Although, OP is present on the PCL surfaces from day 14 to day 28, the percentage of expression does not significantly increase over the course of the culture. Instead, it appears that most of the cells continue to focus proliferation rather than enter a maturing state of osteogenic differentiation. For COL2 expression, the marker protein was present on both surfaces, but at very low percentages in comparison with OP. The standard deviation is very high among both samples at both time points so it is difficult to conclude if there was a significant increase or decrease on either sample type. Since COL2 is a mature chondrocyte marker protein, it may be too early in chondrogenesis for the ADSCs to be producing COL2 even though GAG presence increases on the PCL surfaces over time with alcian blue histological staining as seen earlier.

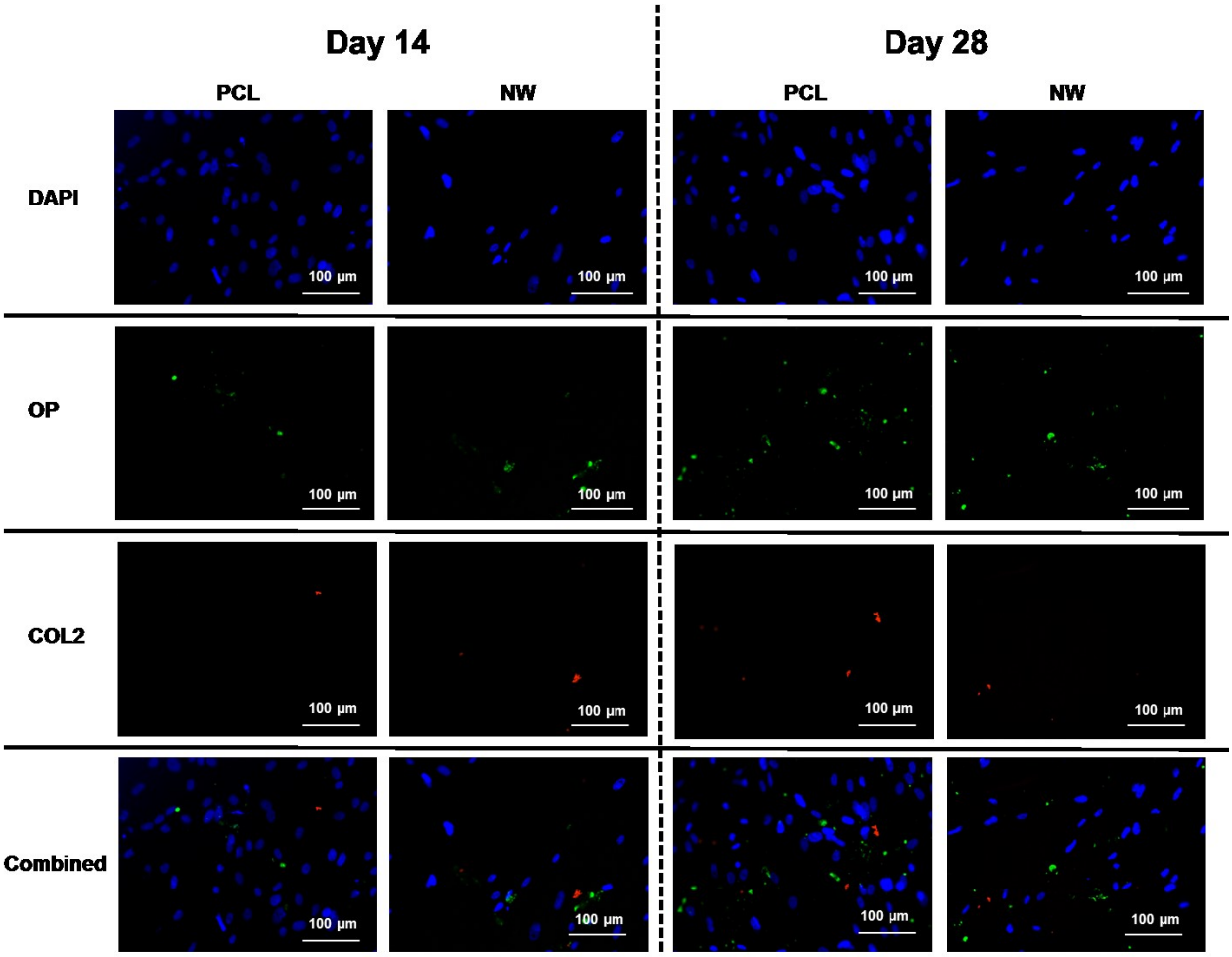

Figure 6.7: (a) Simultaneous immunofluorescence of osteocalcin (OP) and collagen 2 (Col2) on surfaces after 14 and 28 days after initial culture

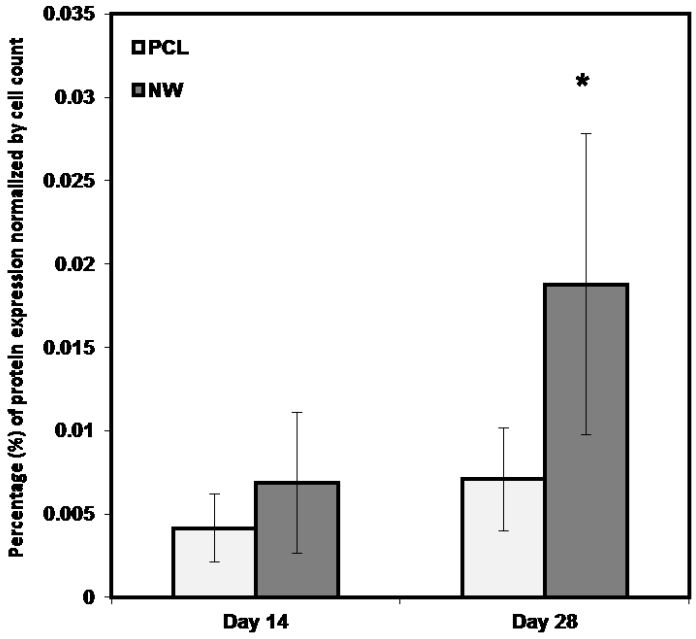

Figure 6.7: (b) Percentage of FITC-labeled osteopontin (OP) normalized by the average total number of cells within the representative images

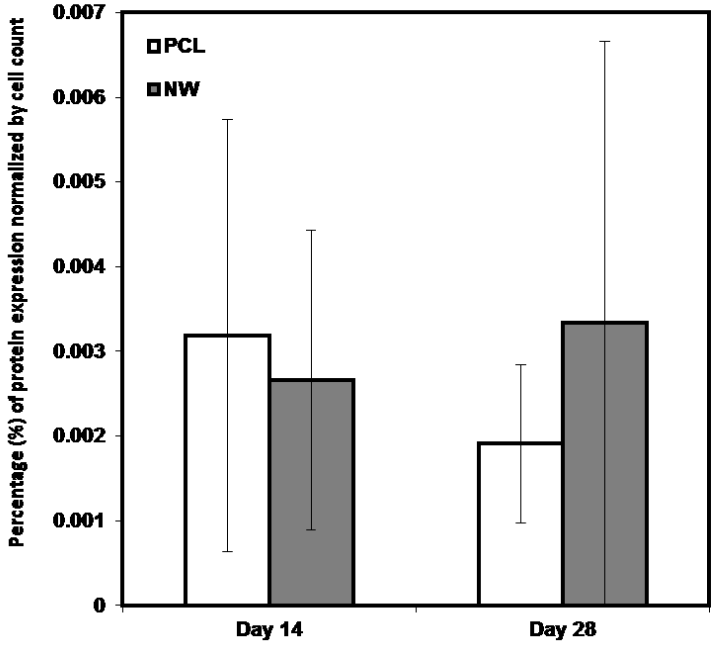

Figure 6.7: (b) Percentage of Texas Red-labeled collagen II (Col2) normalized by the average total number of cells within the representative images

In addition, after 14 and 28 days of culture, ADSCs on different surfaces were simultaneously immuno-labeled for OP and Acrp30 as well as DAPI for the nucleus visualization (**Figure 6.8a**). Acrp30 is a protein hormone secreted by mature adipocytes that regulates the metabolism of lipids. Furthermore, it is also involved in regulating glucose metabolism and the breakdown of fatty acids. The percentage of FITC and Texas Red detected during simultaneous immunofluorescence were normalized by the number of cells within each particular image (**Figures 6.8b and 6.8c**). As expected, the results for OP expression were similar to the simultaneous immunofluorescence with COL2. The OP osteogenic marker protein was present on both surfaces during day 14 and day 28, but the ADSCs on the NW surfaces displayed a large increase in the amount of expression when normalized to the number of nuclei. Although, OP is present on the PCL surfaces from day 14 to day 28, the percentage of expression does not significantly increase over the course of the culture. Instead, it appears that most of the cells continue to focus proliferation rather than enter a maturing state of osteogenic differentiation. For Acrp30 expression, the marker protein was present on both surfaces, but there is no change in the amount of expression on PCL surfaces from day 14 to day 28. Instead, NW surfaces maintained higher levels of Acrp30 expression with a significant difference on day 28 between NW and PCL. However, it is important to note that the percentage of OP on NW surfaces is much greater than the presence of Acrp30 on NW surfaces which indicates that more cells are differentiating towards an osteogenic state.

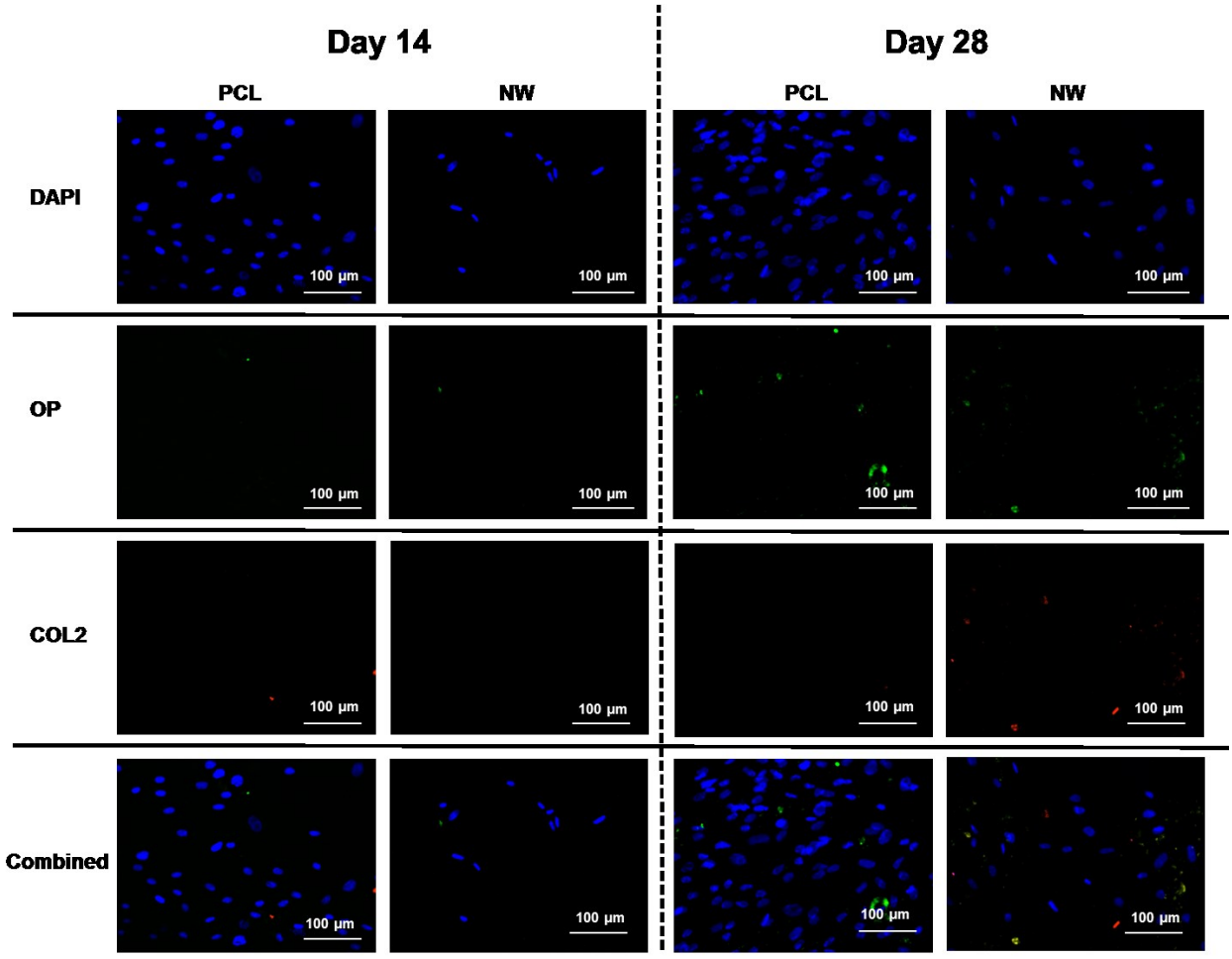

Figure 6.8: (a) Simultaneous immunofluorescence of osteocalcin (OP) and collagen 2 (Col2) on surfaces after 14 and 28 days after initial culture

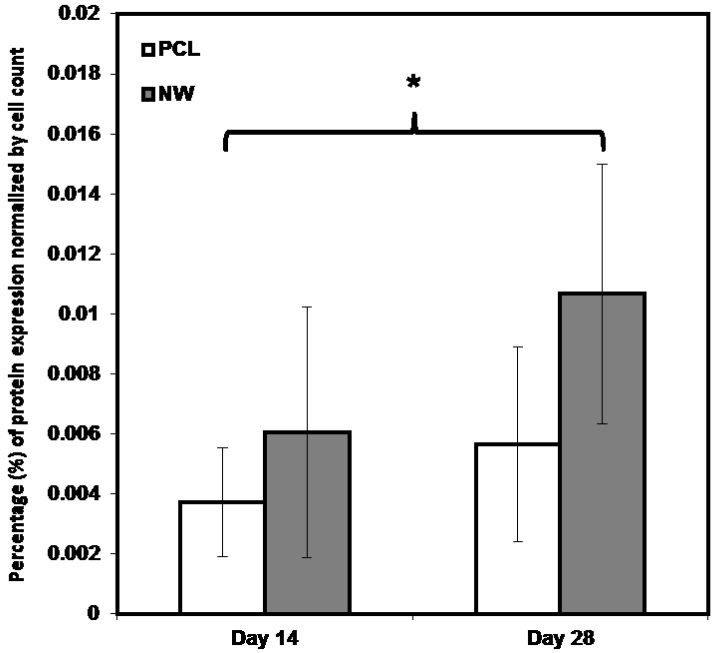

Figure 6.8: (b) Percentage of FITC-labeled osteopontin (OP) normalized by the average total number of cells within the representative images

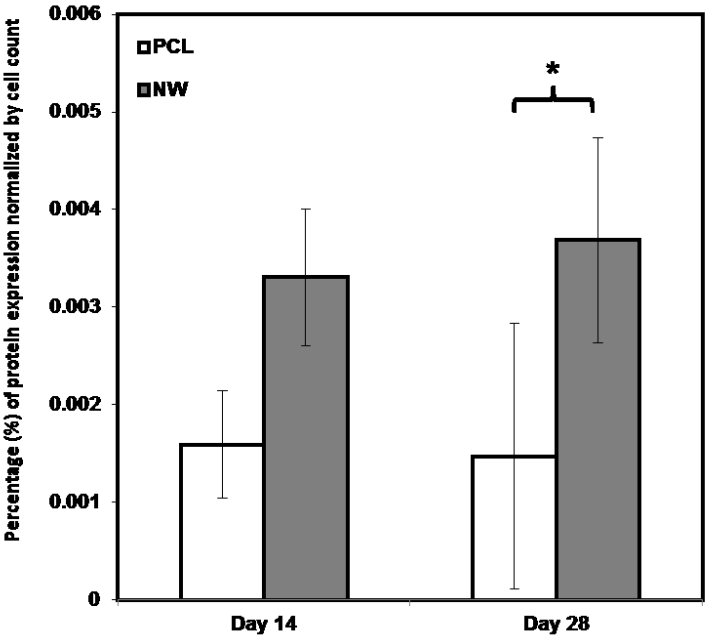

Figure 6.8: (c) Percentage of Texas Red-labeled adiponectin (Acrp30) normalized by the average total number of cells within the representative images

The morphology of the cells after 14, 28, and 42 days of culture was investigated using SEM imaging (**Figure 6.9**). As with fluorescence imaging, the results from the images indicate higher number of cells on PCL with very little increase in the number of cells on NW. However, cells on NW have extended morphologies with cellular extension that interact with the individual nanowires. Fewer cells are seen on day 42 due to delamination of the cells from reaching 100% confluency.

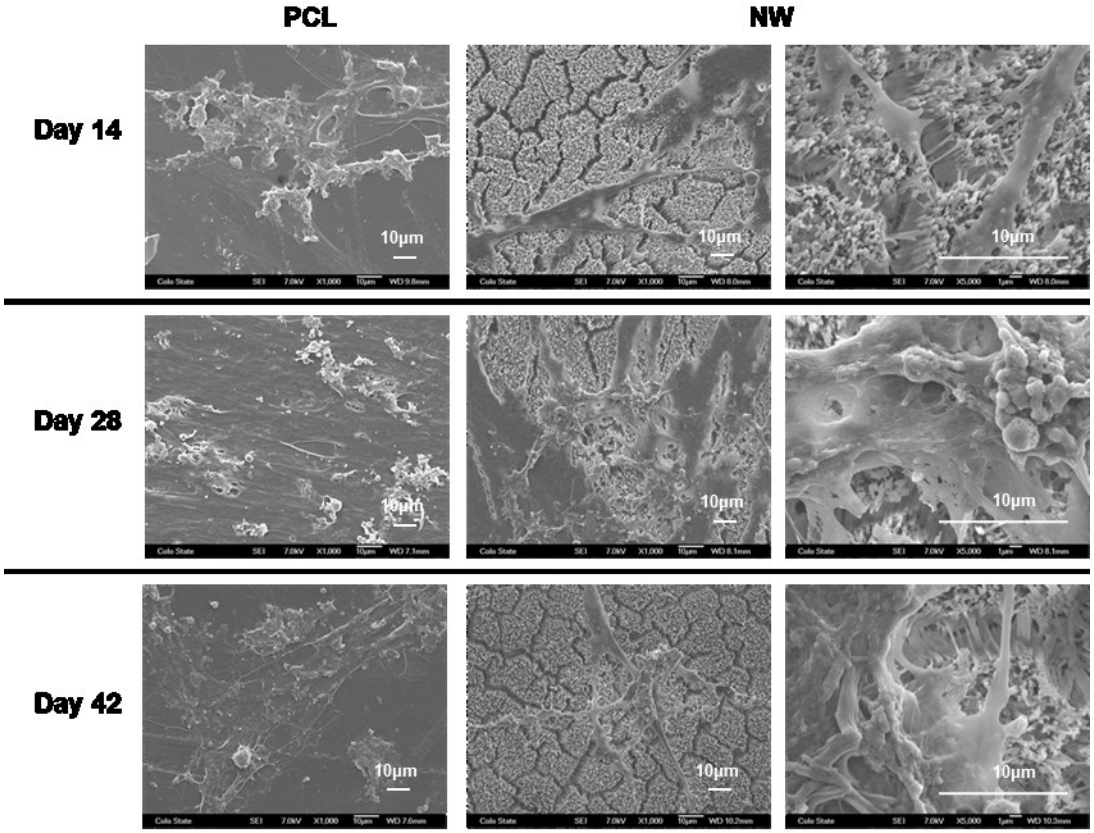

Figure 6.9: Representative SEM images of ADSCs on PCL and NW after 14, 28, and 42 days of culture in growth media conditions.

6.4 Conclusions

This study evaluated the influence of nanowire arrays on ADSC differentiation by investigating the expression of osteogenic, chondrogenic, and adipogenic marker proteins in addition to histological stains. However, this study used minimal essential growth media without differentiation supplements in order to assess how ADSCs are affected by the substrate nanotopography. Although both surfaces promote ADSC adhesion, proliferation, and viability, cells on the PCL surfaces proliferate at a much higher rate than NW surfaces. In addition, ADSCs on NW surfaces had elongated morphologies and lower shape factors similar to the behaviors observed in the previous studies. More ADSCs on the NW surfaces were being signaled to begin the differentiation process and become progenitor cells rather than being signaled to continue proliferation. Differentiation was investigated for 5 weeks of culture, however due to the cells reaching 100% confluency at the final time point, the cell population delaminated on many of the surfaces. However by the third week of culture, the cells were already beginning to show signs of differentiation. Osteopontin marker protein expression was significantly higher on NW in comparison with PCL. Although adiponectin marker protein expression was also higher on NW than PCL, the percentage of osteopontin was much greater than adiponectin. There were no significant differences or noticeable trends with collagen 2 expression. Histological staining also confirmed the results of immunofluorescence and showed that more osteogenic mineralization was occurring on the NW surfaces while more GAG presence was detected on the PCL surfaces. Lipid accumulation and deposition also seemed to be occurring more on the NW surfaces. Overall, these results concluded that attachment of the cells to the nanowire surfaces has a large effect on the mechanostransduction and signaling of the cells to differentiate primarily into osteogenic phenotypes with moderate differentiation into

adipogenic progenitors. Additionally, it was also concluded, that the elongated morphologies of the ADSCs by the nanowire arrays are not conducive towards chondrogenic differentiation.

REFERENCES

1. Hench, L.L. and J.M. Polak, *Third-generation biomedical materials.* Science, 2002. **295**(5557): p. 1014-7.
2. McMurray, R.J., et al., *Nanoscale surfaces for the long-term maintenance of mesenchymal stem cell phenotype and multipotency.* Nature Materials, 2011. **10**(8): p. 637-644.
3. Curtis, A., *Tutorial on the biology of nanotopography.* IEEE Trans Nanobioscience, 2004. **3**(4): p. 293-5.
4. Clark, P., et al., *Cell guidance by ultrafine topography in vitro.* J Cell Sci, 1991. **99 (Pt 1)**: p. 73-7.
5. Clark, P., et al., *Topographical control of cell behaviour. I. Simple step cues.* Development, 1987. **99**(3): p. 439-48.
6. McNamara, L.E., et al., *Nanotopographical control of stem cell differentiation.* J Tissue Eng, 2010. **2010**: p. 120623.
7. Milner, K.R. and C.A. Siedlecki, *Fibroblast response is enhanced by poly(L-lactic acid) nanotopography edge density and proximity.* International Journal of Nanomedicine, 2007. **2**(2): p. 201-211.
8. Dalby, M.J., et al., *Polymer-demixed nanotopography: Control of fibroblast spreading and proliferation.* Tissue Engineering, 2002. **8**(6): p. 1099-1108.
9. Dalby, M.J., et al., *In vitro reaction of endothelial cells to polymer demixed nanotopography.* Biomaterials, 2002. **23**(14): p. 2945-54.
10. Bettinger, C.J., et al., *Enhancement of In Vitro Capillary Tube Formation by Substrate Nanotopography.* Adv Mater, 2008. **20**(1): p. 99-103.

11. Lamers, E., et al., *The influence of nanoscale topographical cues on initial osteoblast morphology and migration.* Eur Cell Mater, 2010. **20**: p. 329-43.

12. Dalby, M.J., et al., *The control of human mesenchymal cell differentiation using nanoscale symmetry and disorder.* Nature Materials, 2007. **6**(12): p. 997-1003.

13. Le Guehennec, L., et al., *Osteoblastic cell behaviour on different titanium implant surfaces.* Acta Biomaterialia, 2008. **4**(3): p. 535-543.

14. Le Guehennec, L., et al., *Osteoblastic cell behavior on nanostructured metal implants.* Nanomedicine, 2008. **3**(1): p. 61-71.

15. Kantawong, F., et al., *Proteomic analysis of human osteoprogenitor response to disordered nanotopography.* J R Soc Interface, 2009. **6**(40): p. 1075-86.

16. Kantawong, F., et al., *Whole proteome analysis of osteoprogenitor differentiation induced by disordered nanotopography and mediated by ERK signalling.* Biomaterials, 2009. **30**(27): p. 4723-4731.

17. Gasiorowski, J.Z., et al., *Alterations in gene expression of human vascular endothelial cells associated with nanotopographic cues.* Biomaterials, 2010. **31**(34): p. 8882-8888.

18. Yim, E.K., et al., *Nanotopography-induced changes in focal adhesions, cytoskeletal organization, and mechanical properties of human mesenchymal stem cells.* Biomaterials, 2010. **31**(6): p. 1299-306.

19. Biggs, M.J., et al., *Regulation of implant surface cell adhesion: characterization and quantification of S-phase primary osteoblast adhesions on biomimetic nanoscale substrates.* J Orthop Res, 2007. **25**(2): p. 273-82.

20. Biggs, M.J.P., R.G. Richards, and M.J. Dalby, *Nanotopographical modification: a regulator of cellular function through focal adhesions.* Nanomedicine-Nanotechnology Biology and Medicine, 2010. **6**(5): p. 619-633.

CHAPTER 7

CONCLUSIONS AND FUTURE WORK

7.1 Summary of Conclusions

The work presented in this dissertation explores the differentiation potential of mulitpotent adipose derived stem cells into osteogenic, chondrogenic, and adipogenic phenotypes based on mechanotransductive signaling from polymeric nanowire surface topographies. The traditional method for inducing stem cell differentiation involves the inclusion of biochemical supplements in the media conditions in order to begin creating progenitor cells which over time will eventually mature into fully differentiated cells. By investigating the differentiation of these cell types without the influence of biochemical cues from the cell media, more focus can be placed on evaluating the effect of surface topography on stem cell adhesion, migration, proliferation, morphology, and the differentiation potential. By creating a biomimetic biomaterial scaffold containing surface features on the nanoscale level, cells will begin to alter their behavior in order to adapt to their new environment.

Since implanted biomedical devices interact with the human physiology at the biomaterial surface interface, it is important that the surface properties are favorable for cell and tissue integration for long-term success. PCL nanowire arrays were fabricated using a solvent-free thermogravimetric template process, a technique developed in the Popat Lab, using anodized alumina membranes with 100 nm pores as the mold. In addition, nanowire arrays were fabricated containing 1 wt% hydroxyapatite nanopowder within the bulk material for osteogenic studies. With the aim of identifying the capabilities of PCL nanowire arrays as interfaces for use in implantable biomedical devices, this research has investigated the characteristics of this specific

nanoarchitecture including nanowire morphology, nanoarchitecture, thermal characteristics, hydrophobicity, bulk material tensile mechanical properties, and nanoindentation properties. All of these characteristics were evaluated using SEM/EDS, TGA, DSC, contact angle, uniaxial tensile testing, and nanoindentation. The simple fabrication, physiologically relevant architecture, strong mechanical properties, low surface energy and large surface area identify PCL nanowire arrays to be promising interfaces for implantable biomedical devices.

Using adipose derived stem cells, the first study evaluated cell functionality and osteogenic differentiation on PCL, hPCL, NW, and hNW surfaces. Surface characterization techniques verified the NW surfaces had a uniform morphology, as well as the presence of HAp on hNW surfaces. The results indicate that the NW and hNW surfaces both demonstrated lower ADSC adhesion and proliferation as compared to PCL and hPCL surfaces. However, ADSCs on NW and hNW surfaces displayed an elongated morphology with cellular extensions interacting with nanotopography. Further, all the surfaces expressed ALP activity for up to 3 weeks of culture in osteogenic conditions. However, NW surfaces expressed highest OC and OP expression, followed by hNW, PCL and hPCL surfaces. Overall this study has shown that the presence of hydroxyapatite nanoparticles does not have a significant effect on enhancing osteogenic differentiation, however the topography of the PCL nanowire surfaces has the most influence on ADSC behavior.

The second and third studies investigated the differentiation potential of ADSCs on polycaprolactone nanowire into chondrogenic and adipogenic phenotypes. ADSC adhesion, proliferation, viability, and morphology were investigated for up to 7 days of culture using fluorescence microscopy imaging, a cell viability assay, and SEM. The results show that the cells on both surfaces, PCL and NW, promote adhesion and proliferation, however the cells on NW

have much more elongated morphologies. Differentiation was investigated after the 7 day growth period for up to 3 weeks of culture using immunofluorescence imaging, histological staining, and SEM. On NW, more cells appear to have differentiated into adipogenic phenotypes, whereas fewer cells appear to have differentiated into chondrogenic phenotypes as compared to cells on PCL. Expression of adipogenic marker proteins (PPARγ and adiponectin) increased, whereas no change in expression was observed for chongrogenic proteins (sox9 and col2) over the 3 weeks of culture on the NW surfaces. In addition, chondrogenic histological staining using alcian blue, indicated lower GAG presence on NW as compared to PCL. Therefore, the results indicate that the nanowire architecture may provide a more favorable template for adipogenic differentiation and less favorable for chondrogenic differentiation of ADSCs.

The final study evaluated the influence of nanowire arrays on ADSC differentiation by investigating the expression of osteogenic, chondrogenic, and adipogenic marker proteins in addition to histological stains. However, this study used minimal essential growth media without differentiation supplements in order to assess how ADSCs are affected by the substrate nanotopography. The results of this study show that although both surfaces promote ADSC adhesion, proliferation, and viability, cells on the PCL surfaces proliferate at a much higher rate than NW surfaces. In addition, ADSCs on NW surfaces had elongated morphologies and lower shape factors similar to the behaviors observed in the previous studies. It was concluded that more ADSCs on the NW surfaces were being signaled to begin the differentiation process and become progenitor cells rather than being signaled to continue proliferation. Differentiation was investigated for 5 weeks of culture, however due to the cells reaching 100% confluency at the final time point, the cell population delaminated on many of the surfaces. However by the third week of culture, the cells were already beginning to show signs of differentiation. Osteopontin

marker protein expression was significantly higher on NW in comparison with PCL. Although adiponectin marker protein expression was also higher on NW than PCL, the percentage of osteopontin was much greater than adiponectin. There were no significant differences or noticeable trends with collagen 2 expression. Histological staining also confirmed the results of immunofluorescence and showed that more osteogenic mineralization was occurring on the NW surfaces while more GAG presence was detected on the PCL surfaces. Lipid accumulation and deposition also seemed to be occurring more on the NW surfaces. Overall, these results concluded that attachment of the cells to the nanowire surfaces has a large effect on the mechanostransduction and signaling of the cells to differentiate primarily into osteogenic phenotypes with moderate differentiation into adipogenic progenitors. Additionally, it was also concluded, that the elongated morphologies of the ADSCs by the nanowire arrays are not conducive towards chondrogenic differentiation.

7.2 Future Work

Conclusions of this work show that the simple fabrication process, the physiological nanoarchitecture, the mechanical properties, thermal characterization, degradation characteristics, and favorable cellular interactions classify PCL nanowire arrays as an advantageous interface for long term implantable biomedical devices. This research helped confirm that these surfaces have the ability to help influence and maintain osteogenic differentiation. The nanowire arrays do not appear to support chondrogencic differentiation and the effect of nanowires on adipogenic differentiation appears to be moderate, at best. Therefore, additional experiments for examining the efficacy of these scaffolds would revolve around improvements for orthopedic applications and specifically bone tissue engineering.

First, the cellular response may be tuned and optimized by varying the size parameters of nanowire arrays using different sized alumina membrane pores and different extrusion times. In addition to obtaining membranes from the manufacture, our lab has the resources and ability to fabricate our own membranes using anodization. Based on the application, it is possible to alter the pore sizes to adequately mimic the feature of the target tissue we are interested in. Extrusion times during the nanowire fabrication process can have a large impact on the surface mechanical properties based on the overall average length of the nanowire arrays. As was discovered in this research, if the surface properties are adjusted, it will greatly influence how cells react and behave. As well as topographical modificiations, further investigation will be necessary regarding biomolecular modifications and the addition of bioactive factors to enhance the long-term effect of nanowire arrays as a biomedical device.

Implications of this work, and the potential use for PCL nanowire arrays as interfaces for use in implantable devices, will require the development of *in vivo* models and research. The primary advantage of i*n vivo* studies is that it will provide us with the ability to investigate the long-term effect and degradation rate of PCL when interfaced with osteogenic tissue. In addition, *in vivo* research will give better insight into the tissue healing, recruitment of cells to the implant site, and development of ECM products. This future research will be beneficial because it will deliver many answers about the long-term functionality of PCL nanowire arrays in various clinical applications as well as determine the best ways to tune and modify the surfaces appropriately for each scenario.